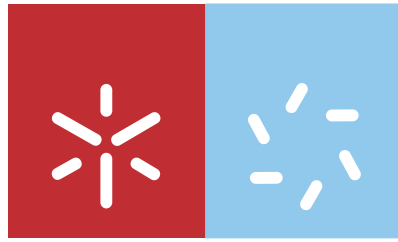


**Universidade do Minho**  
Escola de Ciências

Rómulo Sacramento Sobral

**Characterisation of the molecular interaction between MYB-like transcription factors in the establishment of floral dorsoventral asymmetry in *Antirrhinum majus***



**Universidade do Minho**  
Escola de Ciências

Rómulo Sacramento Sobral

**Characterisation of the molecular  
interaction between MYB-like transcription  
factors in the establishment of floral  
dorsoventral asymmetry in  
*Antirrhinum majus***

Dissertação de Mestrado  
Mestrado de Genética Molecular

Trabalho efectuado sob a orientação da  
**Professora Doutora Maria Manuela Ribeiro Costa**

## DECLARAÇÃO

**Nome:** Rómulo Sacramento Sobral

**Endereço electrónico:** [citfresh@gmail.com](mailto:citfresh@gmail.com)

**Telefone:** 933544209

**Número do Bilhete de Identidade:** 12511652

**Título tese de Mestrado:**

Characterisation of the molecular interaction between MYB-like transcription factors in the establishment of floral dorsoventral asymmetry in *Antirrhinum majus*.

**Orientador:** Maria Manuela Ribeiro Costa

**Ano de conclusão:** 2010

**Designação do Mestrado:** Mestrado de Genética Molecular

É AUTORIZADA A REPRODUÇÃO INTEGRAL DESTA TESE APENAS PARA EFEITOS DE INVESTIGAÇÃO, MEDIANTE DECLARAÇÃO ESCRITA DO INTERESSADO, QUE A TAL SE COMPROMETE.

Universidade do Minho, \_\_\_/\_\_\_/\_\_\_\_\_

Assinatura: \_\_\_\_\_

## **Acknowledgements**

I would like to thank to Prof. Manuela for all her teachings and for being an excellent and supportive supervisor.

To all the people in the lab, I would like to thank for creating an enjoyable environment that allowed me to take pleasure in my work time. In particular, I would like to thank Sara, Juliana, Herlânder and João for all the technical support they gave me since I started my work.

To my family and friends, thank you all for the patience, encouragement and friendship, for being present in the best and worst moments.

Finally to Sara, without her I definitively wouldn't be writing these words. Thank you for all your support, dedication, for the excellent example, and especially for your love...



## Abstract

**Characterisation of the molecular interaction between MYB-like transcription factors in the establishment of floral dorsoventral asymmetry in *Antirrhinum majus*.**

Transcription factor interactions are the cornerstone of combinatorial control, which is a crucial aspect of the gene regulatory system that underlies many developmental processes. In *Antirrhinum majus*, floral dorsoventral asymmetry is controlled by the combined activity of four transcription factors: *CYCLOIDEA* (*CYC*), *DICHOTOMA* (*DICH*), *RADIALIS* (*RAD*) and *DIVARICATA* (*DIV*). *CYC*, *DICH* and *RAD* are expressed dorsally in the floral primordium and promote dorsal petal identity. *DIV* is expressed in the entire floral primordium, even though it only has a phenotypic effect in more ventral regions. Genetic and molecular studies have revealed that *RAD* is a direct target of *CYC* and that *RAD* antagonises the activity of *DIV*. Previous yeast two-hybrid screens led to the identification of two new MYB-like proteins (*RAD-INTERACTING PROTEIN 1* and *2*, *RIP1* and *RIP2*) that interact with both *RAD* and *DIV*. Therefore, the *RIP* proteins might also be involved in the antagonism that *RAD* has on *DIV* activity, essential for the establishment of flower asymmetry in *Antirrhinum*.

The aim of this thesis was to characterise the molecular antagonism between *RAD* and *DIV*, either through direct interaction or indirectly by competition for the *RIP* proteins.

The results from a DNA-binding assay revealed that *RAD* does not target directly *DIV* or the DNA targets of *DIV*, suggesting that the *RIP* proteins might be bridging the molecular antagonism between *RAD* and *DIV*. A sub-cellular localization assay revealed that the *RIP* proteins co-localised with *RAD* and *DIV* in the nucleus, which means that these proteins are able to interact in the same sub-cellular compartment. A quantitative yeast-two hybrid result indicated that *RAD* interacts more strongly with the *RIP* proteins than *DIV*. This result suggest that the *RIP* proteins might be co-factors essential for *DIV* function that are sequestered in the dorsal domain by *RAD*, restricting *DIV* activity to the ventral petal. The role of the *RIP* proteins in the molecular antagonism between *RAD* and *DIV* will be further addressed using protein-protein interaction assays *in vitro* and *in planta*.

## Resumo

**Caracterização da interacção molecular entre factores de transcrição do tipo MYB-like no desenvolvimento da assimetria dorsoventral da flor de *Antirrhinum majus*.**

A interacção entre factores de transcrição é a base do sistema de regulação genética e em maior instância do desenvolvimento. Em *Antirrhinum majus* a assimetria dorsoventral da flor é controlada pela acção combinada de quatro factores de transcrição: *CYCLOYDEA* (*CYC*), *DICHOTOMA* (*DICH*), *RADIALIS* (*RAD*) e *DIVARICATA* (*DIV*). *CYC*, *DICH* e *RAD* são expressos dorsalmente no primórdio floral promovendo a identidade dorsal das pétalas dorsais. *DIV* é expresso em todo o meristema floral, no entanto, os seus efeitos fenotípicos são evidentes apenas nas regiões mais ventrais. Estudos genéticos e moleculares revelaram que *RAD* é responsável pelo antagonismo da actividade de *DIV*. Recentemente num yeast two-hybrid foram identificados dois novos factores de transcrição do tipo MYB (*RAD-INTERACTING PROTEIN 1* e *2*, *RIP1* e *RIP2*) que interagem com *RAD* e *DIV*. É possível que as proteínas *RIP* também estejam envolvidas no antagonismo entre *RAD* e *DIV*.

O principal objectivo desta tese é a caracterização do antagonismo molecular entre as proteínas *RAD* e *DIV*, quer por interacção directa entre *RAD* e *DIV* ou por competição pelas proteínas *RIP*.

O resultado de um ensaio de ligação ao DNA revelaram que *RAD* não interage directamente com *DIV*, nem com os alvos de DNA de *DIV*, sugerindo que as *RIP* poderão ter um papel na mediação do antagonismo molecular entre *RAD* e *DIV*. Um ensaio de sub-localização celular demonstrou que as proteínas *RIP* co-localizam com *RAD* e *DIV* no núcleo, o que indica que as proteínas tem a possibilidade de interagir no mesmo compartimento subcelular. Um ensaio *yeast-two hybrid* quantitativo revelou que *RAD* tem maior afinidade para as proteínas *RIP* que *DIV*. Os resultado sugerem a hipótese que as proteínas *RIP* poderão ser cofactores essenciais para a função de *DIV* e que na presença de *RAD*, as *RIP* são sequestradas, restringindo a actividade de *DIV* ao domínio ventral onde *RAD* não está presente. O papel das proteínas *RIP* no antagonismo molecular entre *RAD* e *DIV* será explorado em ensaios futuros que abrangerão o estudo da interacção das proteínas *in vitro* e *in planta*.

# Table of Contents

<b>Acknowledgements</b>	<b>iii</b>
<b>Abstract</b>	<b>v</b>
<b>Resumo</b>	<b>vi</b>
<b>Table of Contents</b>	<b>vii</b>
<b>Abbreviations and Acronyms</b>	<b>x</b>
<b>1. Introduction</b>	<b>1</b>
1.1 Genetic Regulatory Networks	1
1.2 Genetic Regulatory Networks in the Evolution and Diversity of Plants	2
1.3 Flower Symmetry	4
1.3.1 <i>A. majus</i> as model species for flower symmetry studies	7
1.3.1.1 <i>CYCLOYDEA</i> and <i>DICHOTOMA</i>	8
1.3.1.2 <i>RADIALIS</i>	10
1.3.1.3 <i>DIVARICATA</i>	11
1.3.2 MYB family of transcription factors	13
1.3.2.1 <i>RAD</i> and <i>DIV</i> as MYB-like transcription factors	15
1.3.3 A model for Genetic Regulation of Flower Asymmetry	17
1.3.4 Genetic basis for flower asymmetry among other <i>taxa</i>	20
1.4 Aims of this study	23
<b>2. Material and Methods</b>	<b>25</b>
2.1 Biological material	25
2.1.1 Plant material	25
2.1.1.1 <i>Arabidopsis thaliana</i>	25
2.1.1.2 <i>Nicotiana benthamiana</i>	25
2.1.2 Bacterial material	26
2.1.2.1 <i>Escherichia coli</i>	26
2.1.2.2 <i>Agrobacterium tumefaciens</i>	27
2.1.3 <i>Saccharomyces cerevisiae</i>	27
2.2 DNA Methods	28
2.2.1 Bacterial Transformation	28
2.2.1.1 <i>E. coli</i>	28
2.2.1.2 <i>A. tumefaciens</i>	28
2.2.2 Isolation of plasmid DNA	29
2.2.2.1 P1 P2 P3 method	29
2.2.2.2 Small-scale (mini) isolation of purified plasmid DNA	29
2.2.2.3 Estimation of DNA concentration	29
2.2.3 Agarose Gel Electrophoresis	30
2.2.4 Polymerase chain reaction (PCR) methods for DNA fragment amplification	30
2.2.4.1 Amplification of DNA fragments from plasmid templates	31
2.2.4.2 Amplification of DNA fragments from plasmid templates using <i>Pfu</i> DNA Polymerase	31
2.2.4.3 Amplification of DNA fragments for <i>Gateway</i> ® system based cloning	31
2.2.4.4 Colony PCR amplification	32



2.2.5 DNA purification	33
2.2.5.1 Wizard SV Gel and PCR Clean-Up System	33
2.2.5.2 Phenol/Chloroform DNA extraction method	33
2.2.6 Restriction digestion with endonucleases	33
2.2.6.1 Plasmid DNA	33
2.2.6.2 PCR product	34
2.2.7 Ligation reaction	34
2.3 Cloning procedures	36
2.3.1 Cloning into the pRSET vector	36
2.3.1.1 <i>RIP1</i> and <i>RIP2</i> amplification and digestion	36
2.3.1.2 pRSET digestion	37
2.3.1.3 Ligation and transformation	37
2.3.2 Cloning into pMDC43 and pMDC32	37
2.3.2.1 <i>BP</i> reaction	38
2.3.2.2 <i>LR</i> reaction	38
2.3.3 Cloning into pH7WGF2	39
2.3.3.1 <i>BP</i> reaction	39
2.3.3.2 <i>LR</i> reaction	39
2.3.4 Cloning into pDH51-GW-YFPn and pDH51-GW-YFPc	40
2.3.4.1 <i>BP</i> reaction	40
2.3.4.2 <i>LR</i> reaction	40
2.4 Yeast Methods	41
2.4.1 <i>Saccharomyces cerevisiae</i> transformation	41
2.4.2 3-amino-1, 2, 4-triazole assay	41
2.4.3 Colony-lift filter assay	42
2.4.4 Liquid Culture assay using <i>o</i> -nitrophenyl- $\beta$ - <i>D</i> -galactopyranoside (ONPG) as substrate	42
2.5 Protein Methods	43
2.5.1 Heterologous pilot expression in <i>E. coli</i>	43
2.5.2 Protein electrophoresis	44
2.5.3 Protein gel staining	45
2.5.4 Protein purification	45
2.6 Electrophoretic Mobile Shift Assay (EMSA)	46
2.6.1 Probe preparation and labelling	46
2.6.2 EMSA reaction and electrophoretic separation	46
2.6.3 Electroblotting	47
2.6.4 Detection	48
2.7 Generation of <i>Arabidopsis</i> transgenic lines	48
2.7.1 <i>A. tumefaciens</i> transformation	48
2.7.2 Plant transformation	48
2.7.3 Selection of primary transformants (T1 generation)	49
2.8 <i>N. benthamiana</i> transient transformation	49
2.9 Protein functional analysis	50
<b>3. Results</b>	<b>51</b>
3.1 <i>RIP1</i> and <i>RIP2</i> sequence analysis	51
3.2 Expression of recombinant RAD, DIV and RIP proteins in <i>E. coli</i>	53

3.2.1 Optimization of the expression and purification of RAD recombinant protein	55
3.2.2 Optimization of the expression and purification of <i>DIV</i> recombinant protein	59
3.3 Expression of RIP1 and RIP2 recombinant protein in <i>E. coli</i>	63
3.3.1 Cloning of the RIP1 and RIP2 cDNA into the pRSET plasmid	63
3.3.2 Optimisation of the expression of the RIP1 and RIP2 recombinant proteins	66
3.4 DNA-binding affinity assay	71
3.5 Yeast two-hybrid based assays	75
3.5.1 3-amino-1,2,4 triazole assay	77
3.5.2 RIP1 and RIP2 interact with RAD and DIV in a yeast two-hybrid assay	79
3.5.3 Determination of the interaction strength by the $\beta$ -galactosidase liquid assay	81
3.6 Sub-cellular localisation of RAD, DIV and RIP proteins	84
3.6.1 Plasmids construction	84
3.6.2 Transient expression in <i>N. benthamiana</i>	89
3.6.3 Co-localization assay	93
3.7 Testing the interaction between RAD-RIP and DIV-RIP proteins <i>in planta</i> by Bimolecular Fluorescence Complementation	96
3.7.1 Plasmids construction	96
3.8 Ectopic expression of the RIP proteins in <i>Arabidopsis</i>	103
<b>4. Discussion</b>	<b>105</b>
4.1 RAD does not bind directly to DIV or indirectly to DIV DNA targets.	106
4.2 RAD and DIV interact strongly with the RIP proteins	108
4.3 RAD and DIV co-localise with the RIP proteins in the nucleus	112
4.4 Testing the RAD, DIV and RIPs interactions <i>in planta</i>	114
4.5 The RIPs biological function	116
4.6 Concluding Remarks	116
<b>5. Bibliography</b>	<b>118</b>
<b>6. Supplementary information</b>	<b>131</b>

## Abbreviations and Acronyms

<b>AD</b>	activation domain of GAL4	<b>MM</b>	molecular marker
<b>BD</b>	binding domain of GAL4	<b>mJ</b>	millijoule
<b>bHLH</b>	basic helix loop helix	<b>MM</b>	molecular marker
<b>BiFC</b>	bimolecular fluorescence complementation	<b>mRNA</b>	messenger RNA
<b>Bp</b>	base pairs	<b>MS</b>	Murashige and Skoog
<b>BRET</b>	bioluminescence resonance transfer energy	<b>NLS</b>	nuclear localization signal
<b>CaMV</b>	cauliflower mosaic virus	<b>OD</b>	optical density
<b>cDNA</b>	complementary DNA	<b>ONPG</b>	<i>ortho</i> -Nitrophenyl- $\beta$ -galactoside
<b>Col</b>	<i>A. thaliana</i> ecotype <i>Columbia</i>	<b>ORF</b>	open reading frame
<b>CYC</b>	<i>CYCLOIDEA</i>	<b>PAGE</b>	Polyacrylamide gel electrophoresis
<b>dH<sub>2</sub>O</b>	deionised water	<b>PCR</b>	polymerase chain reaction
<b>DICH</b>	<i>DICHOTOMA</i>	<b>PEG</b>	Polyethylene glycol
<b>DIG</b>	digoxigenin	<b>RAD</b>	<i>RADIALIS</i>
<b>DIV</b>	<i>DIVARICATA</i>	<b>RIP1</b>	<i>RAD INTERACTING PROTEIN1</i>
<b>dNTP</b>	any deoxyribonucleotide	<b>RIP2</b>	<i>RAD INTERACTING PROTEIN2</i>
<b>DTT</b>	dithiothreitol	<b>RNA</b>	ribonucleic acid
<b>DUF</b>	domain of unknown function	<b>rpm</b>	revolutions per minute
<b>EDTA</b>	ethylenediaminetetraacetic acid	<b>SAP</b>	shrimp alkaline phosphatase enzyme
<b>EMSA</b>	electrophoretic mobile shift assay	<b>SD</b>	synthetic minimal medium
<b>EYFP</b>	<i>ENHANCED YELLOW FLUORESCENT PROTEIN</i>	<b>SDS</b>	sodium dodecyl sulphate
<b>FRET</b>	fluorescence resonance energy transfer	<b>ssDNA</b>	single stranded DNA
<b>g</b>	relative centrifugal force	<b>TAE</b>	tris-acetate-EDTA buffer
<b>GFP</b>	<i>GREEN FLUORESCENT PROTEIN</i>	<b>TBE</b>	tris-borate-EDTA buffer
<b>His</b>	histidine	<b>TE</b>	tris-EDTA buffer
<b>HIS3</b>	<i>HISTIDINE3</i>	<b>TEN</b>	tris-EDTA-NaCl buffer
<b>IPTG</b>	Isopropyl $\beta$ -D-1-thiogalactopyranoside	<b>tRNA</b>	transfer RNA
<b>iRNA</b>	interference RNA	<b>UV</b>	ultraviolet
<b>kDa</b>	kilodalton	<b>W</b>	triptofan
<b>LACZ</b>	<i><math>\beta</math>-GALACTOSIDASE</i>	<b>X-GAL</b>	bromo-chloro-indolyl-galactopyranoside
<b>LB</b>	Luria-Bertani medium	<b>YFP</b>	<i>YELLOW FLUORESCENT PROTEIN</i>
<b>Leu</b>	leucine	<b>YPDA</b>	yeast peptone dextrose adenine
<b>M</b>	molar	<b>3-AT</b>	3-Amino-1,2,4-triazole
<b>mJ</b>	millijoule	<b>6xHis</b>	polyhistidine tag

# 1. Introduction

Transcriptional regulation lies at the basis of most biological processes in living organisms. It can be defined as the processing of extracellular and/or intracellular signals that lead to changes in the transcription rate of target genes, and is often characterised by a complex inter-play of protein-protein interactions, sub-cellular translocations and post-translational modifications (Carrol *et al.*, 2001). The study of the evolution of transcription regulation is a common theme for those who are interested in understanding the principles and driving forces whereby new protein-coding genes, new protein structures and new biological functions emerge as a consequence of changes in the genetic material during the course of evolution (Patthy, 2008)

## 1.1 Genetic Regulatory Networks

The organ or body morphology and functionality is the outcome of complex interactions within genetic regulatory networks. It is upon these networks that evolutionary forces act and whose modifications give rise to the vast diversity in morphological form among species (Carroll *et al.* 2001). One particular component of these genetic regulatory networks, which contribute with the most global effects on development, is a family of proteins called transcription factors (Gellon and McGinnis, 1998).

Transcription factors are an important class of proteins involved in regulating the production of mRNA transcripts from genes by binding to DNA *cis*-acting elements. Transcription factors can be a part of the basal transcription machinery or regulatory in nature, whereby they control specific groups of genes in particular cell types, time periods or environmental conditions (Latchman, 1997). Transcription factors are modular in structure and contain distinctive domains: the DNA-binding domain, which attaches to specific sequences of DNA (*cis*-elements) adjacent to regulated genes; and the *trans*-activation domain that contains binding sites for other proteins such as transcription co-regulators (Mitchel and Tjian, 1989).

Transcription factors use a variety of mechanisms to regulate gene expression: stabilise or block the binding of RNA polymerase to DNA; catalyse the acetylation or

deacetylation of histones; or recruit co-activators or co-repressors proteins to the transcription factor complex (Mitchel and Tjian, 1989).

There is ample evidence for the role of transcription factors in developmental modifications during evolution. In the Animal Kingdom, comparative analyses of *Hox* (group of homeodomain transcription factors) gene expression in arthropods, annelids and vertebrates have revealed a consistent correlation between major differences in axis morphology and differences in the spatial and temporal regulation of *Hox* genes (Holland, 1999). As an example, *Hox* genes are expressed at different relative positions along the rostrocaudal axis in the mouse, chick and python (Belting *et al.* 1998; Cohn and Tickle, 1999). Belting *et al.* (1998) provide direct evidence that change in *cis*-regulatory elements has led to the diversification in *Hoxc8* expression that account for part of the morphologic differences between chicks and mice. In the Plant Kingdom a clear example is the *teosinte branched 1* locus (*TB1*) and its role in the domestication of maize. In maize, *tb1* mutants resemble the wild ancestor teosinte with a highly branched architecture that ends in male tassels rather than female ears. Strong selection on the upstream regulatory regions and the resulting altered expression pattern resulted in this change in architecture (Wang *et al.*, 1999; Rosin and Kramer, 2009).

## **1.2 Genetic Regulatory Networks in the Evolution and Diversity of Plants**

An important goal for research is to elucidate how complex gene regulatory networks evolve and how their evolution results in phenotypic change and speciation (Carrol *et al.*, 2005). Two trends seem to be important for plant evolution and diversity: gene duplication and convergent co-option of pre-existent genetic modules.

Duplication of individual genes, chromosomal segments or entire genomes is considered a major source of morphological novelties (Ohno, 1970). Ohno (1970) evolutionary theory suggests three possible outcomes for the duplicated gene as described in figure 1. Copy can be silenced by degenerative mutations (non-functionalization); copy acquires a new function (functional divergence) and is positively selected by natural selection with the other copy maintaining original function (neofunctionalization), or both copies suffer degenerative mutations becoming partially

compromised in a way that the overall capacity is similar to the function of the ancestral gene (Hughes, 1994; He and Zhang, 2005).

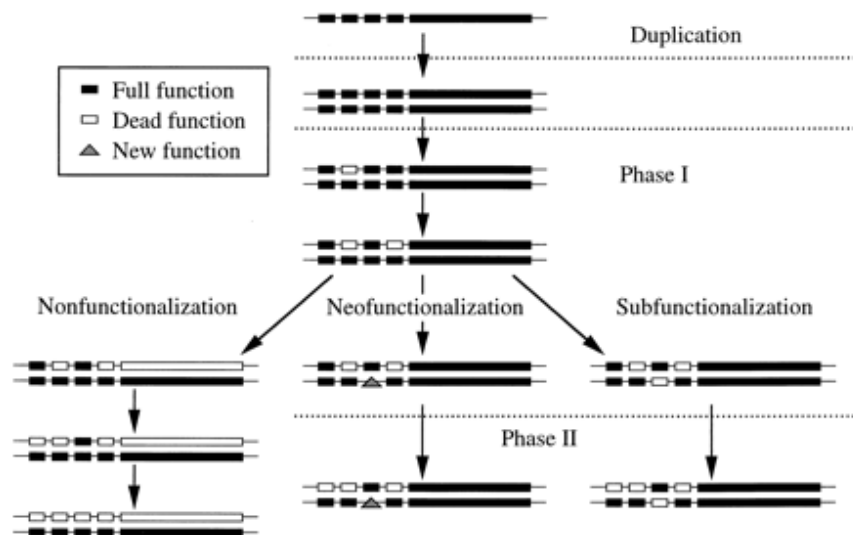


**Figure 1-** Possible outcomes of duplicated genes. Copy can be silenced by degenerative mutations (non-functionalization); copy acquires new function (functional divergence) and is positively selected by natural selection with the other copy maintaining original function (neo-functionalization); or both copies suffer degenerative mutations becoming partially compromised in a way that the overall capacity is similar to the function of the ancestral gene (Hughes, 1994; He and Zhang, 2005).

Lineage-specific gene duplications that led to the expansion of transcription-factor families are widely believed to have an important role in plant diversification and complexity (Levine and Tjian, 2003). Interestingly, there is evidence that the expansion of transcription-factor families is greater in plants than in animals (Shiu *et al.*, 2005). Transcription factors typically contain multiple functional domains, which mediate binding to DNA, interactions with other proteins and the sub-cellular localization of the transcription factor (Latchman, 1997). A transcription factor with a new binding specificity can be created by duplication of an existing transcription factor followed by mutations, often, although not always, in the DNA-binding domain. Transcription factors can also evolve by the acquisition or loss of one of its other functional domains. For example, the loss of a transcriptional activation domain could turn an activator into a repressor, whereas the acquisition of a new protein-protein interaction domain, that facilitates heterodimerisation with a novel binding partner, could significantly alter the targets of the transcription factor (Chen and Rajewsky, 2007).

The other repeated tendency over the course of evolution, which can account for the diversification of several plant traits, is the evolution of convergent morphological features, even at recent time scales through co-option of the same regulatory networks (Rosin and Kramer, 2009). Several cases have now been characterized that show numerous parallel recruitments of homologous genetic pathways to control convergent features. One such case is the independent recruitment of the specific interaction between *KNOTTED-1*-like homeobox (KNOX) transcription factor and *ASYMMETRIC LEAVES1/ROUGH SHEATH2/PHANTASTICA* (*ARP*) genes in the independent evolution of leaves in lycophytes and in seed plants (Harrison *et al.*, 2005).

Plant diversification appears to be closely correlated with modifications in the genetic regulatory networks. There are several described genetic regulatory networks whose function was associated with the control of specific plant features, and among those, is the regulatory network that controls flower symmetry.

### 1.3 Flower Symmetry

Flower symmetry is an architectural trait that accounts for innumerable variations in floral shape (figure 2). Flower symmetry has been chosen as a model for genetic regulatory studies because it is a multiform and integrative morphological trait, genetically determined and set up at various stages during flower development (Endress, 2001). Moreover, mutants for floral symmetry are available in nature and can be obtained in the lab, enabling extensive molecular genetics analysis (Jabbour *et al.*, 2009). But more importantly, is the fact that flower symmetry evolution encompassed not only gene duplications, but also co-option of regulatory networks to a new function.



**Figure 2** – Flower symmetry diversity. (a) *Iris pseudacorus*; (b) *Centaurea cyanus*; (c) *Anthyllis montana*; (d) *Lamprocapnus spectabilis*; (e) *Orchis simia*; (f) *Passiflora coerulea*; (g) *Digitalis purpurea*; (h) *Lobelia tupa*; and (i) *Canna occidentalis*. Adapted from Jabbour *et al.* (2009).

It is possible to distinguish three types of floral symmetry: actinomorphy (or radial symmetry) where the flower can be divided into symmetrical halves by more than one longitudinal plane passing through the axis; zygomorphy (or bilateral symmetry), when a flower is divided by only a single plane into two mirror-image halves; and asymmetry where no symmetry planes are observed (Figure 3) (Endress, 2001).

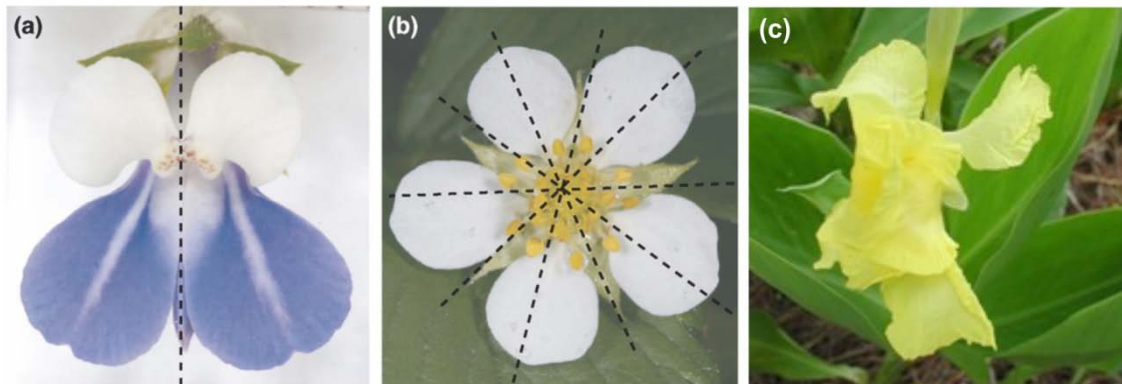


**Figure 3** - Types of floral symmetry: (a) Zygomorphic flower (one symmetry plane); (b) Actinomorphic flower (more than one symmetry planes); and (c) Asymmetric flower (no symmetry planes). Modified from Kalisz *et al.* (2006).

Flower symmetry is generally associated with the perianth whorl but by definition should extend to all floral whorls, however perfect whorl and organ symmetry (actinomorphy, *sensu strictu*) is not very common (Rudall and Bateman, 2004). Floral zygomorphy (flowers with visible differentiation between dorsal and ventral parts) could be the result of a differential organ elaboration by suppression/reduction of the developing flower organs (Endress, 1999). Floral zygomorphy could also be the result of colour alterations or organ orientation but according to Rudall and Bateman (2004) these late secondary changes are not phylogenetically relevant. Fossil and phylogenetic data allowed Endress (1999) to infer that in Angiosperms, actinomorphic flowers predate zygomorphic flowers. The first clearly bisexual flower appears in the fossil record in the beginning of the Cretaceous period (113-90 million years ago.). This flower was completely actinomorphic, with identical organs in each floral whorl (Crane *et al.* 1995). The first distinctive zygomorphic flower is known from the Upper Cretaceous period (Turonian age), 30-40 millions of years after the above mentioned actinomorphic floral fossil (Crepet, 1996). The fact that the basal angiosperms and monocots are almost predominantly actinomorphic, emphasise even more the idea that zygomorphy is a



derived condition (Endress, 1999). Coen and Nugent (1994) suggested a multiple and independent origin of zygomorphy from an actinomorphic ancestor, admitting also the possibility of an independent number or reversions to the ancestral form.

The subclass Asteridae with approximately 65000 species is a particularly good taxonomic group to study the genetic mechanisms underlying floral symmetry transition with about half of the species having actinomorphic corollas and the other half having zygomorphic ones (Ree and Donoghue, 1999) (figure 4).

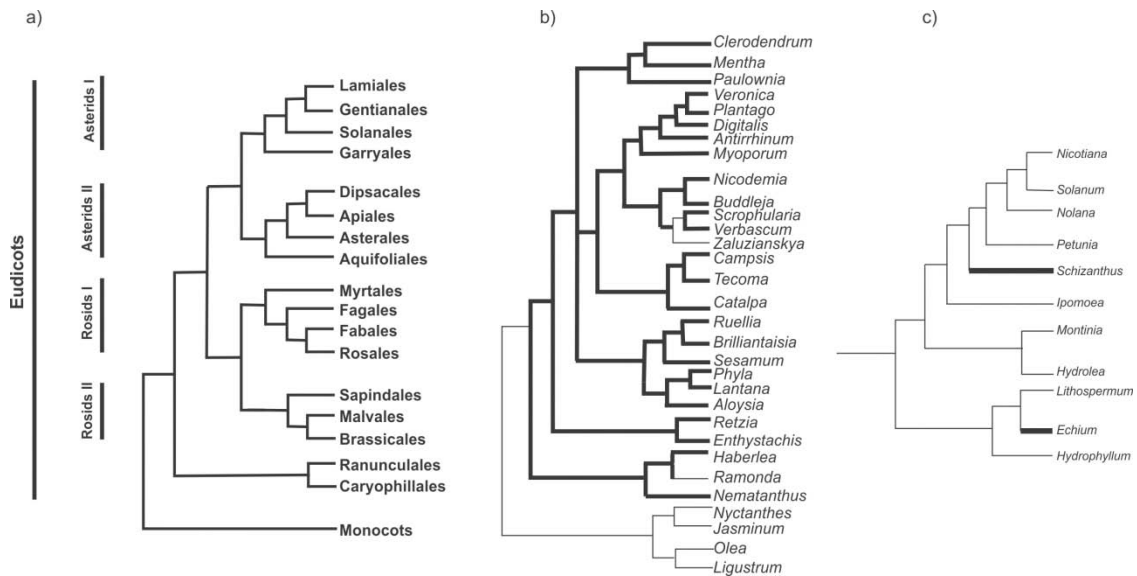


**Figure 4** - Angiosperm simplified phylogenetic tree: **a)** Eudicots phylogeny; **b)** Lamiales phylogeny; and **c)** Solanales phylogeny. Bold branches represent zygomorphic *taxa*. Adapted from Reeves and Olmstead (2003).

According to Donoghue *et al.*, 1998, species deep inside the Asteridae subclass from Rubiaceae, Apocynaceae, Apiales and Ericales, appear to have maintained the actinomorphic ancestral condition, however, phylogenetic data also indicate that some actinomorphic species are derived from zygomorphic ancestors (Endress, 2001), whereas species with zygomorphic flowers (*Plantago*, *Veronica*, *Antirrhinum*) appear to have descended from an actinomorphic ancestral. Floral zygomorphy was probably a preponderant factor in Angiosperms prolific diversification in part because many numerous and complex species (Asteraceae, Fabaceae and Orchidaceae) are predominantly zygomorphic (Cronk, 2001). Sargent (2004) suggested that the high diversity of Angiosperms is due to structural modifications of flower organ that caused shifts in pollination. Animal pollination became a more precise and efficient process in a

zygomorphic background because a zygomorphic flower attracts the pollinator in a particular and precise orientation (Neal, 1998). Moreover, bees, by innate or acquired behaviour, have preference for a monosymmetric pattern (West, 1998). There are, however, several other zygomorphic associated modifications that also enhance pollination efficiency: ventral petals usually exhibit appealing visual features being ideal landing platforms for pollinators; aborted or significantly reduced stamens facilitate pollinator access to nectar and pollen with the other stamens and carpels repositioned to maximize contact with pollinator. Accordingly, it appears that plant and animal co-evolved leading to the development of highly efficient plant/animal groups that eventually originated reproductive isolation (formation of sexual barriers) and initiated the extensive speciation that characterizes Angiosperm radiation (Neal, 1998; Endress, 2001).

The question remaining is to identify the genetic mechanisms that sustain the parallel independent evolutionary shifts between actinomorphy and zygomorphy. At the genetic level the multiple origin of zygomorphy could be explained by non-homologous gene recruitment to a similar function or by repetitive modification of a pre-existent genetic pathway through parallel evolution of *cis*-regulatory elements (Preston and Hileman, 2009).

### **1.3.1 *A. majus* as model species for flower symmetry studies**

Extensive comprehension of the molecular mechanisms underlying floral zygomorphy evolution has been successfully unfolded using *Antirrhinum majus* (Lamiales, Veronicaceae, tribe Antirrhinae) as a model species. In *A. majus*, floral zygomorphy is visible in the corolla and in the stamens (Endress, 2001). The corolla has five petals fused in a tube-like shape where it is possible to differentiate two dorsal petals, two lateral petals and one ventral according to their position, size, shape and epidermal cellular characteristics. The two dorsal petals have bigger lobes than the two lateral petals and ventral petal. The androecium is formed by five stamens (four fertile stamens and a fifth stamen in the dorsal portion that does not develop properly) (Endress, 1994) (figure 5).

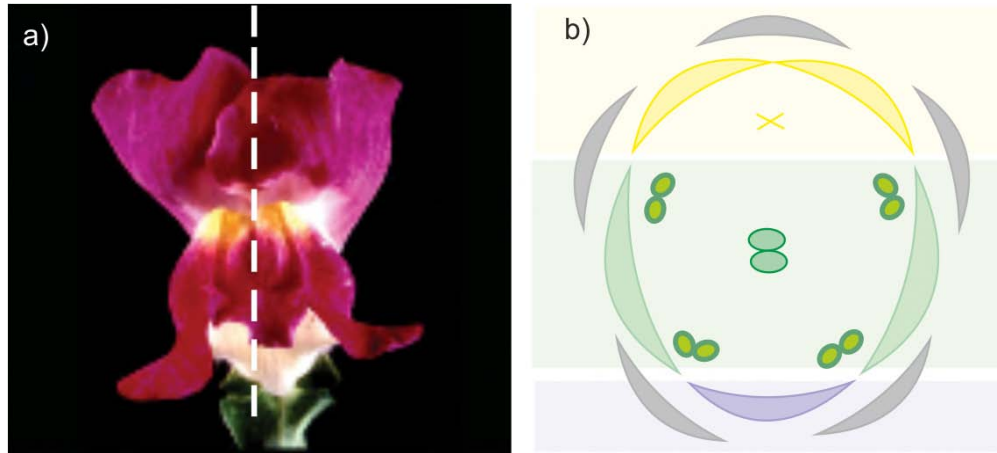


**Figure 5** - *A. majus* floral structure. **(a)** *A. majus* flower: five petals exhibit clear shape and size differences along the symmetry axis (indicated by dashed line). The upper lip consists in two large dorsal petals and the lower lip in two smaller lateral petals and one even smaller ventral petal. **(b)** *A. majus* flower frontal diagram: dorsal petals are shown in yellow, lateral petals in green and ventral petal in purple. Zygomorphy is also observable in the stamen whorl, dorsal stamen (x) is aborted, and the two lateral stamens are smaller than the two ventral stamens. Adapted from Busch and Zachgo (2009).

*A. majus* dorsoventral asymmetry is genetically controlled by four genes, *CYCLOIDEA* (*CYC*), *DICHOTOMA* (*DICH*), *RADIALIS* (*RAD*) and *DIVARICATA* (*DIV*), all codifying for transcription factors (Luo *et al.*, 1996; Almeida *et al.*, 1997; Luo *et al.*, 1999; Galego and Almeida, 2002; Corley *et al.*, 2005).

### 1.3.1.1 *CYCLOIDEA* and *DICHOTOMA*

*CYCLOIDEA* and *DICHOTOMA* are members of the TCP family of transcription factors (Cubas *et al.*, 1999). The TCP genes are transcription factors characterized by the conserved TCP DNA binding domain (plant specific) that adopts a *basic-helix-turn-helix* (bHLH) conformation. TCP genes appear to be specially involved in cellular and plant growth regulation (Cubas *et al.*, 1999; Kosugi and Ohashi, 2002).

In *A. majus*, *CYC* loss of function mutants (*cyc*) have a strong phenotypic effect (figure 6b), with partial loss of the dorsal identity, lateral petal ventralisation and one petal and stamen gain when compared to the *wild type* (figure 6a). Also the remaining dorsal stamen is de-repressed resembling a lateral stamen. *CYC* is necessary to confer dorsal identity and this assumption is supported by the *backpetals* semidominant phenotype. In the *backpetals* mutant, *CYC* is ectopically expressed in the lateral and ventral domain of the flower. This mutant flower has a dorsalised phenotype where the

lateral and ventral petals become mirror images of the lateral half of the dorsal petal (Luo *et al.* 1999).

Together with its paralogous *DICH*, *CYC* is expressed in the meristem dorsal domain. mRNA *in situ* hybridization showed that in the initial stage of flower development, *CYC* is transcribed dorsally in floral meristems. As development of the flower progresses, *CYC* expression becomes restricted to the dorsal petals and to the dorsal staminode (Luo *et al.*, 1999). *CYC* restricts cellular proliferation in the first stages of flower development and in later stages, *CYC* promotes petal lobular growth and repress stamen development (Luo *et al.*, 1996). The ability of *CYC* to enhance or inhibit cellular proliferation depends on *CYC* effect in cellular cycle genes like *CYCLIN D3B* and *HISTONE4* (Gaudin *et al.*, 2000). According to Gaudin *et al.* (2000) *CYC* could be acting as both promotor and repressor of the same cellular cycle regulator or binding to different co-regulators depending on the floral stage development. *DICH* expression is restricted to the dorsal region of the flower meristem, promoting internal asymmetry in the dorsal petals (figure 6a). *DICH* mutation has a much weaker phenotype compared to *cyc*, resulting in the loss of asymmetry in dorsal petals (figure 6c). In *cyc/dich*, the corolla is completely ventralised, with gain of one stamen and one petal (figure 6d) (Luo *et al.*, 1999). *CYC* and *DICH* double mutants produce radially symmetric, completely ventralised flowers which made Luo *et al.* (1999) suggest that *CYC* and *DICH* could be working in an redundant way contributing in different degree to dorsal identity of *A. majus* flower. Hileman and Baum (2003) suggested that *CYC* and *DICH* are the result of a unique duplication event that occurred before the Antirrhinae species radiation. *CYC* and *DICH* functional divergence (66% amino acid identity) could have been due to the accumulation of mutations on *CYC*, *DICH* lineage or in both. The most plausible hypothesis is that *CYC/DICH* ancestor duplicated with both copies undergoing sub-functionalization allowing the retention of both copies in the genome (He and Zhang, 2005).

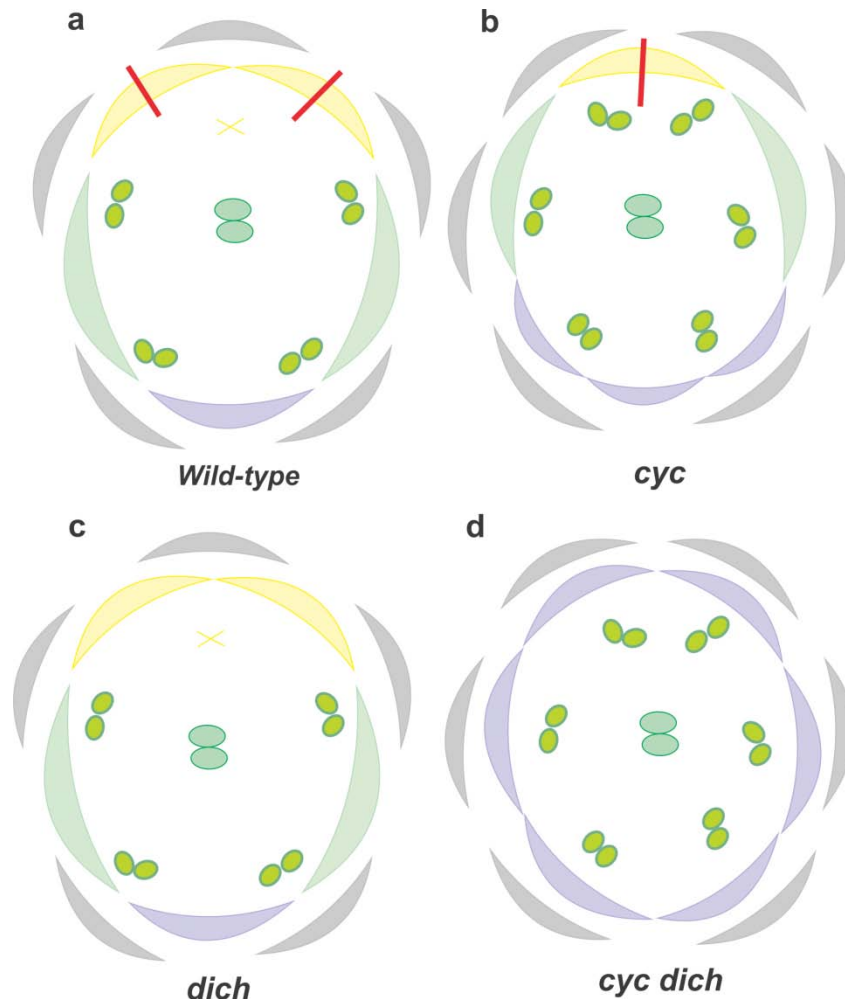


**Figure 6** – *A. majus* floral organ diagram showing phenotypic differences between (a) wild type and (b) *cyc*; (c) *dich*; and (d) *cyc/dich*. Purple colour represents ventral petals, green lateral petals and yellow dorsal petals. X represents the staminode. Grey colour depicts sepals and the red line internal petal asymmetry.

The partial ventralisation of the flower in the *cyc* mutant, together with the *backpetal* mutant phenotype, lead to the assumption that, during flower development, *CYC* might be repressing the genes responsible for ventral identity.

### 1.3.1.2 *RADIALIS*

*RADIALIS* (*RAD*), like *CYC* and *DICH*, promotes dorsal identity, with *rad* mutant flowers giving very similar phenotypes to *cyc*. Mutant flowers with loss of function *rad* have reduced dorsoventral asymmetry and are partially ventralised (Carpenter and Coen, 1990) (figure 7b): the lateral petals and the lower half of the dorsal petals are completely ventralised and the dorsal half of the dorsal petal retains some

lateral identity. The staminode is a bit longer than in the wild type. The number of petals and stamens is similar to wild type (Corley *et al.*, 2005).

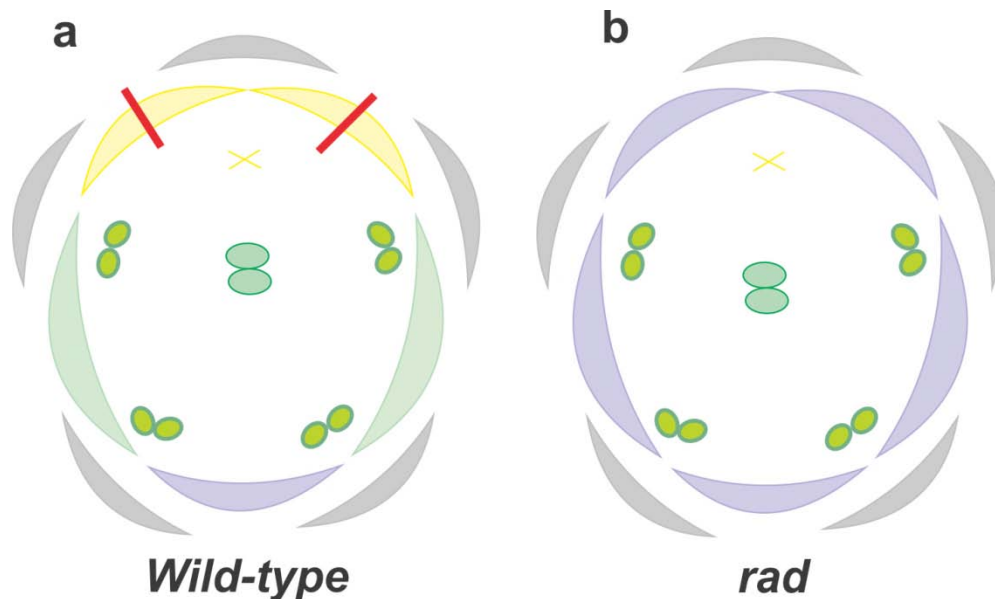


**Figure 7** - *A. majus* floral organ diagram showing phenotypic differences between (a) wild type and (b) *rad*. Purple colour represents ventral petals, green lateral petals and yellow dorsal petals. X represents the staminode. Grey colour depicts sepals and the red line internal petal asymmetry.

mRNA *in situ* hybridization demonstrated that *RAD*, similarly to *CYC* and *DICH*, is expressed dorsally in the flower meristem. Interestingly *RAD* expression is not only delayed relative to *CYC* and *DICH*, but also is absent from *cyc dich* indicating that *RAD* is genetically downstream of *CYC* and *DICH*. Accordingly, Costa *et al.* (2005) proved that the *RAD* promoter and intron contain *CYC*-binding sites and that *RAD* expression can be up-regulated by *CYC in vivo*.

The role of *RAD* in the establishment of flower dorsoventral asymmetry in *A. majus* is still unclear. Similar to the *cyc* mutants, *rad* mutant flowers exhibit partial ventralisation. This fact suggests that *RAD* is mediating *CYC* effects by antagonizing the genes responsible for ventral identity of the flower meristem.

### 1.3.1.3 *DIVARICATA*

*DIVARICATA* (*DIV*) is also a gene that has been associated with the establishment of dorsoventral asymmetry in the *A. majus* flower (Galego and Almeida, 2002). In loss of function *div* mutants the ventral petal adopts a lateral identity. Also,

regions of the lateral petals are affected differently: the dorsal-most and central regions of the lateral petals are unaffected whereas the ventral-most region becomes more similar to the central region of the lateral petal (figure 8b) (Galego and Almeida, 2002). Dorsal petals are unaffected in *div* mutants and stamens develop as the *wild type* (figure 8a).

The lateralisation of *div* mutant phenotype together with the fact that the *cyc:dich:div* triple mutant origins radially lateralized flowers suggest that *DIV* is responsible for establishing petal ventral identity (Galego and Almeida, 2002). It has been proposed that *DIV* establishes ventral identity by interaction with class B floral homeotic genes in order to control downstream genes involved in differentiation and cellular proliferation (Almeida *et al.*, 1997; Perez-Rodriguez *et al.*, 2005).

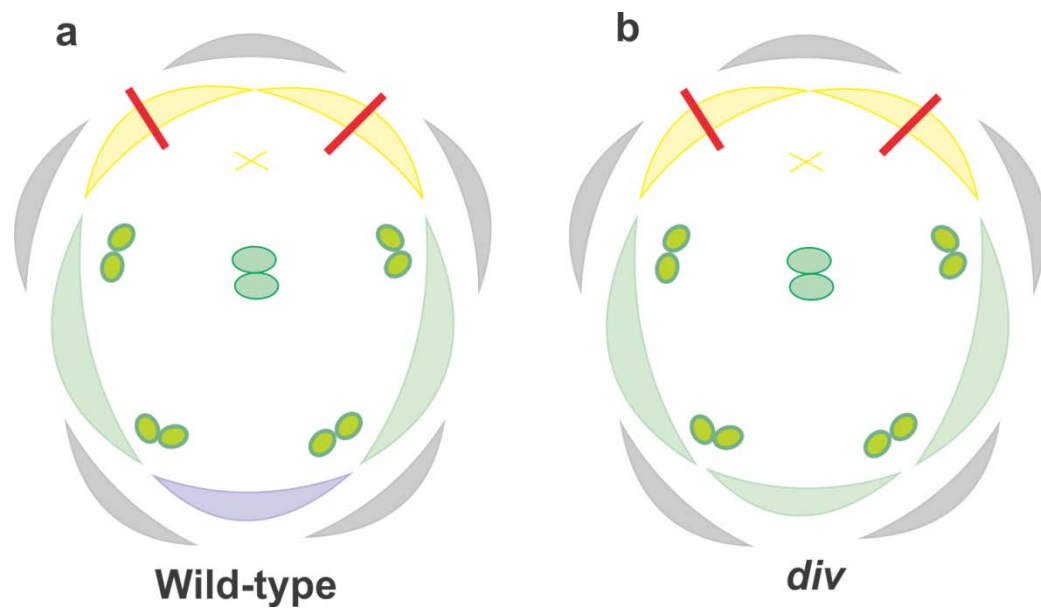


**Figure 8** - *A. majus* floral organ diagram showing phenotypic differences between (a) wild type and (b) *div*. Purple colour represents ventral petals, green lateral petals and yellow dorsal petals. X represents the staminode. Grey colour depicts sepals and the red line internal petal asymmetry.

In the early stages of flower development, *DIV* is expressed in all floral organs regardless of their position along the flower dorsoventral axis. However, its phenotypical affect is only observed in the ventral petal. This suggests that the *DIV* gene product might be post-transcriptionally regulated, probably through the downstream effects of dorsal identity genes (Galego and Almeida, 2002). The first major role of *DIV* is to

increase lateral and ventral petal growth (Galego and Almeida, 2002). In later stages, *DIV* transcripts are observed in the inner epidermal cell layer of the ventral and lateral petals in the region of the petal folds. However, weaker expression is found throughout the dorsal petals. So, in later stages *DIV* activity results in the establishment of a clear difference between lateral and ventral petals together with the increase in lateral petal asymmetry. Together with the fact that *cyc:dich* double mutant has a complete ventralised phenotype it was proposed that somehow *CYC* and *DICH* antagonise *DIV* in the dorsal and part of lateral region of the floral meristem (Galego and Almeida, 2002). One possible explanation for this behaviour would be that *RAD* is mediating the antagonising action of *CYC* over *DIV*. Interestingly, *RAD* and *DIV* code for similar MYB transcription factors which might suggest competition for the same protein or DNA targets.

### **1.3.2 MYB family of transcription factors**

MYB transcription factors are broadly distributed throughout eukaryotes (Yanhui *et al.*, 2006) and have been involved in essential cellular functions such as proliferation and differentiation (Weston, 1999). Jiang *et al.* (2004) admit a high degree of ancestry for the MYB family in plants. The same authors propose that a MYB gene amplification occurred just before monocots and dicots divergence, which lead to the high number of MYB copies present in many plant species. Romero *et al.* (1998) suggested that, in plants, transcription control by the MYB family of transcription factors is particular important, being involved, among others, in circadian clock regulation (Borello *et al.*, 1993), phosphorus deficit response (Rubio *et al.*, 2001), secondary metabolism (Paz-Ares *et al.*, 1987), light and hormonal signalling pathways (Ballesteros *et al.*, 2001), seed and floral meristem development (Schmitz *et al.*, 2002), cellular morphogenesis (Higginson *et al.*, 2003) and cell cycle regulation (Araki *et al.*, 2004).

A MYB protein is formed by one to four repeats of the MYB domain that are referred as R1, R2, R3 and R1/2 (from N-terminus to C-terminus of the protein). A canonical MYB domain has approximately 52 amino acid (Paz-Ares *et al.*, 1987) with three tryptophan residues regularly spaced 18-20 amino acid apart that form an hydrophobic agglomerate that recognizes a specific DNA sequence (Ogata *et al.*, 1995)



(figure 9). The tertiary structure of a MYB domain has three  $\alpha$ -helix assuming a *helix-helix-turn-helix* conformation. The second and third helix intercalate with the major groove of the target DNA (Ogata *et al.*, 1994) (figure 9 and 10).

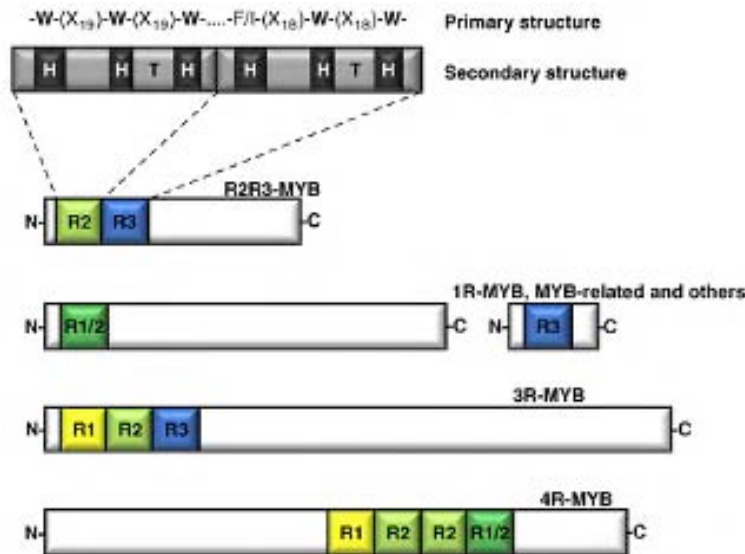


**Figure 9** - MYB transcription factor classes. Illustration showing different plant MYB protein classes, depending on the number of adjacent MYB repeats (R). The primary and secondary structures of a typical R2R3-MYB are indicated. H, helix; T, turn; W, tryptophan; X, amino acid (X). Adapted from Dubos *et al.*, 2010.

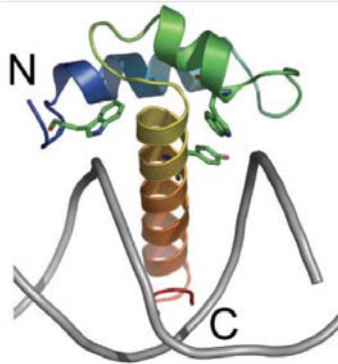


**Figure 10** - Tertiary structure of a MYB domain (helix I, II and III). The MYB protein is shown docked onto a double-stranded DNA fragment. Adapted from Stevenson *et al.* (2006).

MYB proteins can be divided into different classes depending on the number of adjacent MYB repeats (one, two, three or four; figure 9). The smallest class is the 4R-MYB group, whose members contain four R1/R2-like repeats (Dubos *et al.*, 2010). The second class contains R1R2R3-type MYB proteins. Genes encoding R1R2R3-MYB proteins have been found in most eukaryotic genomes, representing a conserved gene

class with roles, despite divergent, in cell cycle control (Ito, 2005). The third heterogeneous class comprises proteins with a single or a partial MYB repeat, collectively designated MYB-like proteins. The majority of plant MYB genes encode proteins of the R2R3-MYB class, which are thought to have evolved from an R1R2R3-MYB gene ancestor, by the loss of the sequences encoding the R1 repeat (Braun and Grotewald, 1999). However, the evolution of R1R2R3-MYB genes from R2R3-MYB genes by the gain of the R1 repeat through an ancient intragenic duplication has also been proposed (Jiang *et al.*, 2004). R2R3-MYB transcription factors have a modular structure, with an N-terminus DNA-binding domain (the MYB domain) and a *trans*-activation or repression domain usually located at the C-terminus (Stracke *et al.*, 2001).

The C-terminus domain of MYB proteins is very variable. This variability could be translated in different protein-protein or protein-DNA interactions, resulting in different transcriptional effects (Jaffé *et al.*, 2007). There is evidence that two MYB domains in the same protein could have different functions and this situation could be correlated to the high proportion of non-conserved amino acids surrounding the DNA-binding domain or alterations in the conserved amino acids of the DNA-binding domain (Rose *et al.*, 1999).

Proteins with MYB repeats that do not have a perfectly conserved DNA-binding domain as the observed in the canonical MYB protein (Paz-Ares *et al.*, 1987) are called MYB-like proteins. In these MYB-like repeats one or more tryptophan residues may be replaced by another aromatic residue or by a similarly sized aliphatic residue (Corley *et al.*, 2005).

#### **1.3.2.1 RAD and DIV as MYB-like transcription factors**

*RAD* codes for a 93 amino acid protein with one single MYB-like repeat (Luo *et al.*, 1999; Corley *et al.*, 2005). *RAD* MYB-like domain has high similarity with the MYB repeat characteristic of the MYB-like/SANT family of transcription factors (Corley *et al.*, 2005). MYB-like/SANT transcription factors have been involved in DNA binding (Aasland *et al.*, 1996), and some proteins in this family were also involved in the chromatin remodelling process (Boyer *et al.*, 2005). Typically, single MYB-like/SANT proteins do not have a *trans*-activation domain downstream of the MYB-like

domain, which could mean that these protein could be mainly involved in transcription repression or protein-protein interactions (Boyer *et al.*, 2005). However, RAD has an incomplete CREB domain that is shared by RAD orthologs in *Arabidopsis* (Baxter *et al.*, 2007). In the animal kingdom, the CREB domain importance in transcription regulation is well established. According to Quinn (1999), the CREB constitutive activation domain interacts with the transcription factor TFIID through one or more of the TATA-binding protein-associated factors in order to control transcription. The importance of the incomplete CREB domain in RAD function is, however, still undetermined. RAD MYB-like/SANT domain is very similar to the one found in *LeFSM1* (Barg *et al.*, 2005). In tomato and *Arabidopsis* ectopic expression of *LeFSM1* results in severe developmental alterations manifested in retarded growth, and reduced apical dominance (Barg *et al.*, 2005). Similarly to *LeFMS1*, *RAD* is involved in the regulation of a evolutionary conserved developmental process, however, the importance of the MYB-like/SANT domain to RAD function remain unclear.

*DIV* is an R2R3MYB-like transcription factor with 307 amino acids (Galego and Almeida, 2002). *DIV* protein is distinctively different from the typical R2R3MYB proteins not only because of the change in the conserved DNA-binding domains residues but also due to a longer linker between the R2 and R3 MYB-like domains (Galego and Almeida, 2002; Howarth and Donoghue, 2009). The two MYB-like domains of *DIV* have distinct functional characteristics: the first domain belongs to the MYB-like/SANT family, whereas the second belongs to MYB-like SHAQKYF class.. The second MYB-like domain of *DIV* has great similarity to the single MYB-like domains of the proteins *CCA1* and *LHY* (Galego and Almeida, 2002). *CCA1* and *LHY* are R3MYB-like transcription factors involved in DNA-binding and transcription activation (Schaffer *et al.*, 1998; Wang and Tobin, 1998). Accordingly, *DIV* might be controlling transcription through the second MYB-like domain. The main feature of the SHAQKYF class is the highly conserved SHAQKYF motif, in the predicted third  $\alpha$ -helix that could be essential in the transcriptional control activity (Schaffer *et al.*, 1998).

*DIV* has significant sequence and structure similarity with *LeMYB1* (Rose *et al.*, 1999; Galego and Almeida, 2002), a transcriptional activator that Rose *et al.* (1999) identified as the first cloned transcription factor able to bind to the I-box DNA sequence

(GATAA) described by Giuliano *et al.* (1988) as the binding sequence of I-box transcription factors. Similar to *DIV*, *LeMYB1* has two MYB-like domains, but only the second MYB-like repeat is involved in DNA transcriptional control (Rose *et al.*, 1999). It is possible that the first MYB-like domain of *DIV*, similar to the first MYB-like repeat of *LeMYB1*, is not involved in transcription control, but functionally involved in protein-protein interactions as suggested for MYB-like/SANT domains by Boyer *et al.* (2005).

Importantly the MYB-like/SANT domain of *DIV* has a great similarity with the MYB-like/SANT domain of *RAD*, which allowed Corley *et al.* (2005) to infer that *RAD* might be resultant from an ancestral similar to *DIV* following a duplication event and posterior loss of the second MYB-like domain. The molecular similarity between the first MYB-like domain of *DIV* and the MYB-like domain of *RAD* suggest that *DIV* and *RAD* could be targeting the same genes or proteins (Corley *et al.*, 2005).

### **1.3.3 A model for Genetic Regulation of Flower Asymmetry**

The lateralised flower phenotype of *cyc:dich:div* triple mutant indicate that lateral identity can be considered a neutral state for petals. *DIV* is responsible for ventral petal identity, and *DIV* function might be suppressed in the dorsal and part of the lateral domain possibly due to *CYC* and *DICH* activity (figure 11) (Galego and Almeida, 2002). As well as antagonizing *DIV* function in the dorsal and lateral petals, *CYC* and *DICH* are responsible for dorsal petal identity (Luo *et al.*, 1999). *CYC* and *DICH* inhibitory action over *DIV* appears to be partially mediated by *RAD*. *RAD* is genetically downstream of *CYC* and *DICH* and is also required for dorsal identity (Corley *et al.*, 2005). However, *CYC* and *DICH* can influence flower asymmetry in a *RAD* independent way because *CYC* and *DICH* function in the dorsal staminoide and dorsal petals lobules do not disappear in loss of function *rad* mutants (Corley *et al.*, 2005). However, it is likely that other target of *CYC* is responsible for dorsal petal specification because neither *rad* single mutants nor *dich rad* double mutants are radially symmetric, whereas *cyc rad* double mutants are (Corley *et al.*, 2005). Nevertheless, it appears that the *CYC* and *DICH* major effects on flower symmetry are mediated by *RAD*. Neither *CYC* or *DICH*, or its downstream target *RAD*, are expressed in the lateral domain (Luo *et al.*, 1996; Luo

*et al.*, 1999; Corley *et al.*, 2005). However, the lateral petals do not have a ventral phenotype as expected by the ubiquitous expression of *DIV* (Galego and Almeida, 2002), so *RAD* must be influencing the lateral petals phenotype in a non-autonomous way possibly by an intercellular transport of *RAD* gene product or protein to the lateral domain (Corley *et al.*, 2005), similar to the non-cell autonomous transport of *DEFICIENS* (*DEF*) and *GLOBOSA* (*GLO*) observed in *Antirrhinum* (Schwarz-Sommer *et al.*, 1992; Perbal *et al.*, 1996).

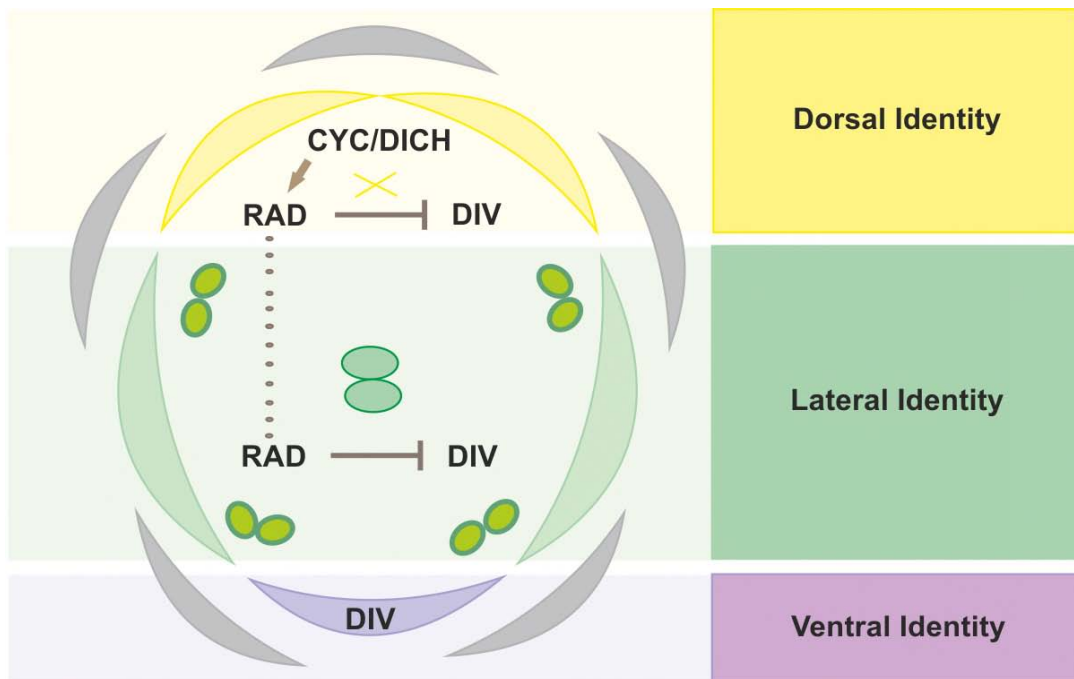


**Figure 11** – Model showing the genetic interactions underlying the establishment of zygomorphy in *A. majus*. *CYC* and *DICH* expression in the dorsal dominion (yellow) leads to *RAD* activation (brown arrow). *RAD* inhibits *DIV* activity in dorsal and lateral regions of the flower.

As previously mentioned, *DIV* is expressed in the entire flower meristem, however, its function is restricted to the ventral domain possibly due to *RAD* function. Thus, *DIV* could be negatively regulated by *RAD* through post-transcriptional mechanisms in the dorsal and lateral domains by direct or indirect competition by competing for the same DNA or protein targets (Galego and Almeida, 2002; Corley *et al.*, 2005). The high similarity between the MYB-like/SANT domain of *RAD* and the MYB-like/SANT domain of *DIV* lead to the hypothesis that *RAD* could be targeting the *DIV*-binding sites in the promoters of *DIV* target genes. This would prevent *DIV* from

DNA-binding and transcription activation (figure 12a). Accordingly, RAD, with no known activation domain, could therefore function as a transcriptional repressor. Moyano *et al.* (1996) described a similar behaviour in *A. majus*. The authors showed that two *A. majus* MYB transcription factors (AmMYB305 e AmMYB340) bind to the same gene promoter using the same *cis*-element having, however, distinct transcriptional activity.

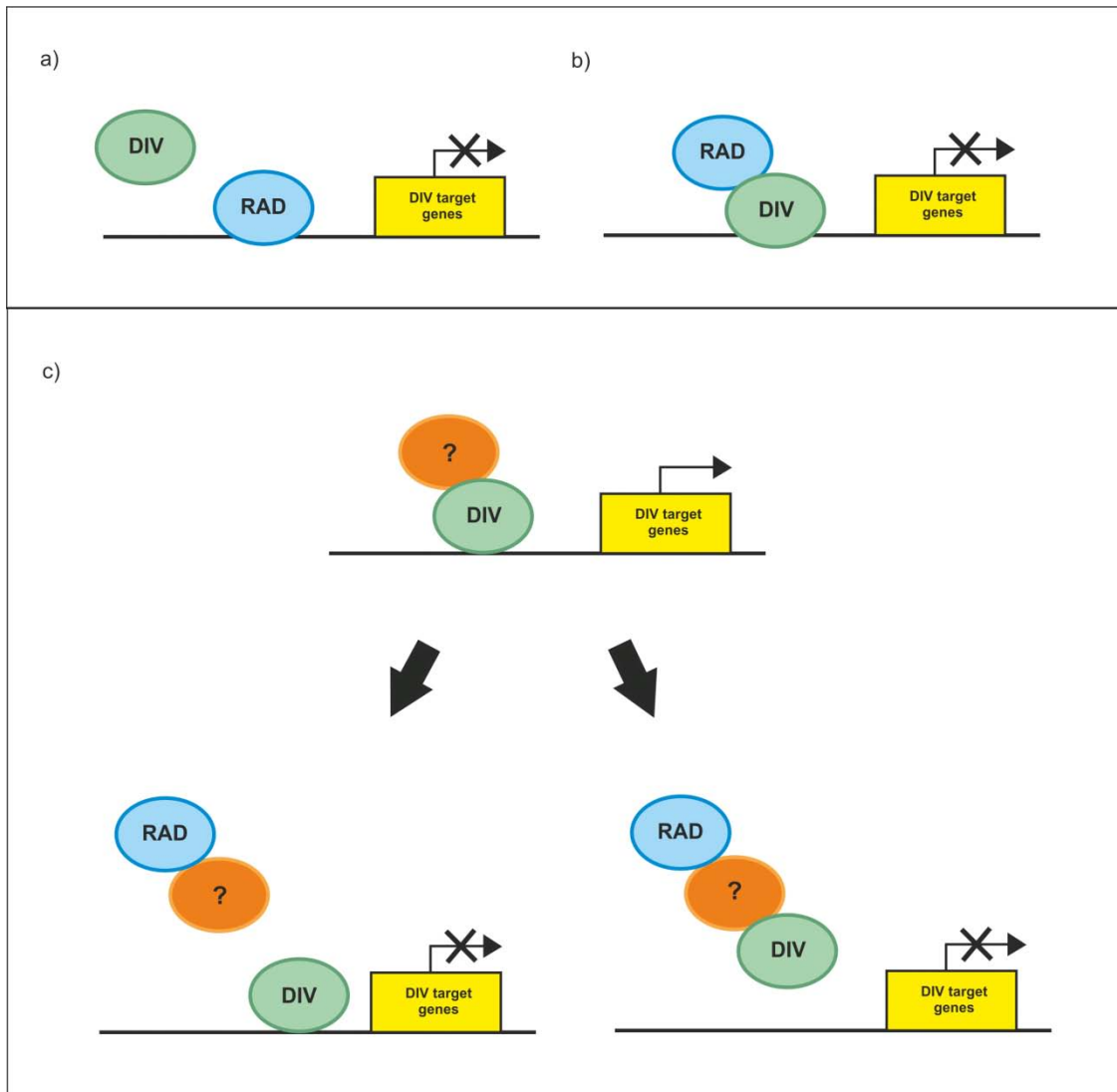


**Figure 12** –Mechanisms of molecular antagonism of RAD over DIV. **a)** RAD could bind to the DNA *cis*-element of DIV; **b)** RAD could form a transcriptional complex with DIV altering DIV transcriptional activity; **c)** To be transcriptional activity, DIV might need a interactor partner, and in this case RAD could be successfully rescuing the interactor partner or DIV, the unknown partner and RAD could form a multi-protein complex that inhibits transcription.

Many proteins mediate their function through the formation of both stable or transient protein complexes (Carrol *et al.*, 2001) and often, the same protein may interact

with various partners in response to different stimuli or at different developmental stages (Hsieh *et al.*, 2003). Taking in consideration the fact that the MYB-like/SANT domain could be involved in the establishment of protein-protein interactions (Boyer *et al.*, 2005), it is possible that RAD might bind directly to DIV preventing its transcriptional activity (figure 12b). It is also possible that DIV might need one or more interacting partners to control transcription (figure 12c), and in this particular case RAD might be inhibiting DIV activity by rescuing its interacting partners. A similar antagonizing pattern is observed in the determination of epidermal cell fate in *Arabidopsis* where the assembling of a transcriptional complex is inhibited by the antagonisation between two MYB proteins. CAPRICE (CPC), TRIPTYCHON (TRY), ENHANCER OF TRY AND CPC1 (ETC1), ETC2 and ETC3 (Simon *et al.*, 2007) are small proteins with a single MYB domain (Simon *et al.*, 2007; Tominaga *et al.*, 2007), that act redundantly as negative regulators in the determination of epidermal cell fate by competition with R2R3-MYB proteins, namely *GLABRA1* (*GL1*) and *WEREWOLF* (*WER*) (Esch *et al.*, 2004; Kirik *et al.*, 2004; Simon *et al.*, 2007).

#### **1.3.4 Genetic basis for flower asymmetry among other *taxa***

Flower asymmetry appears to be controlled by a group of phylogenetic related genes in different *taxa* suggesting a common genetic background for flower asymmetry evolution (Feng *et al.*, 2006). Correspondence between altered expression patterns of genes and change in flower symmetry have been found in some Angiosperm *taxa* phylogenetically distant from *A. majus*, *Mohavea confertiflora* (Plantaginaceae) (Hileman *et al.* 2003); *Chirita hetrotricha* (Gesneriaceae) (Gao *et al.*, 2008), *Bournea* (Gesnereaceae) (Zhou *et al.* 2008), *Lotus japonica* (Fabaceae) (Feng *et al.*, 2006) and *Iberis amara* (Brassicaceae) (Busch and Zachgo, 2007). There is abundant data about *CYC* homologous in *taxa* across the Asteridae and Rosids, however, there is yet little on *RAD*- and *DIV*-like homologues and their putative conserved role in the establishment of the asymmetric dorsoventral pattern of the flower.

Preston *et al.* (2009) work on *Veronica montana* and *Gratiola officinalis* confirmed the conserved ability of *CYC*-like proteins to activate *RAD*-like genes in species belonging to the Veronicaceae family. According to this study, *VmRAD* and

*VmCYC* were expressed in the dorsal region of the flower, becoming detected only in the dorsal petal at late stages of development. Similarly *GoRAD* and *GoCYC* were expressed in the dorsal petals and dorsal staminoide during early to late stages of *G. officinalis* flower development. This is despite an apparent lack of a *CYC*-like binding site in the first intron of *VmRAD*, which is disrupted in several of the well characterized *A. majus rad* mutants (Corley et al., 2005). However, according to the same authors it is unknown whether there are *CYC*-like binding sites upstream of the *VmRAD* coding region, as have been found for *A. majus RAD* (Costa et al., 2005).

The ability of *CYC*-like genes to activate *RAD*-like genes appears to be not only conserved in the Veronicaceae but also in other families of the Lamiales clade. In the Gesneraceae family, work in *Bournea leyophylla* and *Chirita heterotricha* shed some light about the conservation of the genetic mechanisms that support floral dorsoventral asymmetry across the Lamiales (Zhou et al., 2008; Yang et al. 2010).

Yang et al. (2010) suggested that the floral zygomorphy in *Chirita heterotricha* might have been established through the co-option of the *RAD*-like gene into the regulatory network controlled by *CYC*-like genes. The authors found that an appropriate *CYC*-like binding site is present in the *RAD*-like promoter. *B. leyophylla* exhibits actinomorphic flowers at anthesis, however, its very short corolla tube with five filaments adnate to the corolla and the adaxial petals somewhat smaller than others lead Zhou et al. (2008) to suggest evolution from a zygomorphic ancestor (figure 13). The same authors have identified in *B. leiophylla* *CYC*, *RAD* and *DIV* homologues that control flower symmetry. *BICYC1* and *BIRAD* are expressed in the dorsal region of the early meristem but are down regulated during the late stages, which should be responsible for the origin of the derived actinomorphy (Zhou et al., 2008). Interestingly, similarly to *A. majus DIV*, two *DIV* copies, *BIDIV1* and *BIDIV2* were expressed in the entire floral meristem (Zhou et al., 2008). This could mean that the regulatory mechanism that controls the dorsoventral asymmetry of the *A. majus* flower might be conserved in at least some families belonging to the Lamiales. However, there is little published data suggesting *DIV* function outside the Lamiales.

A recent study by Howarth and Donoghue (2009) provided the first phylogenetic analysis of *DIV*-like genes in Dipsicales. Data showed that *DIV* and its homologues in



Dipsicales are the result of a duplication event that occurred in parallel with *CYC*-like genes, their potential interacting partner. The same authors emphasised the fact that *DIV* and *CYC* maintain the same number of copies in eudicots. However, the authors were not clear whether the expression pattern of *DIV* is conserved in *DIV-like* genes and if there is correlation between expression profiles of *DIV-like* genes and *CYC-like* genes and respective shifts in flower symmetry.

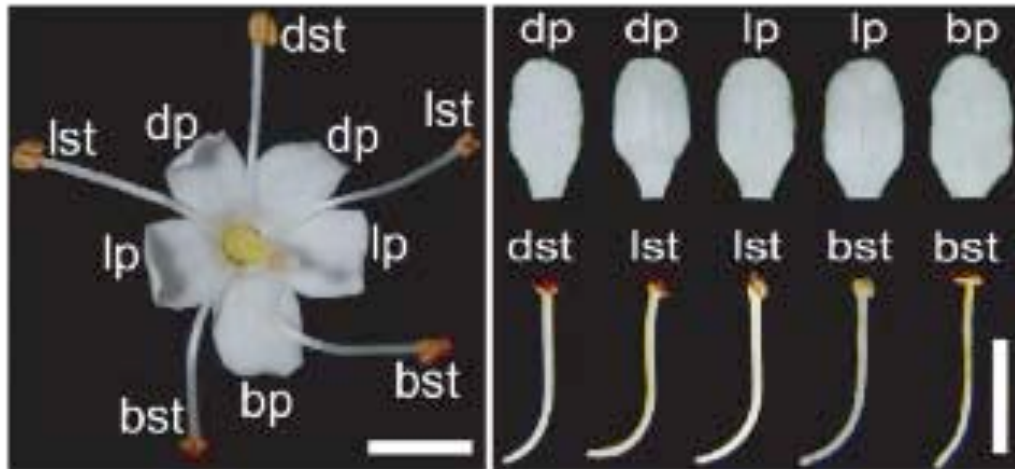


**Figure 13-** Mature whole and dissected flowers of *Bournea leiophylla*. Actinomorphy was observed in mature *Bournea leiophylla* flowers with nearly identical adaxial, lateral and abaxial petals and stamens. bp, abaxial (ventral) petal; bst, abaxial (ventral) stamen; dp, adaxial (dorsal) petal; dst, adaxial (dorsal) stamen; lp, lateral petal; lst, lateral stamen. Bar: 5 mm. Adapted from Zhou *et al.* (2008).

Outside the Asteridae, in two Fabales species, *Lotus japonicus* (Feng *et al.*, 2006) and *Pisum sativum* (Wang *et al.*, 2008), gene expression and functional analyses both implicate *CYC*-like genes in the control of bilateral flower symmetry. In these species, *CYC*-like gene expression is restricted to dorsal or dorsal plus lateral regions of developing flowers, similar to *CYC* expression in *A. majus*. Within the Brassicales, the expression of a *CYC*-like gene seems to be responsible for the bilateral petal symmetry of *Iberis amara*, which deviates from the radial petal symmetry in *Arabidopsis* (Busch and Zachgo, 2007). Also, Zhang *et al.* (2010) described in the Malpighiales, a *CYC*-like gene with a conserved pattern of dorsal gene expression in two distantly related neotropical species, *Byrsonima crassifolia* and *Janusia guaranitica*. These results clearly show that the ability of *CYC*-like genes to control flower asymmetry appears to be

conserved in the core eudicots. However, in this species no data is available confirming the activation of *RAD*-like genes to confer dorsoventral identity to the flower.

Yang *et al.* (1999) described two big large groups of *RAD*-like genes in *Arabidopsis* and *Antirrhinum* that were probably derived from an ancestral gene duplication event following Rosids/Asterids divergence 112-156 million years ago. Costa *et al.* (2005) stated that *CYC* is unable to activate *RAD* orthologues in *Arabidopsis*, however, it is unknown whether the *Arabidopsis* *CYC*-like (*TCPI*) can turn on *Arabidopsis* *RAD*-like genes. Baxter *et al.* (2007) work revealed that *RAD*-like genes are not expressed dorsoventrally in *Arabidopsis*, suggesting that a *cis* or *trans* diversification event occurred that lead to the *RAD* co-option to establish dorsoventral asymmetry in the Asteridae. However, another explanation would be that *Arabidopsis* and its relatives, with radial, four-merous flowers, have lost a pathway that otherwise span the core eudicots (Howarth and Donoghue, 2009).

#### **1.4 Aims of this study**

The main aim of this study is to gain understanding on the molecular mechanisms underlying the antagonizing action of *RAD* over *DIV* function.

In a first approach, *RAD* and *DIV* recombinant proteins will be obtained and used in a DNA-binding assay. This assay will be useful to understand if *RAD* is inhibiting *DIV* by binding to the DNA target of *DIV* or by binding directly to *DIV*.

Recently, to understand if an interactive partner mediates the molecular antagonism between *RAD* and *DIV*, a yeast two-hybrid screening was performed using *RAD* as bait. Two new proteins were identified as *RAD* interactors, and named *RAD* INTERACTING PROTEIN1 (*RIP1*) and *RAD* INTERACTING PROTEIN2 (*RIP2*). Interestingly, both proteins interact with *DIV*.

The second aim of this study is to characterise the interaction of *RIP1* and *RIP2* with *RAD* and *DIV* and to evaluate if this newly identified proteins are responsible for the molecular antagonism between *RAD* and *DIV*. A quantitative yeast two-hybrid assay will be performed to measure the interaction strength of each pair of interactors, and the sub-cellular localisation of *RAD*, *DIV*, *RIP1* and *RIP2* proteins will be identified by

fluorescence microscopy, to determine whether the proteins are able to interact in the same cellular compartment.

The third objective of this study is to develop experimental procedures that will enable further characterisation of RIP1 and RIP2 and their putative role in the molecular antagonism between RAD and DIV. These assays include: the ectopic expression of RIP1 and RIP2 in *Arabidopsis thaliana*; the use of DNA-binding assays to determine if the RIP1 and RIP2 are able to interact with the DNA-target of DIV or to form a multi-protein complex with DIV or/and RAD; and a bimolecular fluorescent complementation assay to further characterize the interaction between RIP1, RIP2, RAD and DIV *in planta*.

## **2. Material and Methods**

### **2.1 Biological material**

#### **2.1.1 Plant material**

##### **2.1.1.1 *Arabidopsis thaliana***

*Arabidopsis thaliana* ecotype Columbia (Col-0) seeds were obtained from public seed banks, and stored in the dark at room temperature. Seeds (20-200 *per tube*) were stratified by water immersion in the dark for 4°C for 3-5 days in order to break dormancy and synchronise germination. The seeds were surfaced sterilised in a horizontal flow laminar chamber (*BBH4 BRAUN Horizontal*) by successive incubations with 1 mL 70% (v/v) ethanol during 5 min, 1 mL commercial 20% (v/v) bleach with 0.1% (v/v) *Tween* for 10 min, followed by three washes with 1 mL sterilised water and two 1 mL 100% (v/v) ethanol. Between incubations, seeds were resuspended by vortex agitation and recovered by centrifugation (10,000g during 1 min). Seeds were sown in Murashige and Skoog agar medium (MS medium, 4.209 mg L<sup>-1</sup>, 1.5% (w/v) sucrose, 1.2% (w/v) plant agar, the pH was equilibrated to 5.7 with KOH) (Murashige and Skoog, 1962) and were incubated vertically under long day conditions (16 hours light / 8 hours dark) at 20°C in controlled environmental growth rooms, with light intensity of 40 μE m<sup>-2</sup> s<sup>-1</sup>. Approximately 10 days after sowing, plantules were transferred to pots containing a 4:1 (v:v) mixture of turf rich soil and vermiculite. The pots were watered and covered with cling film in order to maintain humidity for up to one week after the transplant. Following this period pots were watered every day.

##### **2.1.1.2 *Nicotiana benthamiana***

Material from *N. benthamiana* was used for the transient transformation assay. *N. benthamiana* seeds were stored in the dark at room temperature. *N. benthamiana* seeds (20-30) were sown in pots containing a 4:1 (v:v) mixture of turf rich soil and vermiculite. Plants were grown in a growth chamber at 22°C with 70% relative humidity under a 16 hours light/8 hours dark photoperiod for about 1–1.5 months before the transient transformation assay.

## **2.1.2 Bacterial material**

### **2.1.2.1 *Escherichia coli***

#### **2.1.2.1.1 XL1-Blue strain**

The *E. coli* strain XL1-Blue (*recA1 endA1 gyrA96 (nal<sup>R</sup>) thi-1 hsdR17 supE44 relA1 lac glnV44 F'[proAB<sup>+</sup>lacI<sup>q</sup>ZΔM15 Tn10]*) (Bullock *et al.*, 1987) was used for vector perpetuation and cloning procedures.

#### **2.1.2.1.2 BL21(DE3)pLysE strain**

The *E. coli* strain BL21(DE3)pLysE (*F<sup>-</sup> ompT hsdS<sub>B</sub> (r<sub>B</sub><sup>-</sup>, m<sub>B</sub><sup>-</sup>) dcm gal λ(DE3) pLysE, Cm<sup>r</sup>*) (Studier and Moffatt, 1986) was used for high-stringency heterologous protein expression.

#### **2.1.2.1.3 Preparation of *E. coli* competent cells**

*E. coli* cells were made competent for transformation procedures as follows: 5 ml Luria-Bertani medium (LB medium, 10 g L<sup>-1</sup> Bactotryptone; 5 g L<sup>-1</sup> Yeast extract and 10 g L<sup>-1</sup> NaCl) (Sambrook *et al.*, 1989) was inoculated with a single colony and incubated overnight at 37°C with vigorous shaking (200 rpm) with appropriate antibiotics. One flask containing 100 mL of LB medium was inoculated with 1 mL of the starter culture, and this was grown at 37°C until an OD<sub>600</sub> of about 0.25 was reached (approximately 3 hours after inoculation, depending on the strain). The cells were pelleted in four falcon tubes by centrifugation at 3,000 x g (4°C) for 10 minutes and the supernatant was discarded. Each pellet was carefully resuspended in 8 mL 0.1 M MgCl<sub>2</sub> (sterile and cold) and incubated on ice during 30 min. The cells were then pelleted, as described above, and gently resuspended in 2.5 mL TG salts (75 mM CaCl<sub>2</sub>; 6 mM MgCl<sub>2</sub>; 15% (v/v) glycerol; cold and sterile). Again cells were pelleted as described above, resuspended in 750 μL TG salts and kept on ice for 4-24 hours. 100 μL of cells were pipetted into pre-chilled eppendorfs, frozen in liquid nitrogen and stored at -80°C.

### **2.1.2.2 *Agrobacterium tumefaciens***

The *A. tumefaciens* strain EHA105 was used for *A. thaliana* and *N. benthamiana* permanent and transient transformation procedure, respectively. EHA105 is a derivative of EHA101 (C58 pTiBo542; T-region::aph) (Hood *et al.*, 1986).

#### **2.1.2.2.1 Preparation of *A. tumefaciens* competent cells**

*A. tumefaciens* EHA105 cells were made competent for transformation procedure as follow: a single colony of EHA105 was used to inoculate 100 mL LB medium supplemented with rifampicin ( $100 \mu\text{g mL}^{-1}$ ) and grown overnight at  $30^{\circ}\text{C}$  with vigorous shaking (200 rpm). When the culture reached an  $\text{OD}_{600}$  between 0.5-0.7, the cells were pelleted in four falcon tubes by centrifuging at  $4,000 \times g$  at  $4^{\circ}\text{C}$  for 5 minutes. The supernatant was discarded and the pellet gently resuspended in 25 mL cold 10% (v/v) glycerol. The bacterial solution was centrifuged as described above and the supernatant discarded. The pellet was resuspended in 12.5 mL cold 10% (v/v) glycerol and then centrifuged again under the same conditions. This step was repeated using 500  $\mu\text{L}$  of cold 10% (v/v) glycerol. Finally, the pellet was resuspended in 250  $\mu\text{L}$  of cold 10% (v/v) glycerol. 50  $\mu\text{L}$  of cells were dispensed into pre-chilled eppendorfs, frozen in liquid nitrogen and stored at  $-80^{\circ}\text{C}$ .

### **2.1.3 *Saccharomyces cerevisiae***

The *Saccharomyces cerevisiae* strain AH109 (*MATa trp1-901 leu2-3, 112 ura3-52 his3-200 gal4 $\Delta$  gal80 $\Delta$  LYS2::GAL1<sub>UAS</sub>-GAL1<sub>TATA</sub>-HIS3; GAL2<sub>UAS</sub>-GAL2<sub>TATA</sub>-ADE2; URA3::MEL1<sub>UAS</sub>-MEL1<sub>TATA</sub>-lacZ, MEL1*) was used in the Yeast-two-hybrid assays. The yeast strain AH109 contains distinct *ADE2*, *HIS3*, *lacZ*, and *MEL1* reporter genes, under the control of the GAL promoter, that are only expressed in the presence of the GAL4 reconstituted transcription factor.

Bacterial and *S. cerevisiae* strains were perpetuated as glycerol stocks for long-term storage. In the former case a 500  $\mu\text{L}$  aliquot from an inoculate LB culture was added to an equal volume of 80% (v/v) glycerol. In the latter case an 800  $\mu\text{L}$  aliquot from a culture was added to 200  $\mu\text{L}$  of 80% glycerol (v/v).

## **2.2 DNA Methods**

### **2.2.1 Bacterial Transformation**

#### **2.2.1.1 *E. coli***

An amount of 10 ng (5-10  $\mu\text{L}$ ) of circular DNA was added to 100  $\mu\text{L}$  of competent cells (as described in section 2.1.2.1.3) in an eppendorf tube and incubated on ice for 30 minutes. Cells were heat-shocked at 42°C for 45 seconds, returned to ice for 2 minutes and 900  $\mu\text{L}$  of LB was added to the tube. The cells were incubated at 37°C for 60 minutes with vigorous shaking (200 rpm). A volume of 100  $\mu\text{L}$  of the transformation mix was then spread onto LB-agar plates [LB medium, 1.5% (w/v) agar] containing the appropriate selection antibiotic. Plates were incubated overnight at 37°C.

#### **2.2.1.2 *A. tumefaciens***

An aliquot of thawed *A. tumefaciens* competent cells was added to a pre-chilled electroporation cuvette. A volume containing an amount of 10 ng was carefully added to the cuvette. An electric pulse was applied using the *Gene Pulser II* (Bio Rad) (field strength: 1.25 Kv  $\text{mm}^{-1}$ ; Capacitance: 25  $\mu\text{F}$ ; Resistance: 400  $\Omega$ ; Pulse Field: 8-12 ms). The mixture was transferred to an eppendorf tube with 1 mL LB broth and incubated 3 hours at 30°C with shaking (200 rpm). A volume of 10  $\mu\text{L}$  of the transformation mix was then spread onto LB-agar plates containing the appropriate selection antibiotics. Plates were incubated overnight at 30°C (Inoue *et al.*, 1990).

## **2.2.2 Isolation of plasmid DNA**

### **2.2.2.1 P1 P2 P3 method**

The P1 P2 P3 method was used to isolate plasmid DNA. A single bacterial colony was added to 10 mL LB medium (containing the appropriate antibiotic selection) and grown overnight with shaking (200 rpm) at 37°C. 1.5 mL of the night culture was added to an eppendorf tube and pelleted at 13,000 x g for 2 minutes. The supernatant was discarded and the step repeated two to three times. The bacterial pellet was completely resuspended in 250 µL of P1 solution (50 mM Tris-HCl pH 8; 10 mM EDTA; 100 µg ml<sup>-1</sup> RNase). A volume of 250 µl of P2 solution (0.2 M NaOH; 1% (w/v) SDS) was added, and the tube was gently inverted four to six times to mix the contents before incubating at room temperature for no more than 5 minutes (the solution became white and slurry). 350 µL of P3 solution (3 M KOAc pH 5.5) was added and the contents immediately mixed by inversion (four to six times). The mixture was centrifuged at 13,000 x g for 10 minutes. The supernatant was then transferred to a new eppendorf tube containing 700 µL isopropanol and incubated on ice for 15 minutes. The DNA was pelleted by centrifugation as described above for 30 minutes. The pellet was washed with 100-500 µL with ice cold 70% (v/v) ethanol and centrifuged for 10 minutes. The supernatant was removed, the pellet air-dried for 20 minutes and then resuspended in the desirable dH<sub>2</sub>O volume. The DNA was stored at -20°C.

### **2.2.2.2 Small-scale (mini) isolation of purified plasmid DNA**

The *High Pure Plasmid Isolation Kit* (Roche Applied Science) and protocol were used for small-scale isolation of plasmid DNA according to the manufacturer's instructions. This method was employed when highly pure plasmid DNA samples were required.

### **2.2.2.3 Estimation of DNA concentration**

DNA concentration was estimated by UV spectrophotometry at A<sub>260</sub> assuming that one unit of absorbance at 260 nm corresponds to 50 µg mL<sup>-1</sup> of DNA. Sample quality was established using the A<sub>260</sub>/A<sub>280</sub> (for RNA contamination) and A<sub>260</sub>/A<sub>280</sub> (for protein contamination) ratios. Pure samples were expected to have 1.8-2 for both ratios.



### 2.2.3 Agarose Gel Electrophoresis

DNA samples were resolved by electrophoretic separation when loaded onto a horizontal agarose gel submerged in 0.5 x TAE buffer (0.02 M Tris; 95 mM Acetic acid; 50 mM EDTA.Na<sub>2</sub>, pH 8) after addition of 6x loading buffer (10mM Tris-HCl pH 7.6; 60% (v/v) glycerol; 60 mM EDTA; 0.03% (w/v) bromophenol blue) (1x final concentration) to the DNA samples. *MassRuler DNA Ladder Mix* (Fermentas) was used as the molecular weight marker. PCR reactions with *GoTaq® Flexi* (Promega) were applied directly on the gel without addition of loading buffer. For PCR products and small-scale plasmid digests, 10mm thick gels were prepared using 1% (w/v) agarose. Gels were run at 100 V until the blue bromophenol migration reached two thirds of the gel.

Two methods were used to visualise the DNA on the gel: EtBr (0.1 µg mL<sup>-1</sup>) was added to the agarose gel prior to electrophoresis, or agarose gels were post-stained for approximately 30 minutes in *GelRed* solution (0.5 x *GelRed* Nucleic Acid Gel Stain (Biotium) in 0.1 M NaCl). DNA was visualised on a 610nm (short wave) UV trans-illuminator and photographed.

### 2.2.4 Polymerase chain reaction (PCR) methods for DNA fragment amplification

PCR on plasmid DNA was used to amplify inserts for cloning purposes or to confirm the presence and orientation of plasmid inserts. *Mastercycler Gradient* (Eppendorf) and the *MJ Mini Gradient Thermal Cycler* (Bio-Rad laboratories) were used in the PCR amplification procedures. Primer design followed the parameters suggested by Griffin and Griffin (1994), and were synthesised by *Metabion* (Table I for primer sequences). Specific *primers* were generally 20-30 nucleotides long, with non-complementary nucleotide sequences at both ends. The annealing temperature was calculated based on the Wallace rule (Suggs *et al.*, 1981). In order to maximise annealing strength primers were designed to end (3'end) with a G or C.

#### **2.2.4.1 Amplification of DNA fragments from plasmid templates**

PCR was carried out according to Sakai *et al.* (1988). Total reaction mixtures of 50  $\mu\text{L}$  were set up using water, 5x *GoTaq*<sup>®</sup> (Promega) [100 mM Tris-HCl pH 9; 500 mM KCl], 1 mM  $\text{MgCl}_2$ , 0.1  $\mu\text{M}$  of each forward and reverse *primers*, 0.2  $\mu\text{M}$  *dNTP mix* (Roche), 100 ng plasmid DNA and 0.5  $\mu\text{L}$  *Taq* (*Thermus aquaticus*) DNA Polymerase. The PCR was carried out with an initial 94°C denaturation step for 1 minute; 35 cycles of 94°C for 45 seconds, 55°C annealing for 45 seconds and 72°C extension for 1 minute (depending on the size of the amplification product); and one extension cycle at 72°C for 5 minutes. The samples were stored at 4°C or at -20°C.

#### **2.2.4.2 Amplification of DNA fragments from plasmid templates using *Pfu* DNA Polymerase**

For fragment amplification, using the *Pfu* DNA Polymerase with proofreading activity, total reaction mixtures of 50  $\mu\text{L}$  were set up water, 10x (1x final c.c.) *Pfu DNA Polymerase* buffer (Promega) (200 mM Tris-HCl pH 8.8, 100 mM KCl, 100 mM  $(\text{NH}_4)_2\text{SO}_4$ , 1.0% (v/v) Triton X-100 and 1 mg  $\text{mL}^{-1}$  nuclease-free BSA), 0.5  $\mu\text{M}$  of each forward and reverse *primers*, 0.2  $\mu\text{M}$  *dNTP mix* (Roche), 20 mM  $\text{MgSO}_4$ , 100 ng plasmid DNA and 1  $\mu\text{l}$  *Pfu* DNA Polymerase (*Pyrococcus furiosus* strain Vc1) (Promega). PCR was carried out with an initial 95°C denaturation step for 2 minutes; 35 cycles of 95°C for 45 seconds, 60°C annealing for 45 seconds and 72°C extension for 2-3 minutes (depending on the size of the amplification product); and one extension cycle at 72°C for 5 minutes. The samples were stored at 4°C or at -20°C.

#### **2.2.4.3 Amplification of DNA fragments for *Gateway*<sup>®</sup> system based cloning**

The amplification of DNA fragments for *Gateway*<sup>®</sup> system based cloning was carried out using the *Accuzyme Mix* (Bioline). To avoid using *primers* with a high number of non-homologous nucleotides two different sets of *primers* were used in two different PCR reactions. The first set was used to amplify the open reading frame and a

second step was used to introduce the complete *attB* sequence (adaptor primer *attB1* and *attB2*, table I). In the first PCR reaction, a total reaction mixture of 50  $\mu\text{L}$  were set up in a water, 0.2  $\mu\text{M}$  of each forward and reverse *primers*, 100 ng DNA template and 2x *Accuzyme Mix* (Bioline) (1x final c.c.). PCR was carried out with an initial 94°C denaturation step for 5 minutes; 35 cycles of 94°C for 30 seconds, 55°C annealing for 30 seconds and 72°C extension for 1-2 minutes (depending on the size of the amplified product); one extension cycle at 72°C for 3 minutes. The samples were stored at 4°C or at -20°C. In the second PCR reaction, total reaction mixtures of 50  $\mu\text{L}$  containing 0.6  $\mu\text{M}$  of each adaptor forward and reverse *primers*, 10  $\mu\text{L}$  of the PCR reaction and 2x *Accuzyme Mix* (Bioline) (1x final c.c.). PCR was carried out with an initial 94°C denaturation step for 5 minutes; 5 cycles of 94°C for 30 seconds, 45°C annealing for 30 seconds and 72°C extension for 1-2 minutes (depending on the size of the amplified product); 20 cycles of 94°C for 30 seconds, 55°C annealing for 30 seconds and 72°C extension for 1-2 minutes; one extension cycle at 72°C for 3 minutes. *attB* PCR products were purified as described in section 2.5.1.

#### **2.2.4.4 Colony PCR amplification**

Colony PCR amplification was used to confirm the presence and orientation of plasmid inserts transformed in *E.coli* or *A. tumefaciens*. A small amount of bacterial colony was used as DNA template for the PCR reaction. Total reaction mixtures of 50  $\mu\text{L}$  were set up in water, 5x *GoTaq*® (1x c.c) [100 mM Tris-HCl pH 9; 500 mM KCl] (Promega), 1 mM  $\text{MgCl}_2$ , 0.1  $\mu\text{M}$  of each forward and reverse *primers*, 0.2  $\mu\text{M}$  *dNTP mix* (Roche), 0.5  $\mu\text{L}$  *Taq* DNA Polymerase (*Thermus aquaticus*). PCR was carried out with an initial 94°C denaturation step for 10 minute; 35 cycles of 94°C for 50 seconds, 55°C annealing for 50 seconds and 72°C extension for 1-2 minutes (depending on the size of the amplified product); one extension cycle at 72°C for 5 minutes. The samples were stored at 4°C or -at 20°C.

For colony PCR of *A. tumefaciens*, the protocol was similar, however, colonies prior to the PCR reaction were incubated with 0.02 M NaOH during 10 min at 37°C.

## **2.2.5 DNA purification**

DNA purification methods were used to purify PCR products as well as to clean digested plasmids.

### **2.2.5.1 Wizard SV Gel and PCR Clean-Up System**

The *Wizard SV Gel and PCR Clean-Up System* (Promega) was used to extract and purify DNA from agarose gels and purify PCR products and was performed according to the manufacturer's instructions.

### **2.2.5.2 Phenol/Chloroform DNA extraction method**

A phenol/chloroform based purification method was used to remove protein contaminants from the DNA samples. An equal volume of chloroform was added to the DNA sample and mixed vigorously by vortexing. The tube was then centrifuged at 13000 x g for 10 minutes. The aqueous phase was transferred to a clean eppendorf tube and 100  $\mu$ L of isopropanol and 10  $\mu$ L of a 3 M sodium acetate solution were added to the mixture. The sample was mixed and left for one hour at -20°C and then centrifuged as above described for 15 minutes to precipitate the DNA. The supernatant was discarded and the pellet washed with 200  $\mu$ L of 70% (v/v) ethanol. The mixture was centrifuged as above described for 15 minutes and the supernatant discarded. This step was repeated pellet to remove small traces of ethanol. The pellet was air dried for 10 minutes and resuspended in the appropriate volume of water.

## **2.2.6 Restriction digestion with endonucleases**

### **2.2.6.1 Plasmid DNA**

To linearise plasmids for cloning procedures an amount of 1-5  $\mu$ g of plasmid DNA was digested at 37°C during one to five hours, in a total volume of 20  $\mu$ L, containing 5-10 units of restriction enzyme, 10x restriction buffer and 1  $\mu$ L of *Shrimp Alkaline Phosphatase* (SAP). The enzymes were heat inactivated at 65°C for 15 min and the mixture purified as described in section 2.2.5.1.

### **2.2.6.2 PCR product**

To digest PCR products for cloning procedures, 10-20 µg of amplified PCR product was digested at 37°C during 16 hours, in a total volume of 50 µL, containing 10 units of restriction enzyme and 1x restriction buffer. The enzymes were heat inactivated at 65°C for 15 min. and the mixture purified as described in section 2.2.5.1.

### **2.2.7 Ligation reaction**

To set up the ligation reactions, a molar ratio of purified insert:purified vector of 3:1 was used. The amounts of insert and vector used were calculated using the following formula:  $\text{insert (ng)} = \text{vector (ng)} \times \text{insert size (Kb)} \times 3 / \text{vector size (Kb)}$ . Total reaction mixtures of 10 µL were set up using 10x *T*<sub>4</sub> DNA ligase buffer (1x final c.c.) (60 mM Tris-HCl, 50 mM MgCl<sub>2</sub>, 10 mM DTT, 10 mM ATP, pH 7.5), the appropriate volume of insert and vector, 1 µL *T*<sub>4</sub> DNA ligase (1 unit µL<sup>-1</sup>) (Roche) and water. Control reactions were also prepared (one without insert and the other with just the vector). After mixing carefully with a pipette, reactions were incubated at 4°C for 48 hours or 16°C overnight. The reaction mixture was then transformed in *E. coli* XL1-Blue competent cells and plated in appropriate medium. A colony-PCR was then conducted to confirm the presence and orientation of plasmid inserts.

**Table I** – Oligonucleotide sequences

Oligo	5' or 3' primer	Oligonucleotide sequence	Comments
RIP1Fw	5'	TAGGATCCATGGCTGAAGTGCTAAC	Cloning RIP1 in pRSET A (BamHI)
RIP1Rv	3'	TAGAATTCTCAAGATTTCTTTGCC	Cloning RIP1 in pRSET A (EcoRI)
RIP2Fw	5'	TAGGATCCATGGCAAGCTCAAGTGG	Cloning RIP2 in pRSET A (BamHI)
RIP2Rv	3'	TAGAATTCTTATAACCGGATTGGAAAAC	Cloning RIP2 in pRSET A (EcoRI)
RIP1GTW1F	5'	AAAAAGCAGGCTTAACAATGGCTGCAAGT GCTAACCCCT	RIP1 GATEWAY cloning (1°PCR)
RIP1GTW1R	3'	AGAAAGCTGGGTTTTCAAGATTTCTTTGCCA AGGATGT	
RIP2GTW1F	5'	AAAAAGCAGGCTTAACAATGGCAAGCTAC CGTGGGACA	RIP2 GATEWAY cloning (1°PCR)
RIP2GTW1R	3'	AGAAAGCTGGGTTTTATAACCGGATTGGA AAACTTG	
RADGTW1F	5'	AAAAAGCAGGCTTAACAATGGCTTCGACT CGTGGTTCT	RAD GATEWAY cloning (1°PCR)
RADGTW1R	3'	AGAAAGCTGGGTTTTACGGAATTTTGAGA TTTCTGAA	
DIVGTW1F	5'	AAAAAGCAGGCTTAACAATGGAGATTTTA GCACCAAGT	DIV GATEWAY cloning (1°PCR)
DIVGTW1R	3'	AGAAAGCTGGGTTTCATGCGTTGCGAAAG TGAAGCCC	
RIP1BIFC1R	3'	AGAAAGCTGGGTAAGATTTCTTTGCCAAG GATG	RIP1 GATEWAY cloning (1°PCR) without stop codon
RIP2BIFC1R	3'	AGAAAGCTGGGTATAACCGGATTGGAAAA CTTG	RIP2 GATEWAY cloning (1°PCR) without stop codon
RADBIFC1R	3'	AGAAAGCTGGGTACCGAATTTTGAGATTT CTGAAG	RAD GATEWAY cloning (1°PCR) without stop codon
DIVBIFC1R	3'	AGAAAGCTGGGTATGCGTTCGGAAAGTGA AGCCCCG	DIV GATEWAY cloning (1°PCR) without stop codon
attB1	5'	GGGGACAAGTTTGTAGAAAAAAGCAGGCT	Gateway (2° PCR)

attB2	3'	GGGGACCAGTTTGTACAAGAAAGCTGGCT	Gateway (2° PCR)
T7 Fw	5'	TAATACGACTCACTATAGGG	T7 promoter
T7 Rv	3'	CTAGTTATTGCTCAGCGGTGG	T7 reverse priming site
pDONORFw	5'	TCGCGTTAACGCTAGCATGGATCT	pDONOR specific primers for PCR colony
pDONORRv	3'	GTAACATCAGAGATTTTGAGACAC	
pMDCgfp	5'	GGATTACACATGGCATGGATG	Primer forward for pMDC43 Colony PCR
pMDC32 R2flankfw	3'	CGGCCGCTCTAGAACTAGTTAA	Primer reverse for pMDC32 and 43 Colony PCR
pMDC35S	5'	TTCATTTCAATTTGGAGAGGACC	Primer forward for pMDC32 Colony PCR
YFPn	3'	CCTCGCCCTTGCTCACCAT	Primer reverse for BIFC EYFPn vector Colony PCR
YFPc	3'	CCTTGATGCCGTTCTTCTGCTTG	Primer reverse for BIFC EYFPc vector Colony PCR
P35S	5'	CCACTGACGTAAGGGATGAC	Primer forward for BIFC vectors
F-DOMYB1	5'	CCTTTTAGGATGAGATAAGACTATTCTCAT TCTGA	Primer forward for EMSA DNA probe
R-DOMYB1	3'	AAGGTCAGAATGAGAATAGTCTTATCTCA TCCTAA	Primer reverse for EMSA DNA probe

## 2.3 Cloning procedures

### 2.3.1 Cloning into the pRSET vector

For high-level protein expression in an *E. coli* expression strain, *RIP1* and *RIP2* open reading frames were cloned by PCR amplification, restriction digestion and ligation into the pRSET vector (figure 1, supplemental information).

#### 2.3.1.1 *RIP1* and *RIP2* amplification and digestion

*RIP1* and *RIP2* were amplified (see 2.2.4.1) using the primers listed in table I with different *primer* annealing temperatures (50°C, 55.4°C and 60°C). Samples were

loaded in an agarose gel (see 2.2.3) and the best annealing temperature was chosen. Both *RIP1* and *RIP2* DNA fragments were purified as described above in section 2.2.5.1. Amplified and purified PCR products were digested (see 2.2.6.2) using *EcoRI* and *BamHI* as endonucleases restriction enzymes (10x restriction buffer: 100 mM Tris-HCl, 1 M NaCl, 50 mM MgCl<sub>2</sub>, 10 mM 2-Mercaptoethanol; pH 8.0) for 6 hours at 37°C. The enzymes were heat inactivated at 65°C for 15 min. Digested products were purified as described in section 2.2.5.1.

### **2.3.1.2 pRSET digestion**

7 µg of pRSETa was linearised at 37°C for six hours, in the reaction mixture described in section 2.2.7. The enzymes were heat inactivated at 65°C for 15 min. The remaining restriction enzyme and buffer were removed by phenol/chloroform extraction method for DNA purification (see 2.2.5.2).

### **2.3.1.3 Ligation and transformation**

The ligation reaction was carried out as described in section in section 2.2.7. To 100 ng of pRSETa (2.9 Kb), 80.69 ng of *RIP1* (0.78 Kb) and 74.48 ng of *RIP2* (0.72 Kb) were used. Reactions were incubated at 4°C for 48 hours and then transformed in *E. coli* XL1-Blue competent cells (see 2.2.1.1) and plated in solid LB plus ampicillin (100 µg mL<sup>-1</sup>). Positive colonies were screened using colony PCR (see 2.2.4.4). The primers used in the colony PCR were the T7 forward *primer* and the reverse *primers* of *RIP1* and *RIP2* (table I). PCR samples were resolved by electrophoretic separation (see 2.2.3) and bands visualized on a 610 nm (short wave) UV trans-illuminator. Plasmids of positive clones (vector with insert in the right direction) were isolated (see 2.2.2.1) and sent for sequencing (*STABvida* sequencing services).

## **2.3.2 Cloning into pMDC43 and pMDC32**

*RIP1* and *RIP2* open reading frames were cloned using Gateway® based technology into the pMDC43 vector (Curtis and Grossniklaus, 2003, Invitrogen) (figure



2, supplemental information) to determine the sub-cellular localization by transient expression in *N. tabacum*. *RIP1* open reading frame was also cloned in the pMDC32 vector (figure 3, supplemental information) for permanent expression *in planta*. *RIP1* and *RIP2* open reading frames were amplified as described in section 2.2.4.3. The Gateway® based technology uses the lambda recombination system to facilitate transfer of heterologous DNA sequences (flanked by *att* sites) between vectors (Hartley et al., 2000). Two recombination reactions constitute the basis of Gateway® Technology: BP and LR recombination reactions.

### 2.3.2.1 BP reaction

In the BP reaction an *attB* substrate (*attB*-PCR product) is recombined with an *attP* substrate (donor vector) to create an *attL*-containing entry clone catalysed by *BP Clonase II* enzyme mix (Invitrogen). To preserve equal molarity between vector and *attB* PCR product the amount of the latter was calculated using the following formula:  $\text{ng (attB PCR product)} = \text{fmol} \times N \text{ (nucleotide number)} \times 660 \text{ fg} \times 1 \text{ ng} / 1 \text{ fmol} \times 10^6 \text{ fg}$ . BP recombination reactions of *RIP1* and *RIP2* were carried out in a total volume of 10  $\mu\text{L}$  containing: pDONOR (50 fmol), *RIP1* or *RIP2 attB* products (50 fmol), 2  $\mu\text{L}$  *BP Clonase II* and 5.5  $\mu\text{L}$  TE buffer (10 mM Tris-HCl, 1 mM EDTA, pH 8). Reactions were incubated at 25°C during 2 hours and 30 minutes and then transformed in *E. coli* XL1-Blue competent cells (see 2.2.1.1). Colonies grew in LB plus kanamycin (50  $\mu\text{g mL}^{-1}$ ), and a colony PCR (see 2.2.4.4) was carried out using pDONOR appropriate *primers* (table I). Positive clones were selected (see 2.2.3) and the plasmids isolated (see 2.2.2.1) and sent for sequencing.

### 2.3.2.2 LR reaction

In the LR reaction an *attL* substrate (entry clone) is recombined with an *attR* substrate (destination vector) to create an *attB*-containing expression clone catalysed by *LR Clonase II* enzyme mix (Invitrogen). LR recombination reactions of *RIP1*<sub>pDONOR</sub> and *RIP2*<sub>pDONOR</sub> were carried out in a total volume of 10  $\mu\text{L}$  containing: pMDC43 or pMDC32 (50 fmol) *RIP1/2*<sub>pDONOR</sub> (50 fmol), 2  $\mu\text{L}$  *BP Clonase II* and 5.5  $\mu\text{L}$  TE buffer. Reactions were incubated at 25°C during 18 hours and then transformed in *E. coli* XL1-

Blue competent cells (see 2.2.1.1). Colonies grew in LB plus kanamycin and hygromycin, and a colony PCR (see 2.2.4.4) was carried out using pMDC43 or pMDC32 appropriate *primers* (table I). Positive clones were selected (see 2.2.3) and the plasmids isolated (see 2.2.2.1) and sent for sequencing.

### **2.3.3 Cloning into pH7WGF2**

For sub-cellular co-localization fluorescence studies, *RAD* and *DIV* open reading frames were cloned in to the pH7WGF2 vector (Karimi *et al.*, 2002) using *Gateway* based technology (figure 4, supplemental information). *RAD* and *DIV* open reading frames were amplified as described in section 2.2.4.3.

#### **2.3.3.1 BP reaction**

*BP* recombination reactions of *RAD* and *DIV* were carried out in a total volume of 10  $\mu$ L in containing: pDONOR (50 fmol), *RAD* or *DIV attB* products (50 fmol), 5,5  $\mu$ L TE buffer (pH 8) respectively and 2  $\mu$ L *BP Clonase II*. Reactions were incubated at 25°C during 3 hours and then transformed in *E. coli* XL1-Blue competent cells (see 2.2.1.1). Colonies grew in LB plus kanamycin, and a colony PCR (see 2.2.4.4) was carried out using pDONOR appropriate *primers* (table I). Positive clones were selected (see 2.2.3) and the plasmids isolated (see 2.2.2.1) and sent to sequencing.

#### **2.3.3.2 LR reaction**

*LR* recombination reactions of RAD<sub>pDONOR</sub> and DIV<sub>pDONOR</sub> were carried out in a total volume of 10  $\mu$ L containing; pH7WGF2 (50 fmol), RAD<sub>pDONOR</sub> or DIV<sub>pDONOR</sub> (50 fmol), 2  $\mu$ L *BP Clonase II* and 5.5  $\mu$ L TE buffer (pH 8). Reactions were incubated at 25°C during 16 hours and then transformed in *E. coli* XL1-Blue competent cells (see 2.2.1.1). Colonies grew in LB plus hygromycin and streptomycin, and a colony PCR (see 2.2.4.4) was carried out using pH7WGF2 appropriate *primers* (table I). Positive clones were selected (see 2.2.3) and the plasmids isolated (see 2.2.1) and sent for sequencing.

### 2.3.4 Cloning into pDH51-GW-YFPn and pDH51-GW-YFPc

*RAD*, *DIV*, *RIP1* and *RIP2* open reading frames were cloned using Gateway® based technology into the pDH51-based vector (Zhong *et al.*, 2008) for Bimolecular Fluorescence Complementation (BiFC) based studies (figure 5 and 6, supplemental information). *RAD*, *DIV*, *RIP1* and *RIP2* open reading frames were amplified as described in section 2.2.4.3. *YFP* N' and C' Terminus fragments were downstream of the *attR2* site so to create a viable fusion protein *primers* were designed to remove the stop codon of the four genes.

#### 2.3.4.1 BP reaction

*BP* recombination reactions of *RAD*, *DIV*, *RIP1* and *RIP2* with pDONOR were carried out in a total volume of 10 µl containing: pDONOR (50 fmol), *RAD*, *DIV*, *RIP1* or *RIP2 attB* products (50 fmol), 5,5 µL TE buffer (pH 8) and 2 µL *BP Clonase II*. Total amount of *attB* product necessary was calculated as in section 2.3.2.1 and 2.3.3.1. Reactions were incubated at 25°C during 4 hours and then transformed in *E. coli* XL1-Blue competent cells (see 2.2.1.1). Colonies grew in LB plus kanamycin, and a colony PCR (see 2.2.4.4) was carried out using pDONOR appropriate *primers* (table I). Positive clones were selected (see 2.2.3) and the plasmids isolated (see 2.2.2.1) and sent for sequencing.

#### 2.3.4.2 LR reaction

*LR* recombination reactions of  $RAD_{pDONOR}$ ,  $DIV_{pDONOR}$ ,  $RIP1_{pDONOR}$  and  $RIP2_{pDONOR}$  with appropriate pDEST BiFC vectors were carried out in a total volume of 10 µL containing: pDH51-YFPn or pDH51-YFPc (50 fmol),  $RIP1_{pDONOR}$ ,  $RIP2_{pDONOR}$ ,  $RAD_{pDONOR}$  or  $DIV_{pDONOR}$  (50 fmol), 5,5 µL TE buffer (pH 8) and 2 µL *BP Clonase II*. Total amount of *attB* product necessary was calculated as in section 2.3.2.1 and 2.3.3.1. Reactions were incubated at 25°C during 15 hours and then transformed in *E. coli* XL1-Blue competent cells (see 2.2.1.1). Colonies grew in LB plus ampicillin and chloramphenicol, and a colony PCR (see 2.2.4.4) was carried out using pDH51-GW-YFP appropriate *primers* (table I). Positive clones were selected (see 2.2.3) and the plasmids isolated (see 2.2.2.1) and sent for sequencing.

## **2.4 Yeast Methods**

### **2.4.1 *Saccharomyces cerevisiae* transformation**

The LiAc based method (Ito *et al.*, 1983) was used to introduce *yeast* appropriate plasmids into yeast strains (AH109). Yeast cells from freshly growing plates were scraped into 1 mL water in an eppendorf tube. Cells were pelleted at 13,000 x *g* for 15 seconds. The supernatant was discarded and 1 mL of 0.1 M LiAc was added to the pellet. The mixture was vigorously vortexed to disperse all the clumps. A total volume of 25  $\mu$ L was aliquoted into a separate tube. Total volumes of 240  $\mu$ L of sterile 50% (w/v) PEG<sub>4000</sub>, 36  $\mu$ L of 1 M LiAc (pH 7.5), 50  $\mu$ L of 2 mgmL<sup>-1</sup> *ssDNA* (boiled for 5 minutes and placed on ice) and 25  $\mu$ L of plasmid DNA (1  $\mu$ g of plasmid) were added to the mixture followed by vortexing. Mixture was incubated at 42°C during 120 minutes. The cells were pelleted as described above, resuspended in 100  $\mu$ l of autoclaved water and plated onto appropriate SD minimal media (6.7 g L<sup>-1</sup> Yeast nitrogen without amino acids; 1x Dropout Solution (-T or -L); 20 gL<sup>-1</sup> Agar (w/v); 2% (w/v) glucose, pH 8). SD medium without histidine was used to screen for positive interactions. *LacZ* activity was observed when adding 80 mg mL<sup>-1</sup> of X-gal ( $\beta$ -galactosidase substrate) to the medium.

### **2.4.2 3-amino-1, 2, 4-triazole assay**

3-AT, a competitive inhibitor of the yeast HIS3 protein, was used to inhibit low levels of HIS3 that is expressed in a leaky manner in some reporter strains (including the AH109 strain, Durfee *et al.*, 1993; Fields, 1993). The 3-AT test was used to define the minimal amount of 3-AT necessary to inhibit growth on SD minimal medium without histidine. AH109 cells harboring yeast plasmids were plated on SD -His minimal media containing different 3-AT concentrations (0 mM, 1 mM, 2 mM, 3 mM, 5 mM and 20 mM) and the growth of colonies recorded.

### 2.4.3 Colony-lift filter assay

Colony-lift filter assay (Breeden and Nasmyth, 1985) was used to screen for positive protein-protein interactions by observing  $\beta$ -galactosidase activity of co-transformed yeast cells. X-gal (5-bromo-4-chloro-3-indolyl- $\beta$ -D-galactopyranoside) was used as  $\beta$ -galactosidase substrate for this particular assay. Only colonies less than 2-4 days old and 1-3 mm wide were used in this assay. For each plate of transformants assayed a sterile *Whatman #5* filter was presoaked in 5 mL Z buffer (16.1 g L<sup>-1</sup> Na<sub>2</sub>HPO<sub>4</sub>; 5.50 g L<sup>-1</sup> NaH<sub>2</sub>PO<sub>4</sub>; 0.75 g L<sup>-1</sup> KCl; 0.246 g L<sup>-1</sup> MgSO<sub>4</sub>; 0.27% (v/v) DTT; 0.33 mg mL<sup>-1</sup> X-gal) in a sterile petri dish. A dry sterile filter was placed over the plate of colonies assayed. The filter was gently rubbed to help colonies cling to the filter. The filter was also marked in three or more asymmetric locations to orient the filter and then lifted off the agar plate and transferred (with colonies facing up) to a pool of liquid nitrogen. The filter was completely in liquid nitrogen for 10 seconds and then thawed at room temperature. Carefully, the filter was placed, colony side up, on the presoaked filter. The filters were incubated at 30°C from 30 minutes to 8 hours and appearance of blue color in the colonies “prints” was periodically checked.

### 2.4.4 Liquid Culture assay using *o*-nitrophenyl- $\beta$ -D-galactopyranoside (ONPG) as substrate

The quantification of  $\beta$ -galactosidase activity was performed to compare the relative strength of the protein-protein interactions by expression of the *LacZ* reporter gene. *o*-nitrophenyl- $\beta$ -D-galactopyranoside (ONPG) was used as the  $\beta$ -galactosidase substrate for this particular assay.

Fresh colonies (less than 2 months) were used to inoculate 5 mL SD -His liquid media. The medium was vigorously vortexed for 1 minute to thoroughly disperse the cells. The cultures were incubated at 30°C for 16-18 hours with shaking at 250 rpm until OD<sub>600</sub> reached 1.5. An aliquot (2 mL) of the overnight culture was used to inoculate 8 mL YPDA and the new culture incubated at 30°C for 3-5 hours with shaking at 230 rpm until OD<sub>600</sub> was 0.5-0.8. On the day of the experiment, ONPG was dissolved at 4 mg mL<sup>-1</sup> in Z buffer (see 2.4.3, remove DTT and X-gal). 1.5 mL of the culture was placed in to three eppendorf tubes (3 independent experiments) and the cells pelleted at 14,000 x g

for 30 seconds. The supernatants were carefully removed and 1.5 mL of Z-buffer was added to each tube. The mixture was vortexed until all the cells were resuspended. The cells were pelleted again as before and resuspended in 300  $\mu$ L Z-buffer. 100  $\mu$ L of the cell suspension was transferred to a new eppendorf tube and subjected to three-freeze/thaw cycles (freezed in liquid nitrogen and thawed at 37°C). A control tube was set-up with 100  $\mu$ L of Z-buffer. 700  $\mu$ L of Z-buffer plus 0.27% (v/v) DTT was added to the reaction and control tubes. Immediately, 160  $\mu$ L of ONPG was added to the reaction and control tubes. Start time was recorded. The tubes were incubated at 30°C. When the yellow color developed 400  $\mu$ L 1 M Na<sub>2</sub>CO<sub>3</sub> was added to the reaction tubes to stop the reaction. Time was again recorded. Reaction tubes were centrifuged as described above for 10 minutes to pellet cell debris. Supernatants were transferred to clean cuvettes. A spectrophotometer was calibrated against the blank at A<sub>420</sub> and the values of absorbance of the samples recorded.

$\beta$ -galactosidase units were calculated assuming that 1 unit is defined as the amount of  $\beta$ -galactosidase that hydrolyzes 1  $\mu$ mol of ONPG to *o*-nitrophenol and *D*-galactose *per minute per cell* (Miller, 1972; Miller, 1992):  $\beta$ -galactosidase units:  $1000 \times A_{420} / (t \times V \times OD_{600})$ ; where t was the elapsed time of incubation; V: 0.1 x concentration factor, and OD<sub>600</sub> the is the optical density of the initial culture.

## 2.5 Protein Methods

### 2.5.1 Heterologous pilot expression in *E. coli*

RAD<sub>pRSET</sub>, DIV<sub>pRSET</sub>, RIP1<sub>pRSET</sub> and RIP2<sub>pRSET</sub> were transformed into the *E. coli* BL21(DE3)pLysE expression strain, as described in section 2.2.1.1. Colonies grew in LB plus ampicillin, chloramphenicol and kanamycin. A pilot expression experiment was conducted to define the optimal inducer concentration that maximized protein expression and the best time point to collect the sample. One colony was used to inoculate 10 mL LB medium plus amp, chl and kan. The cultures were incubated at 37°C overnight with shaking at 200 rpm. 500  $\mu$ L of the overnight culture was used to inoculate 25 mL LB medium with the antibiotics described above. The new culture was incubated at 37°C for 3 hours with shaking at 200 rpm until OD<sub>600</sub> reached 0.4-0.6. 1 mL

of the culture was retrieved ( $OD_{600}$  was recorded) and pelleted at 14,000 x g for 2 min. Pellet was frozen at  $-20^{\circ}\text{C}$  (time 0). Isopropyl  $\beta$ -D-1-thiogalactopyranoside (IPTG) was added to the culture to a final concentration of 0.4 or 1 mM. During the following 4 hours, 1 mL of the culture was retrieved in one hour intervals, the  $OD_{600}$  recorded and the cells pelleted as described above. Pellets were frozen at  $-20^{\circ}\text{C}$  (time 1, 2, 3 and 4). To each frozen pellet 100  $\mu\text{L}$  lysis buffer (0.02 M HEPES pH 7.8; 0.8 M KCl; 0.1% (v/v) *Triton-X*) was added, and the mixtures vortexed until the pellet was completely resuspended. Soluble and insoluble fractions were obtained by centrifuging the samples 15 minutes at 14,000 x g. The supernatant was transferred to a new tube (soluble fraction). The insoluble fraction was solubilised adding 100  $\mu\text{L}$  of lysis buffer to the pellet.

### **2.5.2 Protein electrophoresis**

To analyse the protein profile of the culture in each time point samples (total, soluble and insoluble fractions) were boiled  $95^{\circ}\text{C}$  for 5 minutes after adding 2x SDS sample buffer (1x final c.c.) (0.125 M Tris-HCl pH 6.8; 0.5% (v/v) SDS; 20% (v/v) glycerol; 5% (v/v) DTT; 0.025% (w/v) blue bromophenol) and then centrifuged at 14,000 x g for 15 minutes to pellet cellular debris. Samples were then loaded into an appropriate discontinuous polyacrylamide gel (Raymond and Weintraub, 1959; Laemmli, 1970). In this system, by using different buffers in the gel and in the running solution and adding a stacking gel to the resolving gel, samples are compressed into a thin starting band and individual proteins are finely resolved and separated. The Laemmli system buffer system is a system that incorporates SDS in the buffer. The denatured polypeptides (by heat) take on a rod-like shape and a uniform charge-to-mass ratio proportional to their molecular weight.

The stacking gel was prepared adding 1.3 mL of a 30% (w/v) Bis-acrylamide solution (30:0.8), 100  $\mu\text{L}$  of a 10% (w/v) SDS solution, 2.5 mL of a 0.5 M Tris-HCl (pH 6.8) solution, 50  $\mu\text{L}$  of a 10% (w/v) APS solution and 12  $\mu\text{L}$  TEMED. The resolving gel was prepared adding 5 mL of a 30% (w/v) Bis-acrylamide solution (30:0.8), 100  $\mu\text{L}$  of a 10% (w/v) SDS solution, 2.5 mL of a 1.5 M Tris-HCl (pH 8.8) solution, 50  $\mu\text{L}$  of a 10%

(w/v) APS solution and 16  $\mu$ L TEMED. A 10  $\mu$ L SDS-PAGE Molecular Weight Standard (Broad Range, Bio-Rad) was also added to each gel. The gel was run at 120 V for 1 hour in Tris-glycine electrophoretic buffer (0.08 M Tris-HCl pH 8.3; 1.45% (w/v) glycine; 0.1% (w/v) SDS).

### **2.5.3 Protein gel staining**

Coomassie staining (Meyer and Lambert, 1965) solution (50% (v/v) methanol; 10% (v/v) acetic acid; 0.25% (w/v) Coomassie Brilliant Blue R-250) was used to detect proteins after electrophoretic separation. The gels were covered with 400 mL of the Coomassie solution and stained at room temperature for 3 to 4 hr with gentle agitation. The Coomassie stain solution was then removed by aspiration. The gels were covered with 250 mL of destain solution (10% (v/v) methanol; 5% (v/v) acetic acid) and allowed to destain with gentle agitation. The destain solution was changed several times, removing it at each time by aspiration. The destaining was continued until the protein bands were seen without background staining of the gel.

### **2.5.4 Protein purification**

The recombinant proteins expressed in *E.coli* had an N-Terminus 6xHIS-tag that allowed purification based on the affinity between the histidines and a resin containing immobilised cobalt, the *TALON* resin (Clontech). The resin (500  $\mu$ L bed volume) was equilibrated adding 5 mL equilibration buffer to the resin bed by centrifugation at 3,000 x *g* for 2 minutes. This step was repeated one more time. After defining the best expression conditions of the protein of interest, a 50 mL induced culture was harvested by centrifugation at 3,000 x *g* for 15 min at 4°C. The pellet was then resuspended in 4 mL equilibration buffer (50 mM sodium phosphate, 300 mM NaCl). Samples were subjected to three successive freeze/thaw cycles in liquid nitrogen. The cell extract was then centrifuged at 5,000 x *g* for 20 min at 4°C to pellet any insoluble material. The supernatant was then transferred to the equilibrated resin. The resin plus soluble sample was agitated at room temperature for 20 min to allow the recombinant polyhistidine-tagged protein to bind to the resin. The mixture was then centrifuged at 700 x *g*. The



supernatant was removed and discarded. The resin was then washed with 20 mL of equilibration buffer. The suspension was agitated at room temperature for 10 min and centrifuged as before for 5 min. The supernatant was discarded. This step was repeated two times to promote thorough washing. The protein was eluted by adding 5 mL of elution buffer to the resin (50 mM sodium phosphate, 300 mM NaCl, 150 mM imidazole) followed by centrifugation at 700 x g for 1 min. Eluates were collected in 500  $\mu$ L fractions. To the eluates a similar volume of 100% (v/v) glycerol was added, and samples stored at -80°C.

## **2.6 Electrophoretic Mobile Shift Assay (EMSA)**

The study of DNA-protein interactions was performed using the electrophoretic mobile shift assay (Fried and Crothers, 1981). This technique is based on the separation of free DNA from DNA-protein complexes due to the differences in the electrophoretic mobility in native (nondenaturing) polyacrylamide gels.

### **2.6.1 Probe preparation and labelling**

The DIV probe (36 bp) was prepared by mixing the complementary oligonucleotides (table I) in TEN buffer (10 mM Tris; 1 mM EDTA; 0.1M NaCl; pH 8.0) in a 1:1 molar ratio. The mixture was incubated at 95°C for 10 minutes and cooled to 15-25°C at 0.5°C/minute. The probe was diluted to 4 pmol/ $\mu$ L with TEN buffer (ng DS DNA=pmol x 0.66 x N, where N is the probe size). The probe was DIG-labeled in a total reaction mixture of 20  $\mu$ L containing: probe (3,85 pmol), 5x labeling buffer (1 M potassium cacodylate; 0.125 M Tris-HCl; 125 mg mL<sup>-1</sup> bovine serum albumin; pH 6.6), 5 mM CoCl<sub>2</sub>; 0.05 mM DIG-ddUTP; Terminal Transferase (20 U  $\mu$ L<sup>-1</sup>) and water. The mixture was mixed and centrifuged briefly at 12,000 x g, incubated at 37°C for 15 minutes and then placed on ice. Reaction was stopped by adding a final concentration of 1 mM EDTA (pH 8.0) to the reaction. The labeled probe was stored at -20°C.

### **2.6.2 EMSA reaction and electrophoretic separation**

Reaction mixtures were prepared containing: DIG-labeled probe (0.4 ng  $\mu$ L<sup>-1</sup>),

poly L-lysine ( $0.1 \mu\text{g } \mu\text{L}^{-1}$ ), poly [d(I-C)] ( $1\mu\text{g } \mu\text{L}^{-1}$ ), 5x binding buffer, protein and water. Three binding buffers were used in this study:

**Buffer 1-** 100 mM HEPES pH 7.6; 5 mM EDTA, 50 mM  $(\text{NH})_4 \text{SO}_4$ ; 5mM DTT; 1% (v/v) *Tween*; and 150 mM KCl.

**Buffer 2-** 50 mM Tris-HCl pH 8.0; 5 mM EDTA; 150 mM KCl; 5 mM DTT; and 1% (v/v) *Tween*.

**Buffer 3-** 50 mM HEPES pH 7.6; 5 mM EDTA; 150 mM NaCl; 5 mM DTT; 40 mM  $\text{MgCl}_2$ ; and 4mM spermidine.

The components of the reaction were mixed carefully and incubated at room temperature for 15 min. Tube was then placed on ice and 5x loading buffer (60% (v/v) TBE buffer; 40% (v/v) glycerol; 0.2% (w/v) bromophenol blue) was added do the samples. Samples were then loaded in a pre-run 6% native continuous polyacrylamide gel. A Native PAGE is an electrophoretic technique commonly used in the separation of biologically active proteins. The mobility in a native gel depends on both size and charge of the proteins. The gel was prepared by adding 2 mL of a 30% (w/v) Bis-acrylamide solution, 5 mL of a 2x TBE buffer, 50  $\mu\text{L}$  of a 10% (w/v) APS solution and 10  $\mu\text{L}$  TEMED. The gel was pre-run during 30 minutes at 120 V to remove traces of APS and TEMED from the gel. Samples were run at 80 V for 60 minutes in 0.5x TBE buffer (45 mM Tris; 45 mM Boric acid; 1 mM EDTA; pH 8.0).

### 2.6.3 Electroblotting

After electrophoresis one glass plate was carefully removed from one side of the gel. In the meantime a nylon membrane trimmed to the size of the gel was equilibrated for 5 minutes in transfer buffer (0.5x TBE). The nylon membrane was then placed in the top of the gel avoiding air bubbles. Four layers of gel-sized Whatman 3MM sheets (presoaked in transfer buffer) were placed on the top of the gel/membrane. The pad Whatman/membrane/gel was then removed from the other glass plate, and another four pre-soaked layers of gel-sized Whatman 3MM sheets were added to the other side of the gel. The ‘sandwich’ was then placed in the gasket of an electroblot device. Transfer was performed in 0.5x TBE buffer for 30 min at 400 mA. Following the transfer the membrane was cross-linked at 120 mJ in a Stratalinker.

## 2.6.4 Detection

The membrane was transferred to a plastic recipient with washing buffer (0.1 M Maleic acid; 0.15 M NaCl; 0.3% (v/v) *Tween*; pH 7.5) and incubated at room temperature for 2 minutes. The membrane was then incubated for 30 minutes with 100 mL of a 1x blocking solution (DIG Gel shift Kit, 2<sup>nd</sup> generation) (1% (w/v) blocking reagent dissolved in maleic acid). The membrane was then incubated with antibody solution (1:10,000 Anti-Digoxigenin in 1x blocking solution) for 30 minutes. The membrane was washed two times with washing buffer for 15 minutes and then equilibrated in detection buffer (0.1 M Tris-HCl; 0.1 M NaCl pH 9.5) for 5 minutes. The membrane was then placed DNA facing up on a folder and covered with 0.1 mL of a CSPD solution (1:100 CSPD in detection buffer). Immediately, the membrane was covered with the second sheet of the folder to spread the substrate evenly and incubated at room temperature for 5 minutes. The membrane was incubated at 37°C for 10 minutes. Chemiluminescent signal was detected two hours later in a ChemiDoc XRS (Bio-Rad laboratories).

## 2.7 Generation of *Arabidopsis* transgenic lines

Two constructs [RIP1<sub>pMDC32</sub> (see section 2.3.2) and RIP2<sub>pBI121</sub>] were introduced into *A. thaliana* ecotype *Columbia* using the floral dip method with *A. tumefaciens* (Clough and Bent, 1998)

### 2.7.1 *A. tumefaciens* transformation

*A. tumefaciens* was transformed with both constructs as described in section 2.2.1.2. RIP1<sub>pMDC32</sub> transformation mix was plated onto LB plates containing rifampicin and hygromycin, RIP2<sub>pBI121</sub> plated onto LB plates containing rifampicin and kanamycin.

### 2.7.2 Plant transformation

The floral dip method (Clough and Bent, 1998) was used to generate *A. thaliana* transgenic plants. *A. thaliana* plants were grown in 10 cm width pots, 4 plants per pot until the flowers were open. LB medium (10 mL) containing the appropriate antibiotic

was inoculated with a single colony of *A. tumefaciens* harbouring the construct. The culture was grown at 30°C with vigorous shaking (200 rpm) until the OD<sub>600</sub> reached 0.8. 500 µL was used to inoculate 200 mL LB (pH 5.4, supplemented with 19.6 µg mL<sup>-1</sup> acetosyringone). The culture was grown overnight at 30°C and then centrifuged at 4,000 x g for 12 min and the pellet resuspended in 250 mL infiltration medium (5% sucrose (w/v) supplemented with 500 µL<sup>-1</sup> *Silwett L-77*) in an 500 mL plastic container. The aerial regions of the plants were submerged in the infiltration medium for 1 to 10 minutes and then left to dry horizontally in obscurity covered with a plastic bag for 2 days. Plants were grown as described in section 2.1.1.1.

### **2.7.3 Selection of primary transformants (T1 generation)**

T1 seeds were recovered after approximately 8 weeks growth, when the siliques were dehydrated. A thin metallic net enabled the separation between seeds and the rest vegetal material. Seeds were then sterilised, sown in appropriate plate medium and stratified as described in section 2.1.1.1. Positive transformants were selected by their survival in medium plus antibiotic.

### **2.8 *N. benthamiana* transient transformation**

Constructs described in section 2.3.2 and 2.3.3 were used in the transformation of *N. benthamiana* leaves. Leaves were grown for 5 weeks as described in section 2.1.1.2 LB medium (10 mL) containing the appropriate antibiotics was inoculated with a single colony of *A. tumefaciens* harbouring the construct, and the culture grown overnight at 30°C with vigorous agitation (200 rpm) until the OD<sub>600</sub> reached 2. 5 mL of the previous culture was used to inoculate 30 mL LB (without antibiotics) and the culture grown at 30°C with vigorous shaking (200 rpm) until OD<sub>600</sub> reached 2. The culture was centrifuged at 4000 x g for 10 min and the pellet gently resuspended in infiltration solution (5% (w/v) sucrose; 200 µM acetosyringone; 5 mM MES pH 5.6). For one optical density unit, 7.5 mL of infiltration solution was added to the pellet. The mixture was gently incubated with slow shaking for 30 minutes and then aspirated to a sterile syringe. The syringe was put against the leaf abaxial zone and the fluid infiltrated

applying pressure. In a successful infiltration the liquid spreads to the entire leaf. Following infiltration the plants were kept in the dark for 48 hours. 3 days after the infiltration a section of the infiltrated tissue was checked for fluorescence emission using an epifluorescence *Leica DM5000 B* microscope or an *Leica SP2 AOBs SE* fluorescent laser scanning confocal microscope.

## 2.9 Protein functional analysis

RIP1, RIP2, RAD and DIV proteins molecular mass weight was retrieved from the Swiss-Prot *protparam* tool (Gasteiger *et al.*, 2005) at [ca.expasy.org/tools/protparam.html](http://ca.expasy.org/tools/protparam.html). RIP1, RAD, DIV and RIP2 protein motifs/domains were screened against the *InterProScan* database program at the EMBL - European Bioinformatics Institute website ([www.ebi.ac.uk/Tools/InterProScan/](http://www.ebi.ac.uk/Tools/InterProScan/)). Sub-cellular localization was predicted using the *ProtComp v. 9.0* software at [linux1.softberry.com/berry.phtml](http://linux1.softberry.com/berry.phtml) and the *ESLPred* program (Bhasin and Raghava, 2004) at [www.imtech.res.in/raghava/eslpred/](http://www.imtech.res.in/raghava/eslpred/). Protein function was predicted using the *ProtFun 2.2 Server* (Jensen *et al.*, 2002 and Jensen *et al.*, 2003) at [www.cbs.dtu.dk/services/ProtFun/](http://www.cbs.dtu.dk/services/ProtFun/). The presence and location of Twin-arginine signal peptide cleavage sites in bacteria was identified using the TatP 1.0 Server at <http://www.cbs.dtu.dk/services/TatP-1.0/> (Brendtsen *et al.*, 2005). RIP1, RIP2 and DIV codon usage for expression in *E. coli* was analysed using the Rare Codon Caltor at [www.doe-mbi.ucla.edu/~sumchan/caltor.html](http://www.doe-mbi.ucla.edu/~sumchan/caltor.html). Nuclear localisation signals were identified using the PSORT database (Nakai and Kanehisa, 1991).

### 3. Results

Phenotypic analysis of loss of function mutants and expression data suggest that the dorsal identity of the *A. majus* flower meristem is partially controlled by the activity of RAD, and that RAD function by inhibiting post-transcriptionally *DIV*, the gene responsible for ventral identity. This was emphasised by the high similarity of the MYB-like/SANT domain of RAD to the first MYB-like/SANT domain of *DIV* (figure 14). This similarity could suggest a molecular competition for the same DNA or protein targets.

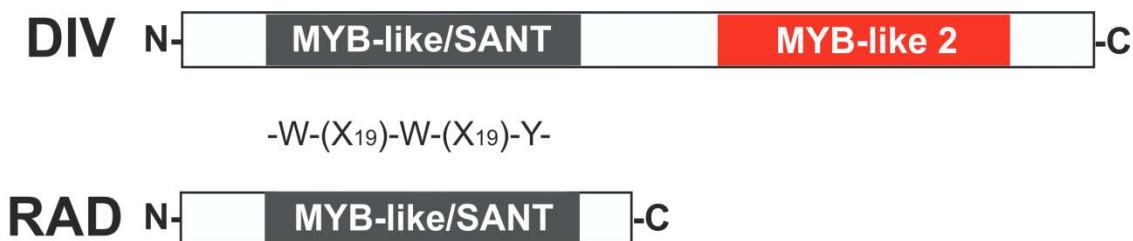


**Figure 14-** Homology between the MYB-Like domains of RAD and DIV proteins. The first MYB-like domain of DIV and the MYB-like of RAD share a conserved sequence that generates a helix-helix-loop-helix. Also both domains share a W-W-Y motif typical of the MYB-like domains.

Three hypotheses that could explain the molecular antagonism between RAD and DIV proteins were tested in this study: RAD could bind to the *DIV* binding *cis*-elements in the promoter of *DIV* targets preventing *DIV* from activating the transcription of these genes. Another hypothesis tested was the possibility that RAD could be antagonizing directly *DIV* through a direct protein-protein interaction. Finally, a possibility arose that RAD could be sequestering co-factors of the *DIV* transcriptional complex, or could be forming a multi-protein complex with *DIV* and its co-factors that alters the transcription rate of the genes controlled by *DIV*. Previous to this work, a yeast two-hybrid screening of an *A. majus* cDNA floral library allowed the identification of two proteins that interact with RAD and *DIV*, and they were named RIP1 and RIP2.

#### 3.1 RIP1 and RIP2 sequence analysis

The alignment of the primary sequences of RIP1 and RIP2 (figure 15) shows that RIP1 and RIP2 are very similar (65%), sharing 113 identical amino acids (45%). The screening of RIP1 and RIP2 primary sequences against the InterProScan database lead to

the identification of two conserved protein domains: a MYB-like/SANT domain and a domain of unknown function 3755 (DUF3755) in the protein C' Terminus region (figure 15).

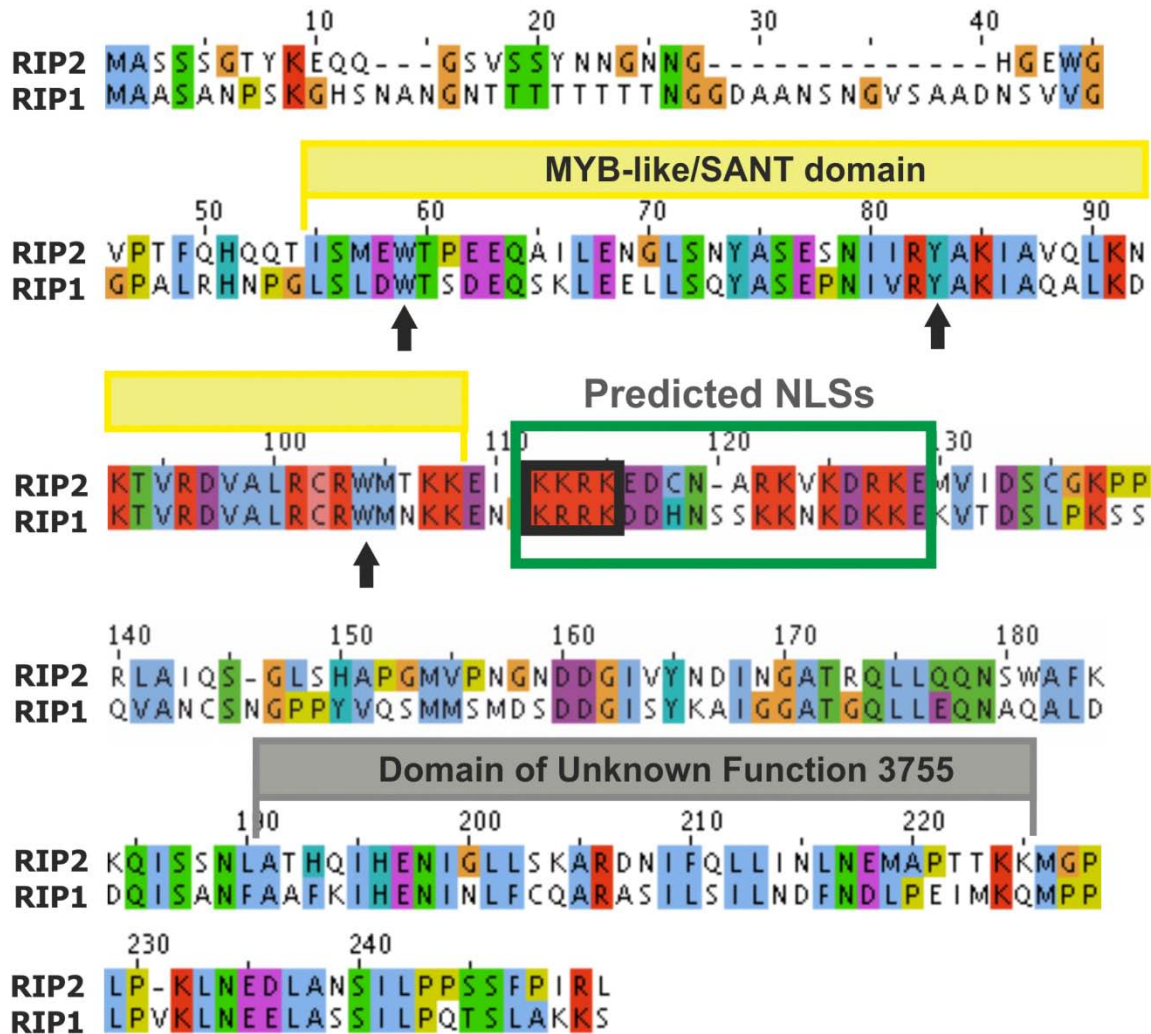


**Figure 15-** RIP1 and RIP2 primary sequences were aligned using the program Clustal-X. Two conserved domains were identified using the *InterProScan* program available at EBI-EMBL and are highlighted (a MYB-like/SANT domain and a DUF3755 domains). Black arrows indicate the canonical MYB-like/SANT conserved residues (W-Y-W). Green and black boxes show the NLSs of the RIP1 and RIP2 proteins predicted by the pSORT program. Alignment was visualized using JalView.

The MYB-like/SANT domain found in RIP1 and RIP2 is similar to the ones found in RAD and DIV sequences. However, the canonical MYB-like/SANT conserved amino acids W-W-Y observed in the RAD and DIV sequences is substituted in the RIP1 and RIP2 MYB-like/SANT domains by a conserved W-Y-W amino acidic combination (figure 15, black arrows), a substitution that could be functionally significant. Screening

all the annotated proteins with MYB-like/SANT domains revealed that this amino acidic combination in the RIP1 and RIP2 MYB-like/SANT domain is unique. This means that the MYB-like/SANT domain of RIP1 and RIP2 belong to a new class of MYB-like transcription factors.

According to the *Protcomp* database (Bhasin and Raghava, 2004), RIP1 and RIP2 proteins should be localised in the nucleus. A nuclear localisation often implies the presence of a nuclear localisation signal (NLS). A NLS sequence is an amino acid sequence that acts like a tag on the exposed surface of a protein and is used to target the protein to the cell nucleus through the nuclear pore complex (Kalderon *et al.*, 1984). Typically, this signal consists of one or more short sequences of positively charged lysines or arginines. The most common type of NLS is that of the SV40 large T antigen characterised by the sequence PKKKRKV (Kalderon *et al.*, 1984). Robbins *et al.* (1991) proposed another type of nuclear targeting signal that is characterised by two basic residues, a ten-residue spacer, and another basic region consisting of at least three basic residues out of five residues. According to PSORT (Nakai and Kanehisa, 1991) The RIP1 and RIP2 sequences contain these two described types of NLSs (figure 15, green and black boxes).

RIP1 and RIP2 function was predicted using the *ProtFun 2.2 Server* (Jensen *et al.*, 2002 and Jensen *et al.*, 2003), and both were identified as DNA-binding proteins.

### **3.2 Expression of recombinant RAD, DIV and RIP proteins in *E. coli***

In order to test the DNA binding activity of RAD, DIV and RIPs recombinant proteins, a gel-shift assay was planned. To accomplish this, RAD, DIV and RIPs proteins were obtained through heterologous expression in *E. coli* cells. To obtain the proteins, a plasmid containing the *open reading frame* (ORF) of each of these genes, fused in frame with a His•tag and under the control of the strong bacteriophage *T7* promoter (pRSET, Invitrogen), was used to transform *E. coli* BL21(DE3)pLysE strain competent cells. In this strain, the *DE3* gene that codes for both the *T7* RNA polymerase promoter and gene is under the control of a lac operator (Moffatt and Studier, 1987). This strain also carries the natural promoter and coding sequence for the *lac* repressor



(Studier *et al.*, 1990; Dubendorff and Studier, 1991). In normal physiological conditions, the *lac* repressor acts at the *lac* gene promoter to repress transcription of the *T7* RNA polymerase gene. However, in the presence of isopropyl  $\beta$ -D-1-thiogalactopyranoside (IPTG, a lactose analogue), the *lac* repressor is inactivated and the *T7* RNA polymerase is generated, leading to the transcription of the genes under the control of the *T7* promoter. This particular *E. coli* strain used also carried the pLysE vector, a plasmid that codes for the *T7* lysozyme. Accordingly, when no inductor is added to the medium the production of the *T7* lysozyme inhibits the residual production of *T7* RNA polymerase (Moffatt and Studier, 1987; Studier, 1991).

To avoid unspecific protein binding in the DNA-binding assay, purified protein samples were required. As mentioned earlier, proteins were cloned in frame with a 6xHis tag that allowed purification based on the Immobilized metal affinity chromatography (IMAC) principle that there is a reversible interaction between the histidines side chains and cobalt ions immobilized on a resin (Porath *et al.*, 1975).

In this assay, the proteins tagged with the polyhistidines were added to a resin containing sepharose beads bearing the tetradent chelator of the  $\text{Co}^{2+}$  metal ion. Under conditions of physiological pH (pH 7), the polyhistidines tagged proteins attached to the resin by sharing the electron density of one of the imidazole nitrogen atoms with the electron-deficient orbitals of the cobalt (figure 16).

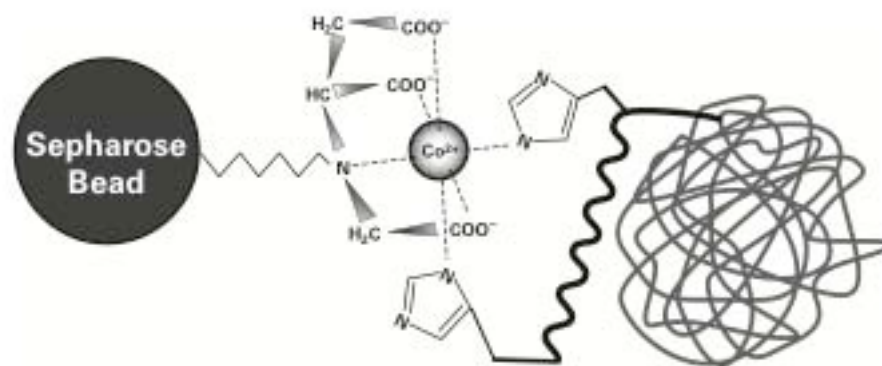


**Figure 16-** Schematic diagram of the immobilized metal affinity chromatography method used in the purification of polyhistidines fusion proteins. The polyhistidine- tagged recombinant protein binds to the resin containing sepharose beads bearing the tetradentate chelator of the  $\text{Co}^{2+}$  metal ion.

Protein elution occurred when the imidazole nitrogen bound to the resin was protonated (by alteration of pH, 7 to 5) generating a positively charged ammonium ion,

which is repelled by the positively charged metal atom (elution by a drop in pH) or alternatively, the bound polyhistidine-tagged protein was competitively eluted by adding imidazole to the elution buffer (Hochuli *et al.*, 1987). The imidazole compound competed for the binding on the resin with the histidines, leading to the release of the recombinant proteins from the resin.

### **3.2.1 Optimization of the expression and purification of RAD recombinant protein**

To express RAD recombinant protein, the pRSET plasmid (Invitrogen) containing the *RAD* cDNA as a *Bam*HI-*Hind*III fragment (a construct previously obtained) was introduced into *E. coli* BL21(DE3)pLysE strain competent cells.

The characteristics of each gene product are unique and, therefore, the optimal conditions for induction of gene expression are variable. The next step was to establish optimal conditions for growth of the cells and expression of the recombinant protein. To study the time course of the recombinant protein expression after induction with different concentrations of IPTG (0.4 and 1 mM), 1 mL aliquots of the culture were harvested at 60 min intervals and the total protein extracts were analysed by SDS-PAGE (the sample were normalized by the culture OD<sub>600nm</sub> at each time point). RAD protein has a molecular weight of 12 kDa as predicted from the primary sequence but when fused to the His•tag, the molecular mass reaches 15 kDa (*protparam* program, Gasteiger *et al.*, 2005). Figure 17 shows the total cellular polypeptides present in an identical volume of culture when induced with the two different concentrations of IPTG. A band corresponding to the molecular mass of RAD recombinant protein (15 kDa) was observed in all the induced samples. The expression of the recombinant protein could be observed one hour after induction with 0.4 mM IPTG (figure 17, lane 2). The maximum amount of protein per cell was obtained 2 hours after induction, in both concentrations of inductor (figure 17, lanes 3 and 6). After this time point, the level of protein expression appears to decrease slightly despite the OD<sub>600nm</sub> of the culture continued to increase, an explication for this could be that the culture may have become overgrown with cells that lost the plasmid.

According to these results, in order to obtain the higher amount of RAD recombinant protein, cultures were induced with 0.4 mM IPTG during 2 hours.

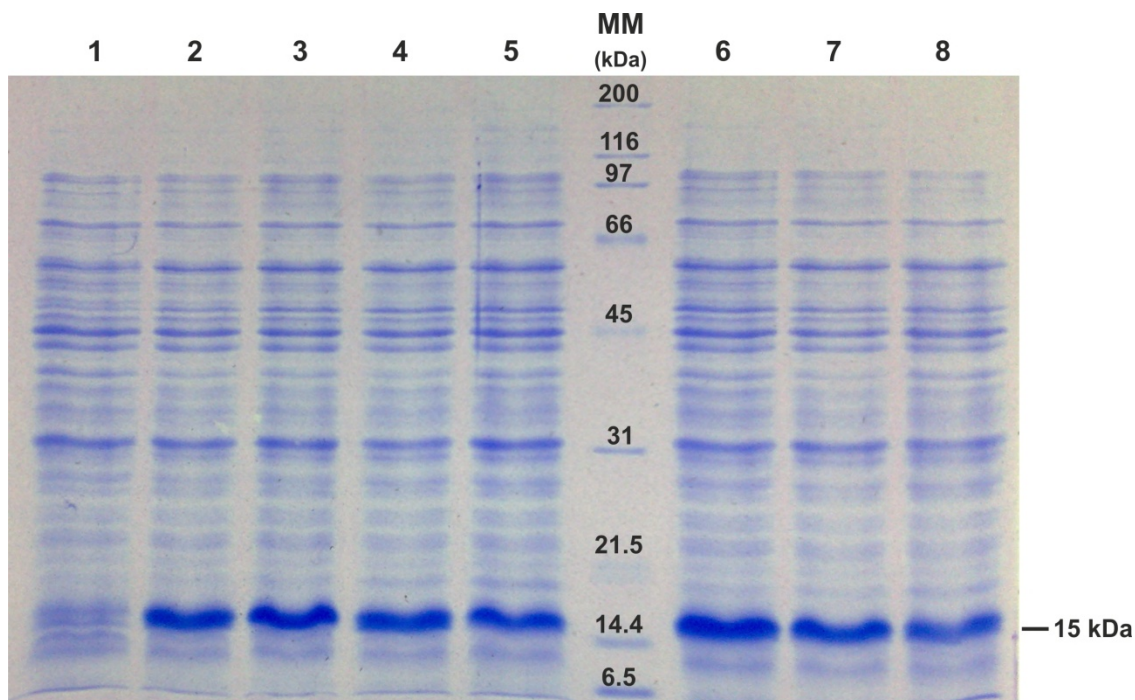


**Figure 17-** Analysis of RAD heterologous polypeptide expression in BL21(DE3)pLysE *E. coli* cells carrying the RAD<sub>pRSETa</sub> plasmid at different time points after IPTG induction (0.4 and 1 mM final concentrations). Samples were run on an SDS-PAGE discontinuous 15% polyacrylamide gel. The samples were normalized by the culture OD<sub>600nm</sub> at each time point. The polypeptides were detected on the gel by Coomassie Blue staining.

Lane 1- no induction,

Lane 2- 1h after induction with 0.4 mM IPTG;

Lane 3- 2h after induction with 0.4 mM IPTG;

Lane 4- 3h after induction with 0.4 mM IPTG;

Lane 5- 4h after induction with 0.4 mM IPTG;

Lane 6- 2h after induction with 1 mM IPTG;

Lane 7- 3h after induction with 1 mM IPTG;

Lane 8- 4h after induction with 1 mM IPTG;

MM- molecular weight marker, broad range (Bio-Rad). Arrow represent the RAD recombinant protein.

A cellular fractioning method was performed to determine whether the protein is soluble in the cytoplasm or insoluble and localised in inclusion bodies. The presence of the RAD recombinant protein in the soluble fraction would ensure that the protein would be closest to its functionally active state. Clarified and insoluble fractions of RAD induced and non-induced samples were obtained and analysed by SDS-Page.

According to the results observed in figure 18, RAD recombinant protein was found in the soluble fraction (lane 4), but also in the insoluble fraction (lane 6).

Nevertheless, the amount of RAD protein in the soluble fraction was enough for subsequent studies.

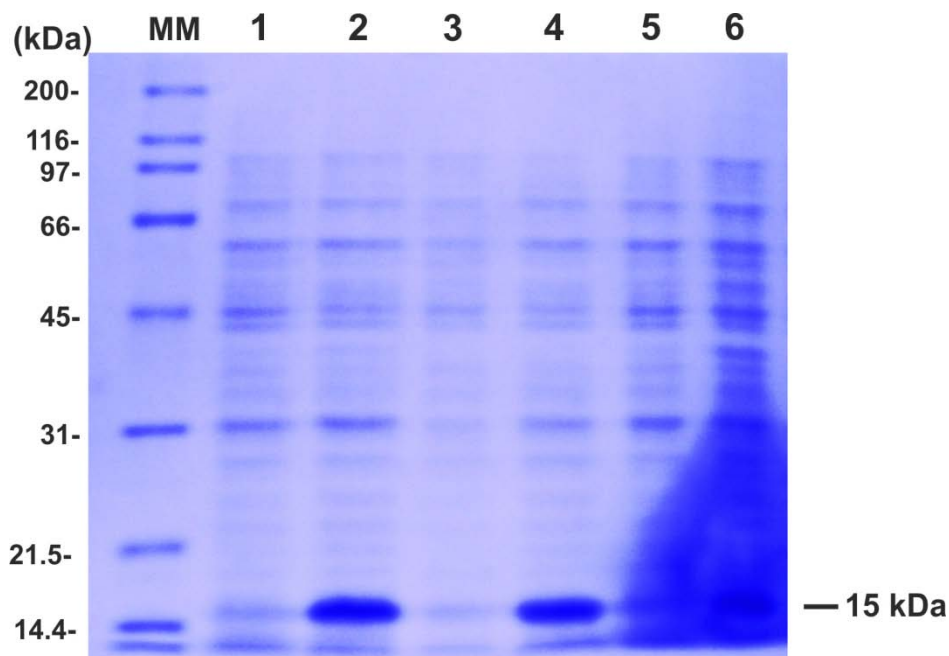


**Figure 18-** Analysis by SDS-PAGE of cellular localisation of RAD recombinant protein in BL21(DE3)pLysE *E. coli* cells carrying the RAD<sub>pRSETa</sub> plasmid. The culture was grown at 37° C and induced with a final concentration of 0.4 mM IPTG. Samples were run on an SDS-Page descontinuous 15% polyacrylamide gel. The polypeptides were detected on the gel by Coomassie Blue staining.

lane 1- total fraction (no induction);  
 lane 2- total fraction with 2 h induction;  
 lane 3- soluble fraction (no induction);  
 lane 4- soluble fraction with 2 h induction;  
 lane 5- insoluble fraction (no induction);  
 lane 6- insoluble fraction with 2 h induction.

MM- molecular weight marker, broad range (Bio-Rad). Arrow represent the RAD recombinant protein.

The RAD recombinant protein was purified using a batch purification method. Accordingly, a metal affinity resin was used to which the RAD proteins, fused to the 6xHis, bind. The soluble fraction containing RAD recombinant protein was loaded onto the TALON<sup>TM</sup> resin (Clontech) and RAD recombinant protein elution was performed by adding imidazole to the resin or by a drop in the solution pH (pH 7 to pH 5). For each elution method, eluates were recovered in four fractions. RAD recombinant protein was successfully obtained using both elution methods (figure 19). Elution of RAD protein by adding imidazole retrieved a larger amount of protein in the first eluate fraction (figure 19a, lane 2), whereas in the case of the elution with a drop in pH a

higher amount of RAD recombinant protein was obtained in the second eluate fraction (figure 19b, lane 5). Comparing both elution methods it appears that elution by a drop in pH yields a smaller amount of purified protein than the elution by imidazole method, however, the elution with a pH drop method was preferred. This method was preferred because there are studies with a variety of eukaryotic transcription factors, which have shown that molecules containing imidazole are potent inhibitors of protein–DNA interactions (Melander *et al.*, 2004). Thus, as the main aim of generating recombinant protein is to perform a DNA-binding assay, the use of imidazole was avoided.

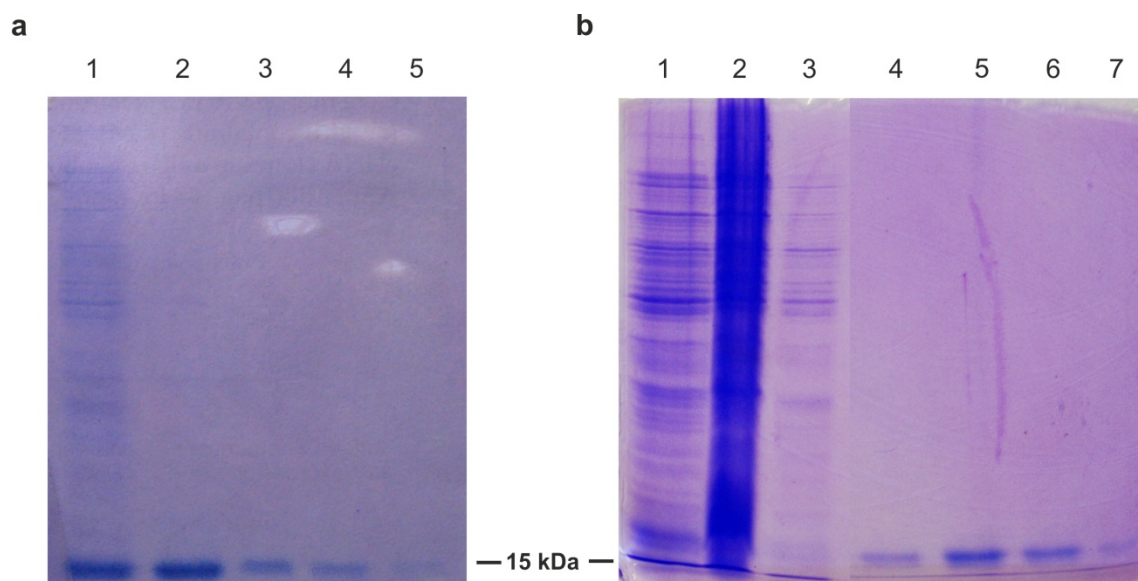


**Figure 19-** Analysis by SDS-PAGE of different steps of the purification of RAD recombinant protein using TALON affinity resin and elution by (a) adding imidazole or (b) with a drop in pH. Samples were run on an SDS-Page descontinuous 15% polyacrylamide gel and the polypeptides were detected on the gel by Coomassie Blue staining. Arrow represent the RAD recombinant protein.

**a)** Elution of RAD protein by adding Imidazole:

Lane 1- soluble fraction of an induced sample (2 hours with 0.4 mM IPTG);

Lane 2- first eluate fraction;

Lane 3- second eluate fraction;

Lane 4- third eluate fraction;

Lane 5- fourth eluate fraction;

**b)** Elution of RAD protein by a drop in pH:

Lane 1- soluble fraction (no induction);

Lane 2- soluble fraction of an induced sample (2 hours with 0.4 mM IPTG);

Lane 3- flow-through;

Lane 4- first eluate fraction;

Lane 5- second eluate fraction;

Lane 6- third eluate fraction;

Lane 7- fourth eluate fraction.

### 3.2.2 Optimization of the expression and purification of *DIV* recombinant protein

To express *DIV* recombinant protein, the pRSET plasmid (Invitrogen) containing the cDNA of *DIV* as a *Bam*HI-*Hind*III fragment (a construct previously obtained) was introduced into *E. coli* BL21(DE3)pLysE competent cells. A pilot expression was conducted to analyse the expression profile of the *DIV* recombinant protein expression, similar to the one performed for RAD expression profile. 1 mL aliquots of the culture were harvested at 60 min intervals, before and after induction, and the total protein extracts were analysed by SDS-PAGE (the samples were normalized by the culture OD<sub>600nm</sub> at each time point). *DIV* protein has a molecular weight of 41 kDa as predicted from the primary sequence but when fused to the His•tag, *DIV* recombinant protein has a molecular weight of 44 kDa (*protparam* program, Gasteiger *et al.*, 2005). Figure 20 shows the total *E. coli* protein extracts at different time points present in an identical volume of culture when induced with two different concentrations of IPTG (0.4 mM and 1 mM final concentrations). One hour after induction with 0.4 mM IPTG, the expression of *DIV* recombinant protein could be observed (figure 20a, lane 2), however, the highest amount of recombinant protein was observed three hours after induction (figure 20a, lane 4). A similar amount of *DIV* recombinant protein was observed after four hours following induction with 1 mM IPTG (figure 20b, lane 2). Thus, *DIV* recombinant protein expression appears to follow a steady increase rate culminating in the highest accumulation on the third and fourth hour following induction with IPTG (figure 20). In further experiments, *DIV* recombinant protein was obtained from *E. coli* cultures induced with 0.4 mM IPTG during 4 hours.

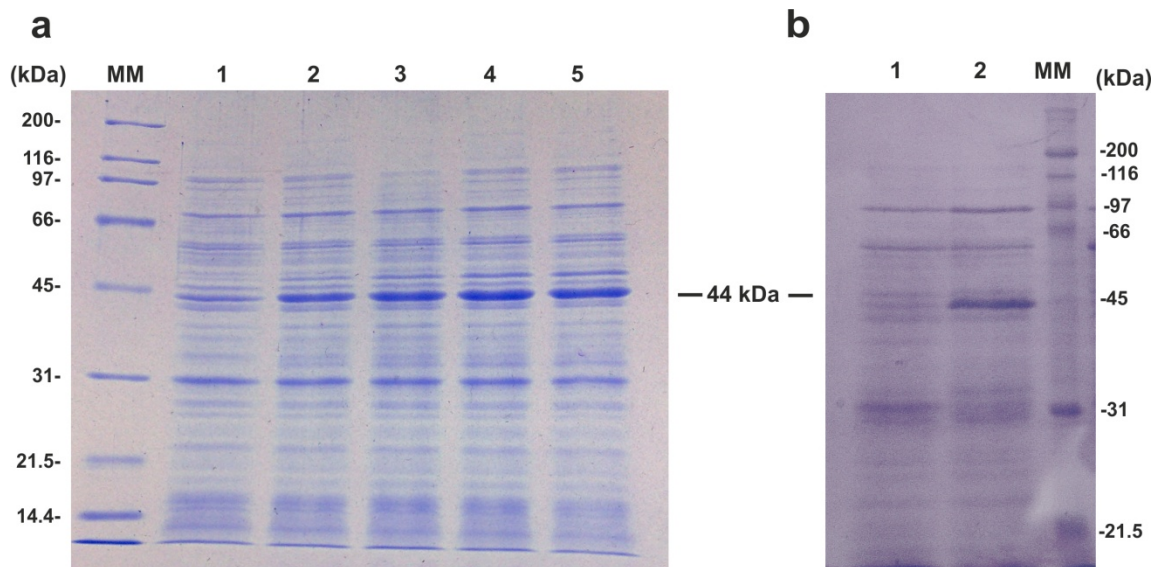


**Figure 20-** Analysis of DIV heterologous polypeptide expression in BL21(DE3)pLysE *E. coli* cells carrying the DIV<sub>pRSETc</sub> plasmid at different time points after IPTG induction. The samples were normalized by the culture OD<sub>600nm</sub> at each time point. Samples were run on an SDS-PAGE descontinuous 12% polyacrylamide gel and the polypeptides detected on the gel by Coomassie Blue staining.

**a)**

Lane 1- no induction;

Lane 2- 1h after induction with 0.4 mM IPTG;

Lane 3- 2h after induction with 0.4 mM IPTG;

Lane 4- 3h after induction with 0.4 mM IPTG;

Lane 5- 4h after induction with 0.4 mM IPTG;

**b)**

Lane 1- no induction;

Lane 2- 4h after induction with 1 mM IPTG;

MM- molecular weight marker, broad range (Bio-Rad). Arrow represent the DIV recombinant protein.

It is clear, however, that in all time points the amount of DIV recombinant protein expressed was never as high as RAD recombinant protein (figure 17). One possible explanation is that DIV recombinant protein could be toxic to the cells; however, the OD<sub>600nm</sub> of the culture grew continuously throughout induction similarly to the RAD induced cultures. Another explanations could be that the mRNA secondary structure of DIV could be inhibiting protein translation in *E. coli*, or the presence of rare codons in the mRNA sequence could be leading to the incorporation of incorrect amino acids during translation in *E. coli*, originating truncated or altered protein forms.

A cellular fractioning method was performed to determine whether DIV recombinant protein is soluble in the cytoplasm or insoluble and located in inclusion bodies. The presence of DIV recombinant protein in the soluble fraction would ensure that the protein would be closest to its functionally active state. Clarified and insoluble

fractions of induced and non-induced samples were obtained and analysed by SDS-Page. By analysis of figure 21, it is possible to verify that DIV recombinant protein is present in the soluble fraction (figure 21, lane 4) and none was observed in the insoluble fraction (figure 21, lane 6).

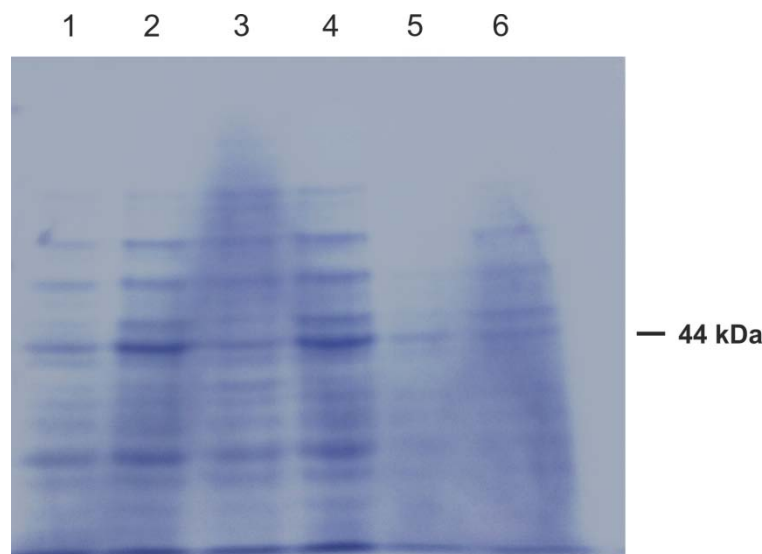


**Figure 21-** Analysis by SDS-PAGE of cellular localisation of DIV recombinant protein in BL21(DE3)pLysE *E. coli* cells carrying the DIV<sub>pRSETc</sub> plasmid. The culture was grown at 37° C and induced with a final concentration of 0.4 mM IPTG. Samples were run on an SDS-Page discontinuous 12% polyacrylamide gel and the polypeptides detected on the gel by Coomassie Blue staining.  
lane 1- total fraction (no induction);  
lane 2- total fraction following 4 h induction;  
lane 3- soluble fraction (no induction);  
lane 4- soluble fraction following 4 h induction;  
lane 5- insoluble fraction (no induction);  
lane 6- insoluble fraction following 4 h induction. Arrow represent the DIV recombinant protein.

The purification of DIV recombinant protein, similarly to RAD recombinant protein, was also performed based on the affinity between the histidines tagged DIV proteins and a cobalt-based resin. Due to the success in the purification of RAD recombinant protein using a drop in pH as the elution method, the elution of DIV recombinant protein was performed using the same method. Similarly to the RAD elution strategy, the use of an elution buffer with imidazole was avoided due to its inhibitory effects in DNA-protein interactions (Melander *et al.*, 2004). In figure 22, lanes 4-6 show the DIV purified recombinant protein recombinant protein in the three eluate fractions obtained.



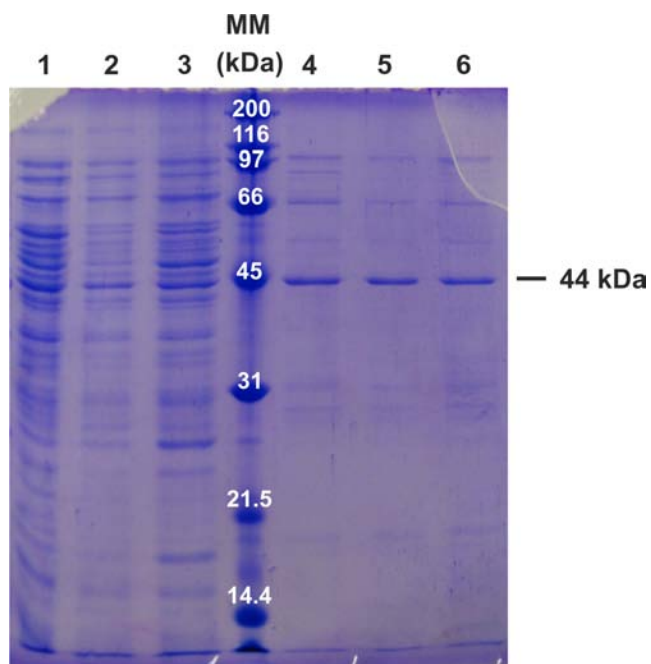


**Figure 22-** Analysis by SDS-PAGE of different steps of the purification of DIV recombinant protein using TALON affinity resin. The culture was grown at 37° C and induced with a final concentration of 0.4 mM IPTG. Samples were obtained four hours after induction and the clarified sample added to the resin. DIV recombinant protein was eluted by a drop in pH in three different fractions. Samples were run on an SDS-Page discontinuous 15% polyacrylamide gel and the polypeptides detected on the gel by Coomassie Blue staining.

Lane 1- soluble fraction of the induced culture;

Lane 2- first resin flow through;

Lane 3- second resin flow through;

Lane 4- first eluate fraction;

Lane 5- second eluate fraction;

Lane 6- third eluate fraction.

MM- molecular weight marker, broad range (Bio-Rad). Arrow represent the DIV recombinant protein.

### 3.3 Expression of RIP1 and RIP2 recombinant protein in *E. coli*

#### 3.3.1 Cloning of the RIP1 and RIP2 cDNA into the pRSET plasmid

To obtain RIP1 and RIP2 recombinant protein, a strategy was designed to clone the *open reading frames* of the *RIP1* and *RIP2* in the pRSET expression plasmid (Invitrogen). The genes were cloned under the transcriptional control of the T7 promoter and in fusion with a His•tag (figure 23). These features allowed expression in an *E. coli* expression strain and purification using a metal affinity resin, respectively.

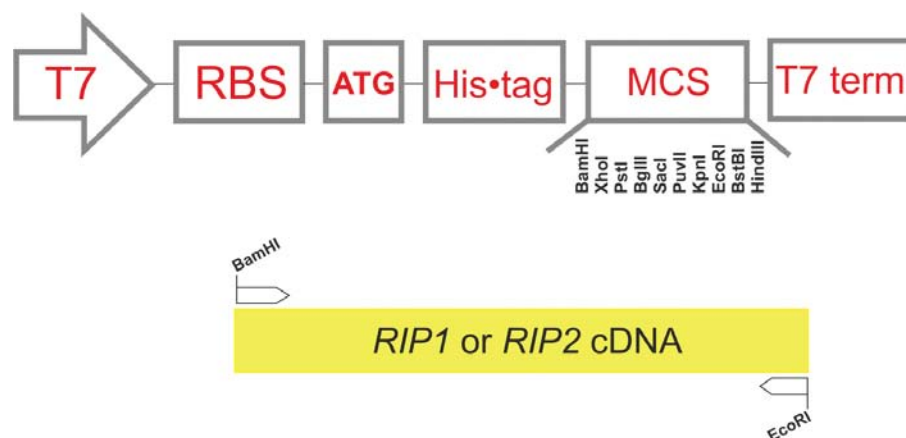


**Figure 23-** Strategy for cloning *RIP1* and *RIP2* cDNA in the pRSET expression vector. The pRSET plasmid sequence contains the T7 promoter, a ribosome binding site (RBS), a initiation codon (ATG), the His•tag, a multiple cloning site (MCS) and the T7 terminator. Specific *RIP1* and *RIP2* primers were designed to introduce the recognition sites of the endonucleases *Bam*HI and a *Eco*RI in the amplification products.

*Primers* were designed to introduce the endonucleases *Bam*HI (5') and *Eco*RI (3') recognition sites in the amplification products. The 5' *primer* was further designed to allow cloning *in frame* with the His•tag. To test for primer specificity, the *RIP1* and *RIP2 ORFs* were amplified by PCR using three different *primer* annealing temperatures (50°C, 55.4°C and 60°C). As seen in figure 24, a single band was observed corresponding to the expected *RIP1* amplified product (780 bp) and *RIP2* amplified product (740 bp). As expected no unspecific amplification occurred. To perform the *RIP1* and *RIP2* cDNA amplification by PCR, the lower *primer* annealing temperature (50°C) was chosen. Amplification by PCR was then performed with *Pfu* DNA

Polimerase to avoid the occurrence of any mutation. Following amplification, the PCR products were purified and digested with *Bam*HI and *Eco*RI endonucleases. The pRSET plasmid was also linearised with *Bam*HI and *Eco*RI. The digestion product was run on an agarose gel and two bands were visible: the expected band (3000 bp) and a smaller size band (figure 24, lane 1). Due to the presence of the smaller size band, the expected band containing the linearised pRSET plasmid was extracted from the agarose gel and purified.

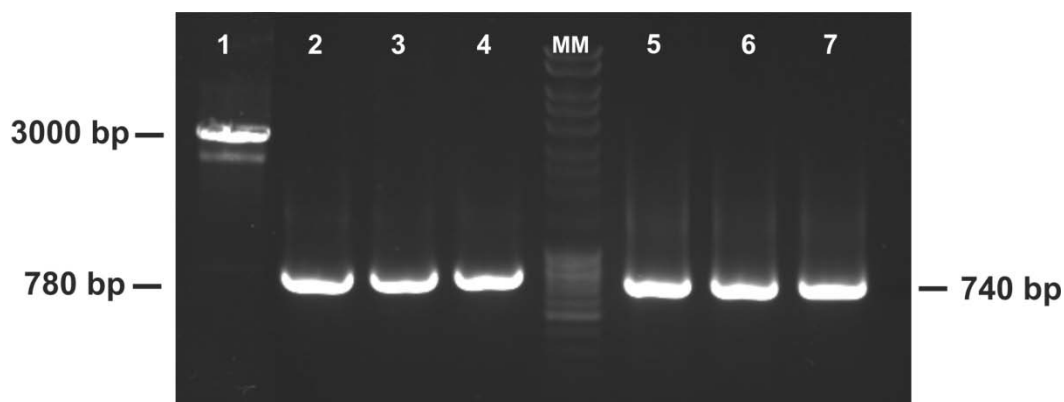


**Figure 24-** pRSET digestion and *RIP1* and *RIP2* cDNA PCR amplified products. A 10 kb ladder was run in the middle lane of the 1% agarose gel.  
 Lane 1 - linearized pRSET a plasmid (expected size: 3000 bp);  
 lane 2-4 *RIP1* amplified product using different *primer* annealing temperatures (50°C, 55,4°C and 60°C respectively) (expected size: 780 bp);  
 lane 5-7 *RIP2* amplified product using different *primer* annealing temperatures (50°C, 55,4°C and 60°C respectively) (expected size: 740 bp).

The restricted fragments were ligated and transformed in *E. coli* XL1-Blue competent cells. Colonies transformed with the construct were capable of growing in medium supplemented with ampicillin (100 µg mL<sup>-1</sup>).

A colony PCR was then conducted to select positive clones. The T7 *primer* forward that amplifies from the T7 promoter and the T7 *primer* reverse that amplifies from the T7 terminator were used for *RIP1*<sub>pRSET</sub> colonies screening (figure 25a), whereas the screening of clones harbouring the *RIP2*<sub>pRSET</sub> construct was conducted using the T7 forward *primer* and the *RIP2* reverse *primer* (anneals at the end of the gene) (figure 25b). For *RIP1*<sub>pRSET</sub>, an 1100 bp amplified product was expected for a positive clone whereas for *RIP2*<sub>pRSET</sub> an amplified product of 940 bp was expected.

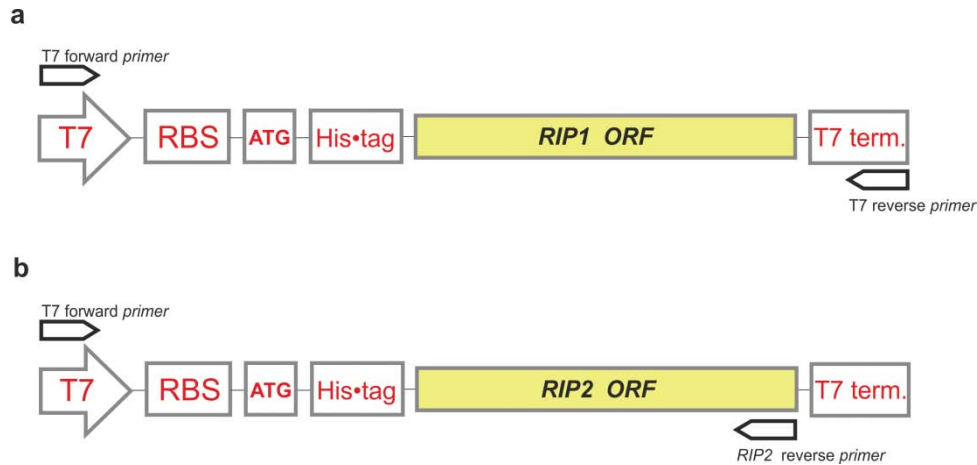


**Figure 25-** Primers chosen for the screening of  $RIP1_{pRSET}$  and  $RIP2_{pRSET}$  positive clones by colony PCR. **a)** for  $RIP1_{pRSET}$  screening, the T7 forward and reverse *primers*; **b)** for  $RIP2_{pRSET}$ , the T7 forward *primer* and the *RIP2* reverse *primer*.

At least four  $RIP1_{pRSET}$  positives clones were observed with the expected amplification product size (figure 26a, lanes 2, 3, 5 and 9). Similarly, four  $RIP2_{pRSET}$  positives clones were observed with the expected amplification product size (figure 26b, lanes 7, 11, 12 and 14).

Plasmids of clone 9 ( $RIP1_{pRSET}$ ) (figure 26a) and clone 14 ( $RIP2_{pRSET}$ ) (figure 26b) were isolated and sent for sequencing. Both *RIP1* and *RIP2* ORFs were properly orientated, without mutations and *in frame* with the His•tag.

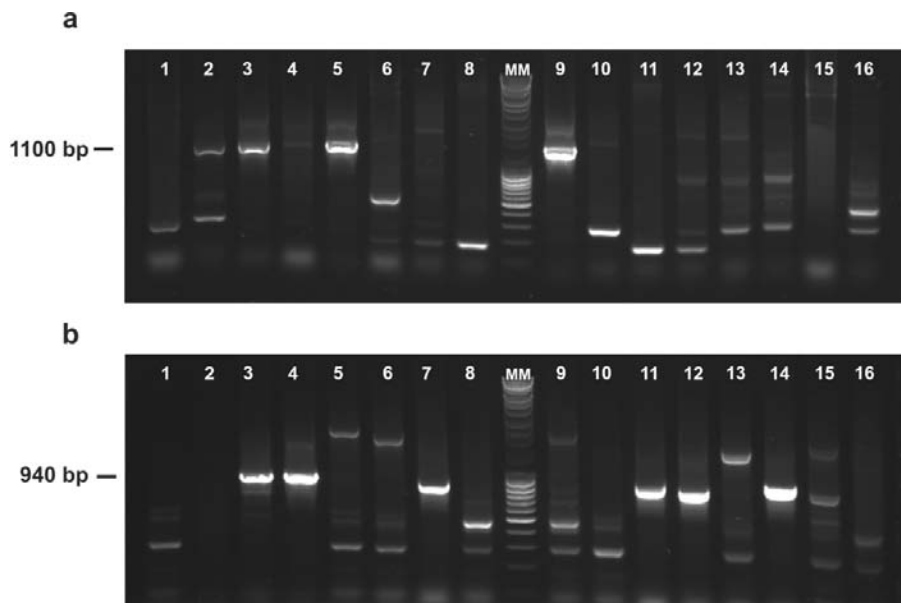


**Figure 26-**  $RIP1_{pRSET}$  and  $RIP2_{pRSET}$  clones screening by colony PCR amplification. A 10 kb ladder was run in the middle lane of each 1% agarose gel. **a)**  $RIP1_{pRSET}$  colonies screening (expected size for a positive clone: 1100 bp); **b)**  $RIP2_{pRSET}$  colonies screening (expected size for a positive clone: 940 bp).

### 3.3.2 Optimisation of the expression of the RIP1 and RIP2 recombinant proteins

*E. coli* BL21(DE3)pLysE competent cells were then transformed with RIP1<sub>pRSET</sub> and RIP2<sub>pRSET</sub> and the conditions of expression of the RIP1 and RIP2 proteins optimised. A pilot expression was conducted to analyse the expression profile of RIP1 and RIP2, similar to the one used for RAD and DIV recombinant protein expression profiles. 1 mL aliquots of induced culture were harvested at 60 min intervals and the total protein extracts were analysed by SDS-PAGE (the samples were normalized by the culture OD<sub>600nm</sub> at each time point).

RIP1 protein has a molecular weight of 27 kDa as predicted from the primary sequence but when fused to the His•tag, RIP1 recombinant protein has a molecular weight of 30 kDa (*protparam* program, Gasteiger *et al.*, 2005). Figure 27 shows the total *E. coli* protein extracts at different time points present in an identical volume of culture when induced with two different concentrations of IPTG (0.4 mM and 1 mM final concentrations). As observed in figure 27 (lanes 1 and 7), prior to induction, a band with the approximate molecular weight of the RIP1 recombinant protein is observed. Following induction with either 0.4 or 1 mM IPTG the band corresponding to the strongly expressed protein before induction can not be detected in induced cultures. Instead, there is a band of smaller molecular weight (figure 27, lanes 2, 3, 4, 6, 8 and 9) that could correspond to the RIP1 recombinant protein. Assuming that the band that appeared following induction is the RIP1 recombinant protein, it appears that induction with 1 mM IPTG generates a higher amount of protein when compared to induction with a final concentration of 0.4 mM IPTG. Also, the highest amount of protein was observed two hours after induction with 1 mM IPTG, however, the amount of putative RIP1 recombinant protein decreases in the following time points. After 4 hours of induction, the OD<sub>600nm</sub> value of the cultures stabilised, however, in a smaller value than the ones observed in RAD and DIV induced cultures (data not shown), which indicates that the expression of the RIP1 recombinant protein could be toxic to the bacterial cells.

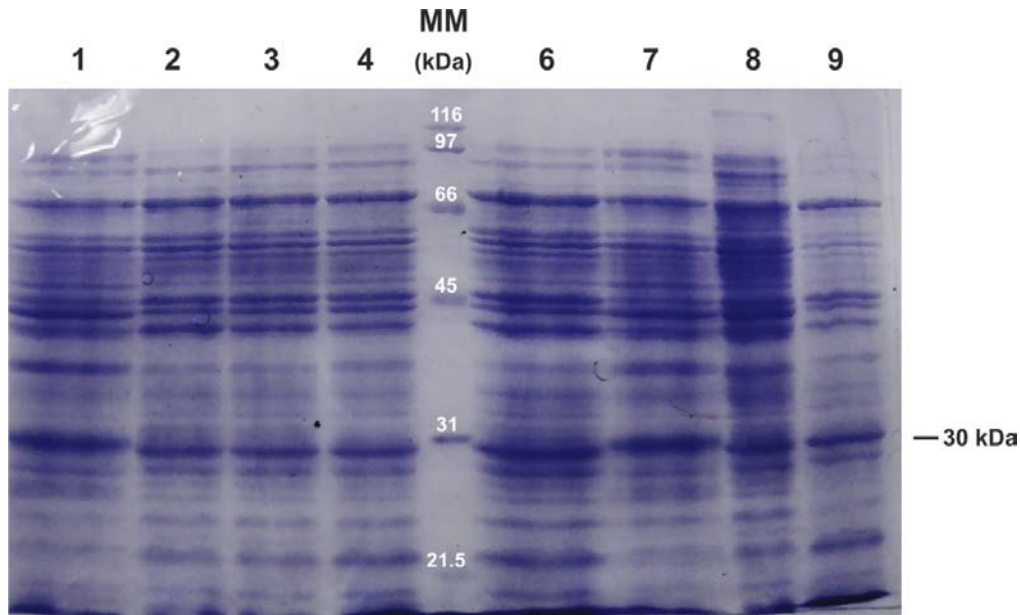


**Figure 27-** Analysis of RIP1 recombinant protein expression in BL21(DE3)pLysE *E. coli* cells carrying the RIP1<sub>PRSET</sub> plasmid following induction with two concentrations of IPTG (0.4 and 1 mM) at different time points. The samples were normalized by the culture OD<sub>600nm</sub> at each time point. Samples were run on an SDS-PAGE discontinuous 12% polyacrylamide gel and the polypeptides detected on the gel by Coomassie Blue staining.

Lane 1- no induction;

Lane 2- 2 hours following induction with 0.4 mM IPTG;

Lane 3- 3 hours following induction with 0.4 mM IPTG;

Lane 4- 4 hours following induction with 0.4 mM IPTG;

Lane 6- 2 hours following induction with 1 mM IPTG;

Lane 7- no induction;

Lane 8- 3 hours following induction with 1 mM IPTG;

Lane 9- 4 hours following induction with 1 mM IPTG.

MM- molecular weight marker, broad range (Bio-Rad). Arrow represent putative RIP1 recombinant protein.

The RIP2 protein has a molecular weight of 26 kDa as predicted from the primary sequence but when fused to the His•tag, RIP2 recombinant protein has a molecular weight of 29 kDa (*protparam* program, Gasteiger *et al.*, 2005). Figure 28 shows the total *E. coli* protein extracts at different time points present in an identical volume of culture when induced with two different concentrations of IPTG (0.4 mM and 1 mM final concentrations). The RIP2 recombinant protein pilot expression was found very similar to the RIP1 expression profile. However, in this case the difference between the strongly expressed band of the non induced samples (figure 28, lane 1 and 5) and the putative RIP2 recombinant protein is not clear (figure 28, lanes 2, 3, 4, 6, 7 and 8), which means that it is nor possible to assume clearly that the RIP2 recombinant protein is being produced.

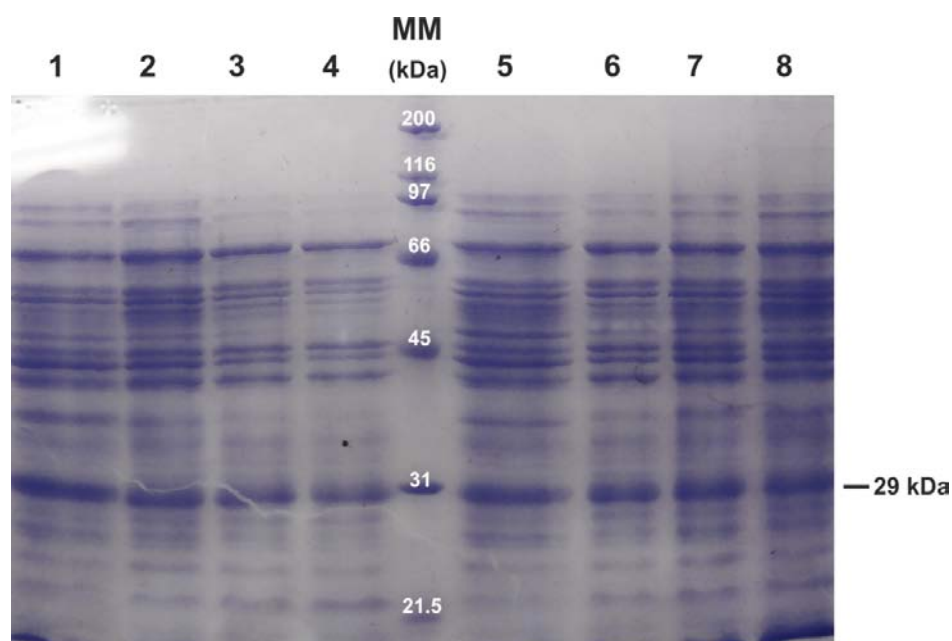


**Figure 28-** Analysis of RIP2 heterologous polypeptide expression in BL21(DE3)pLysE *E. coli* cells carrying the RIP2<sub>prSET</sub> plasmid following induction with two concentrations of IPTG (0.4 and 1 mM) at different time points. The samples were normalized by the culture OD<sub>600nm</sub> at each time point. Samples were run on an SDS-PAGE descontinuous 12% polyacrylamide gel and the polypeptides detected on the gel by Coomassie Blue staining.

Lane 1- no induction;

Lane 2- 2 hours following induction with 0.4 mM IPTG;

Lane 3- 3 hours following induction with 0.4 mM IPTG;

Lane 4- 4 hours following induction with 0.4 mM IPTG;

Lane 5- no induction;

Lane 6- 2 hours following induction with 1 mM IPTG;

Lane 8- 3 hours following induction with 1 mM IPTG;

Lane 9- 4 hours following induction with 1 mM IPTG.

MM- molecular weight marker, broad range (Bio-Rad). Arrow represent putative RIP2 recombinant protein.

Assuming that the band of expected molecular weight in the induced samples is RIP2 recombinant protein, it is possible to observe that the highest amount of putative RIP2 recombinant protein was observed two hours following induction (figure 28, lanes 2 and 5). Similarly to the RIP1 protein expression profile, a higher amount of RIP2 recombinant protein was produced following induction with 1 mM IPTG (figure 28).

To test if the proteins that appeared following induction were indeed due to RIP1 and RIP2 recombinant protein expression and not due to the expression of a bacterial protein of the same molecular weight, a new expression protocol was conducted using *E. coli* cells harbouring the prSET empty vector as a negative control. By analysis of

figure 29, it is possible to observe a difference between the band profile of the induced empty vector (figure 29, lane 3) and the band generated an induced RIP1 recombinant protein culture (figure 29, lane 6). However, this is not the case of *RIP2*, where no differences could be detected when the RIP2 induced expression profile (figure 29, lane 9) was compared with the induced empty vector profile (figure 29, lane 3).

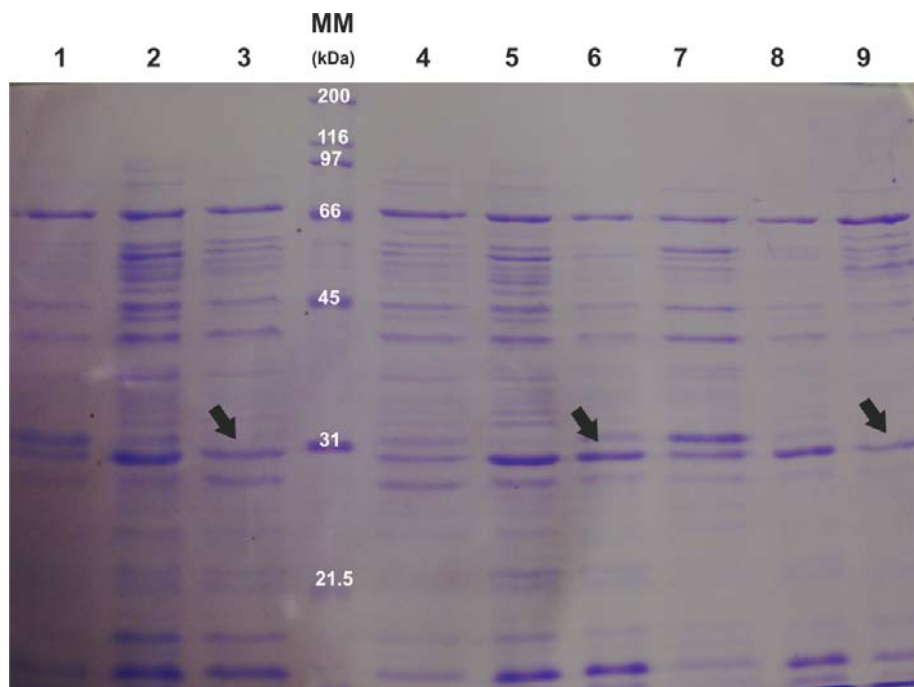


**Figure 29-** Analysis of the difference between RIP1<sub>pRSET</sub>, RIP2<sub>pRSET</sub> and pRSET expression profiles following induction with 1 mM IPTG for 3 hours. The samples were normalized by the culture OD<sub>600nm</sub> at each time point. Samples were run on an SDS-Page discontinuous 12% polyacrylamide gel and the polypeptides detected on the gel by Coomassie Blue staining.

Lane 1, pRSET, at the time of induction;

Lane 2- pRSET, no induction, sample taken at the same time as the induced one;

Lane 3- pRSET induced;

Lane 4, RIP1<sub>pRSET</sub>, at the time of induction;

Lane 5- RIP1<sub>pRSET</sub> no induction, sample taken at the same time as the induced one;

Lane 6- RIP1<sub>pRSET</sub> induced;

Lane 7, RIP2<sub>pRSET</sub>, at the time of induction;

Lane 8- RIP2<sub>pRSET</sub> no induction, sample taken at the same time as the induced one;

Lane 9- RIP2<sub>pRSET</sub> induced.

MM- molecular weight marker, broad range (Bio-Rad). Black arrows indicate a band with the same molecular weight of RIP1 RIP2 recombinant protein.

Taking together the results, it is not possible to assume clearly that the recombinant RIP proteins are being expressed, especially the RIP2 recombinant protein. Nevertheless, when comparing to both RAD and DIV protein profile expression (figure



17 and 20), the amount of RIP1 recombinant protein and putative RIP2 recombinant protein expressed was found significantly lower.

According to figure 29, a small amount of RIP1 recombinant protein appeared to be produced. Thus, a purification protocol was conducted with a culture of cells expressing the RIP1 recombinant protein. A RAD recombinant protein induced sample was used as positive control. As seen in figure 30 (lane 2), no amount of purified RIP1 recombinant protein was detected. This result could have three explanations: the amount of putative purified RIP1 recombinant protein might not be sufficient to be detected using Coomassie blue staining; the RIP1 recombinant protein expressed could be in an insoluble form or RIP1 is not expressed.

The expression protocol of the recombinant RIP proteins needs to be optimized. If, as the results indicate, there is no expression of RIP2 recombinant protein in *E. coli*, another expression system must be used. Concerning RIP1, it is possible that a small amount of recombinant protein is being generated, however, a cellular fractioning method needs to be performed to determine whether the RIP1 protein is in a soluble or insoluble form. Also, the purification needs to be optimised to ensure that enough amount of protein is available to use in the DNA-binding assay.

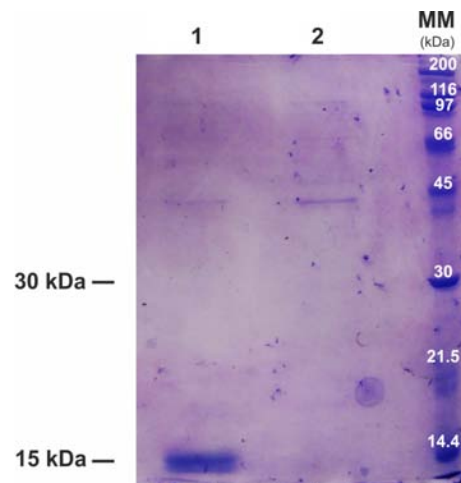


**Figure 30-** Analysis by SDS-PAGE of the purified RIP1 recombinant protein obtained using TALON affinity resin and elution by a drop in pH. RAD induced culture was used as positive control. Samples were run on an SDS-Page descontinuous 15% polyacrylamide gel and the polypeptides were detected on the gel by Coomassie Blue staining.

Lane 1- RAD recombinant protein eluate fraction;

Lane 2- RIP1 recombinant protein eluate fraction.

MM- molecular weight marker, broad range (Bio-Rad). Arrows represent RIP1 and RAD recombinant proteins.

### 3.4 DNA-binding affinity assay

One of the objectives of this work was to use the Electrophoretic Mobile Shift Assay (EMSA) to study the binding affinity of the RAD, DIV and RIP recombinant proteins for the same DNA target sequence and also to test the ability of these proteins to form a multi-protein complex *in vitro*. However, due to the results showed on the previous section, no RIP recombinant protein was obtained. Therefore, the DNA binding assay focused only on the binding ability of RAD and DIV recombinant proteins to target the same DNA sequence. The EMSA assay is based upon the observation that the migration rate of stable protein-DNA complexes through polyacrylamide gels is different from unbound DNA. The speed at which different molecules move through the gel is determined by their size and charge (Garner and Revzin, 1981).

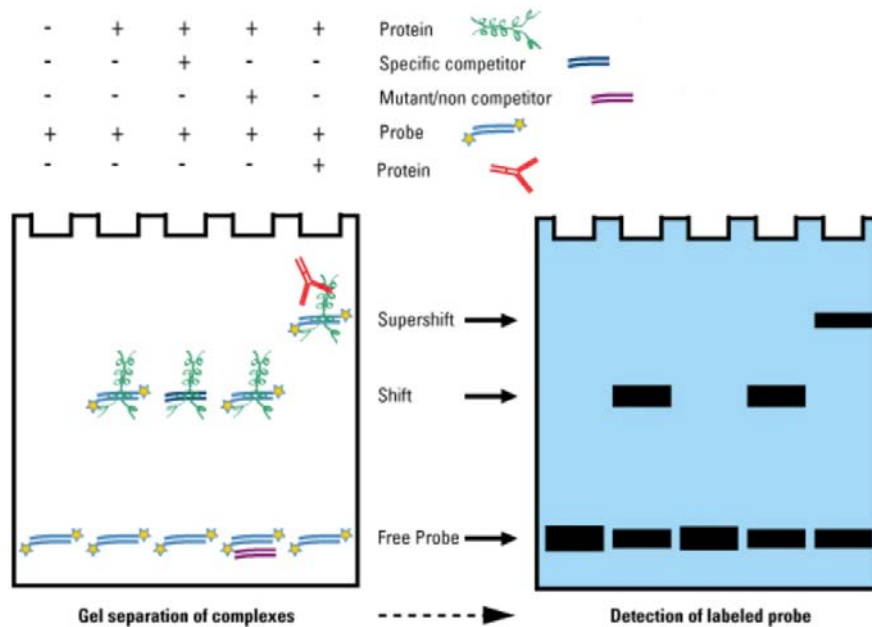


**Figure 31-** Overview of the Gel Shift Assay Method. The EMSA is based on the principle that the migration rate of stable protein-DNA complexes through polyacrylamide gels is different from unbound DNA. In the binding reaction, if a protein binds to a labeled DNA probe a shift is observed in the gel. Adding increasing amounts of competitive unlabeled DNA probe to the reaction allows the evaluation of the specificity of the DNA-protein interaction (if the interaction is specific, the complex DNA-protein should disappear as the amount unlabeled of probe increases). Adding a nonspecific competitor provides an excess of nonspecific sites to adsorb proteins that will bind to any general DNA sequence, this enhances the efficacy of the specific DNA-protein interaction. The EMSA assay could also be used to study protein-protein interactions. If a second protein interacts with the DNA-protein complex a super-shift is observed in the gel. Adapted from Hellman and Fried (2007).

Assuming that the protein is capable of binding to the fragment, the lane with protein and probe will contain another band that represents the larger, less mobile complex of nucleic acid probe bound to protein, which is 'shifted' up on the gel (since it has moved more slowly) (Garner and Revzin, 1981) (figure 31). An important element of the EMSA assay is the addition of a nonspecific competitor (Hellman and Fried, 2007) (figure 31). Nonspecific competitor is any irrelevant, unlabeled nucleic acid used as a blocking/quenching agent in the binding reaction to minimize the binding of nonspecific proteins to the labeled target DNA (Fried and Crothers, 1981). The most common nonspecific competitors used in DNA gel shift assays are sonicated salmon sperm DNA and poly (dI•dC). These repetitive fragments or polymers provide an excess of nonspecific sites to adsorb proteins that will bind to any general DNA sequence. A common test to evaluate the affinity of the protein to the DNA probe is to add increasing amounts of unlabeled probe to the reaction (figure 31). In this case, when adding increasing amounts of unlabeled probe the DNA-protein complex should become lesser and lesser visible in the gel (Kozmik *et al.*, 1990). The EMSA assay also allows discrimination of protein-protein interactions and competition between different proteins for the same DNA target. A super-shift is visible in the gel when two or more proteins are able to form a multi-protein complex with the DNA probe. If a protein of different molecular weight is able to compete for the probe a different shift should be observable in the gel (Hellman and Fried, 2007). Nucleic acids can be labeled with radio-isotopes (Maxam and Gilbert, 1977), covalent or non-covalent fluorophores (Forwood and Jans, 2006) or digoxigenin (Kang *et al.*, 2005) and can be detected by autoradiography, fluorescence imaging, chemiluminescent imaging and/or chromophore deposition, respectively (Hellman and Fried, 2007).

In a previous work, a Random Binding-Site Selection was performed to define the DNA consensus binding site of DIV. All the nucleotides obtained contained the sequence GATAA. Therefore, a probe was constructed containing this DNA consensus sequence. An EMSA assay was then performed not only to test if RAD recombinant protein is able to bind to the probe (figure 32a), but also to test if the RAD recombinant protein is able to form a multi-protein complex with DIV (figure 32c) or able to disrupt the DIV-probe complex (figure 32b).

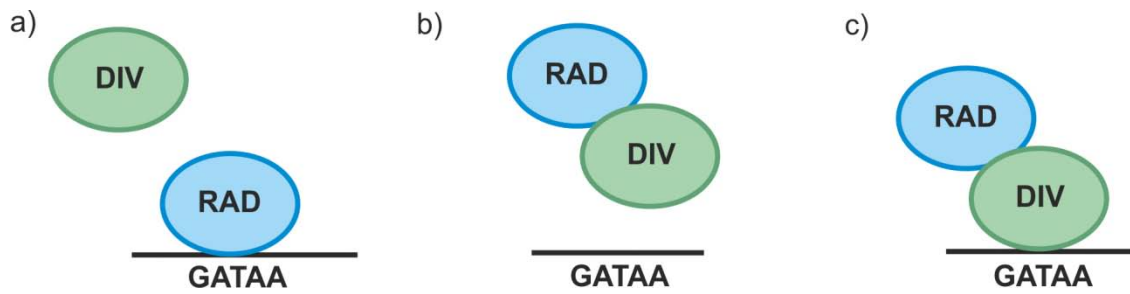


**Figure 32-** Potential mechanisms of molecular antagonism of RAD over DIV tested using the EMSA. **a)** RAD might bind to the DIV DNA binding site; **b)** RAD might sequester DIV, inhibiting the binding to the DNA element; and **c)** RAD and DIV might be forming a transcriptional complex that prevents DIV from activating transcription of target genes.

There are several factors that affect the strength and specificity of DNA-protein interactions, including the ionic strength and pH of the binding buffer, the presence of nonionic detergents, glycerol or carrier proteins or the presence/absence of divalent cations (Kozmik *et al.*, 1990). In this assay, three binding buffers were used:

- **Buffer 1-** 20 mM HEPES pH 7.6; 1 mM EDTA; 12.5 mM  $(\text{NH}_4)_2\text{SO}_4$ ; 1 mM DTT; 0.25% (v/v) *Tween*; 40 mM KCl.
- **Buffer 2-** 12.5 mM Tris-HCl pH 8.0; 1 mM EDTA; 40 mM KCl; 1 mM DTT; 0.25% (v/v) *Tween*.
- **Buffer 3-** 12.5 mM HEPES pH 7.6; 1 mM EDTA; 35 mM NaCl; 1 mM DTT; 10 mM  $\text{MgCl}_2$ ; 1 mM spermidine.

The buffers differed in pH (7.6-8), in the presence or absence of *Tween* (a nonionic detergent), the presence and absence of spermidine (a carrier protein) and in the presence or absence of  $\text{Mg}^{2+}$  (divalent cation). Poly(dI•dC) was added as a nonspecific competitor to each reaction.

If somehow RAD recombinant protein was capable of binding to the probe, a RAD-probe complex had to be visible on the gel, however by analysing figure 33, it is possible to observe that RAD was not able to bind to the probe in any of the three different binding buffers tested (figure 33, lanes 2-5). As expected, DIV formed a complex with the probe when using the three different binding buffers (figure 33, lanes 6-8). When mixing the probe, RAD and DIV recombinant proteins a complex was

formed with the same size of DIV-DNA complex (figure 33 lane 8). The shift of this band is similar to the shift when using only DIV protein in the reaction implying that RAD does not bind to the DIV-DNA complex nor able to disrupt it.

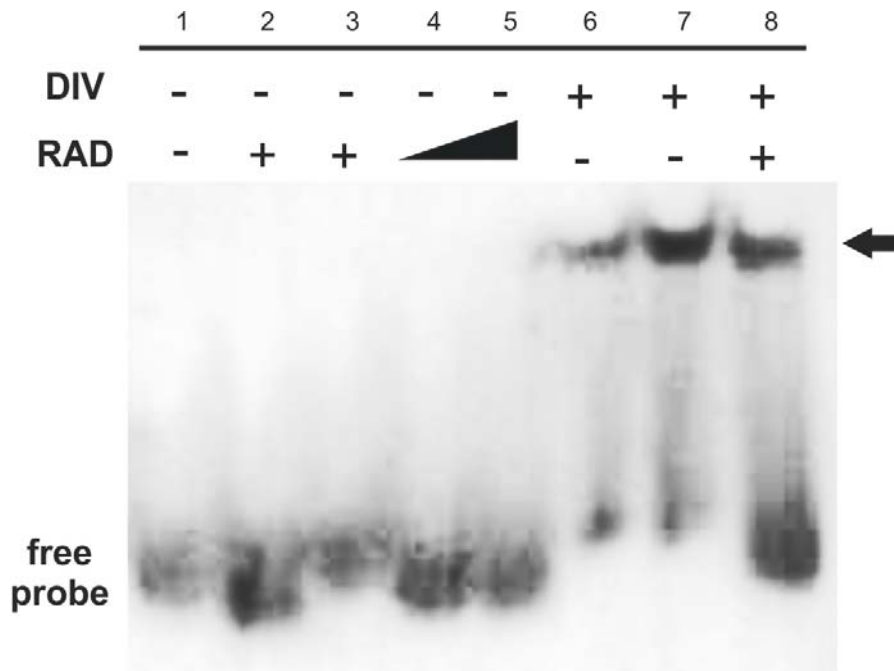


**Figure 33-** Analysis by EMSA of the DNA binding affinity of RAD and DIV recombinant proteins for the probe (digoxigenin labelled) containing the DNA binding consensus of DIV. Mix samples were run in an 5% Native Page gel and the probe detected by DIG chemiluminescence.

- Lane 1- free probe;
- Lane 2- probe, RAD recombinant protein, buffer 3;
- Lane 3- probe, RAD recombinant protein, buffer 2;
- Lane 4- probe, RAD recombinant protein, buffer 1;
- Lane 5- probe, RAD recombinant protein, buffer 1;
- Lane 6- probe, DIV recombinant protein, buffer 1;
- Lane 7- probe, DIV recombinant protein, buffer 2;
- Lane 8- probe, RAD and DIV recombinant proteins, buffer 3.

The results described suggest that RAD and DIV are not able to interact *in vitro* and also that RAD does not inhibit DIV by competitively binding to its targets DNA. This DNA-binding assay needs to be repeated not only to optimise the gel-shift protocol but also to confirm the results obtained.

### 3.5 Yeast two-hybrid based assays

*In vitro* binding assays suggested that RAD and DIV do not interact directly, and a possibility arose that a common interaction partner could be mediating the molecular antagonism between RAD and DIV. As described previously, yeast two-hybrid screening of an *A. majus* cDNA floral library using RAD as bait allowed the identification of the RIP1 and RIP2 proteins. Interestingly the RIP proteins also were found to interact with DIV. In this study, and using the yeast two-hybrid system the nature of the interaction between RAD and DIV and the RIP proteins was further analysed.

The yeast two-hybrid system has been used extensively in plant research to analyse known interactions between proteins and to isolate new interaction partners. Examples of this are the studies of protein-protein interactions involved in a number of processes such as hormonal regulation (Zhang et al. 2009), floral development (Moon *et al.*, 1999), phytohormone signaling (Ballesteros *et al.*, 2001) or regulation of the cell cycle (Trémousaigue *et al.*, 2003). It is a system that offers a number of advantages over many of the biochemical procedures often used for the analysis of protein-protein interactions, one of which is that it is a technology relatively inexpensive since it avoids costly procedures such as antibody production and protein purification. Finally this system is often more sensitive than many *in vitro* techniques and could be more suited to the detection of weak or transient interactions (Causier and Davis, 2002). On the basis of the yeast two-hybrid assay, is the assumption that two non-functional halves of a transcription factor when brought together can reconstitute an active transcription factor. Widely used in yeast two-hybrid assays, the GAL4 transcription factor can be divided in two distinct domains: the activation domain (AD<sub>GAL4</sub>) that is responsible for transcription activation and the binding domain (BD<sub>GAL4</sub>), which is responsible for DNA binding. When interacting partners are fused to either the AD<sub>GAL4</sub> or BD<sub>GAL4</sub>, the GAL4 transcription factor is reconstituted promoting the transcription of reporter genes. The positive interaction can then be monitored by yeast growth in selective medium or using colorimetric assays (Fields and Song, 1989).

To perform the yeast two-hybrid assays, the *RIP1*, *RIP2*, *RAD* and *DIV open reading frames* were cloned in fusion with the activation domain of GAL4 into the

pGAD424 vector (*GAL4*<sub>(768-881)</sub> AD, *LEU2*) or in fusion with the binding domain of GAL4 into the pGBT9 vector (*GAL4*<sub>(1-147)</sub> DNA-BD, *TRP1*) (Bartel *et al.*, 1993) (figure 34). The yeast strain AH109 (*MATa trp1-901 leu2-3, 112 ura3-52 his3-200 gal4Δ gal80Δ LYS2::GAL1<sub>UAS</sub>-GAL1<sub>TATA</sub>-HIS3; GAL2<sub>UAS</sub>-GAL2<sub>TATA</sub>-ADE2; URA3::MEL1<sub>UAS</sub>-MEL1<sub>TATA</sub>-lacZ, MEL1*) was the chosen strain to conduct the yeast two-hybrid based assays. This strain has the *HIS3* and *LacZ* genes downstream of minimal promoters containing the GAL4 binding site (figure 34). The *LacZ* gene codes for β-galactosidase an enzyme that cleaves the disaccharide lactose into glucose and galactose. Adding specific lactose analogous it is possible to detect positive interactions by a colorimetric reaction. The *HIS3* gene codes for the imidazoleglycerol-phosphate dehydratase that catalyses the sixth step in histidine biosynthesis, enabling surviving of yeast cells in medium lacking histidine. (Feilotter *et al.*, 1994; West *et al.*, 1984).

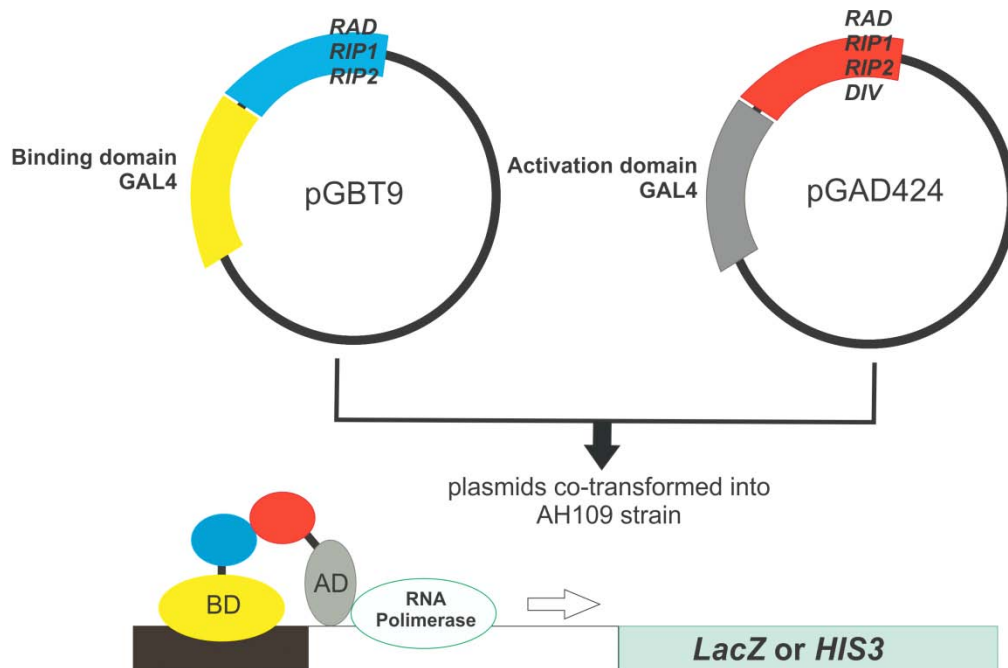


**Figure 34-** Yeast two-hybrid assay diagram. A yeast strain is co-transformed with prey (AD) and bait vectors (BD) fused to different proteins. If the proteins interact, the GAL4 transcription factor is reconstituted and transcription of the reporter genes, *LacZ* or *HIS3* is activated.

### 3.5.1 3-amino-1,2,4 triazole assay

The AH109 yeast strain is, however, able to grow in medium lacking histidine due to the production of minimal amounts of imidazoleglycerol-phosphate dehydratase (Causier and Davies, 2002). If the screening of the positive interacting partners is performed based on the ability of the yeast cells to grow in medium lacking histidine, the basal amount of imidazoleglycerol-phosphate dehydratase production has to be reduced to a minimum. 3-amino-1,2,4-triazole (3-AT) is a chemical compound that, when added to the medium, competes directly with imidazoleglycerol-phosphate dehydratase, suppressing the minimal biosynthesis of histidine (Brent and Finley, 1997). So, before testing the interaction in the yeast two-hybrid assay, AH109 yeast competent cells were transformed with the yeast vectors containing the available fusion proteins (RAD, DIV, RIP1 and RIP2 fused to either the AD<sub>GAL4</sub> or the BD<sub>GAL4</sub>) and plated onto appropriate selection medium supplemented with different final concentrations of 3-AT. Cells expressing with proteins fused to the AD<sub>GAL4</sub> domain grew in medium without leucine (-Leu) as observed in figure 35 (first column), whereas cells expressing proteins fused to the BD<sub>GAL4</sub> domain were capable of growing in medium lacking triptofan (-Trp) (figure 36, first column). However, every transformant also grew in medium lacking histidine (-His) (figure 35 and 36, second column), which confirmed the ability of this strain to grow in selective medium without histidine. Adding just 1 mM of 3-AT to the media, managed to abolish growth in selective medium without histidine (figure 36 and 37, respectively, third column from the left). According to previous work, adding 1-5 mM final concentration of 3-AT was sufficient to inhibit unspecific growth in selective medium (Brent and Finley, 1997), which is similar to the result here demonstrated. Thus, for further experiments using the *HIS3* as a reporter gene, the selective medium was supplemented with a final concentration of 3 mM 3-AT.



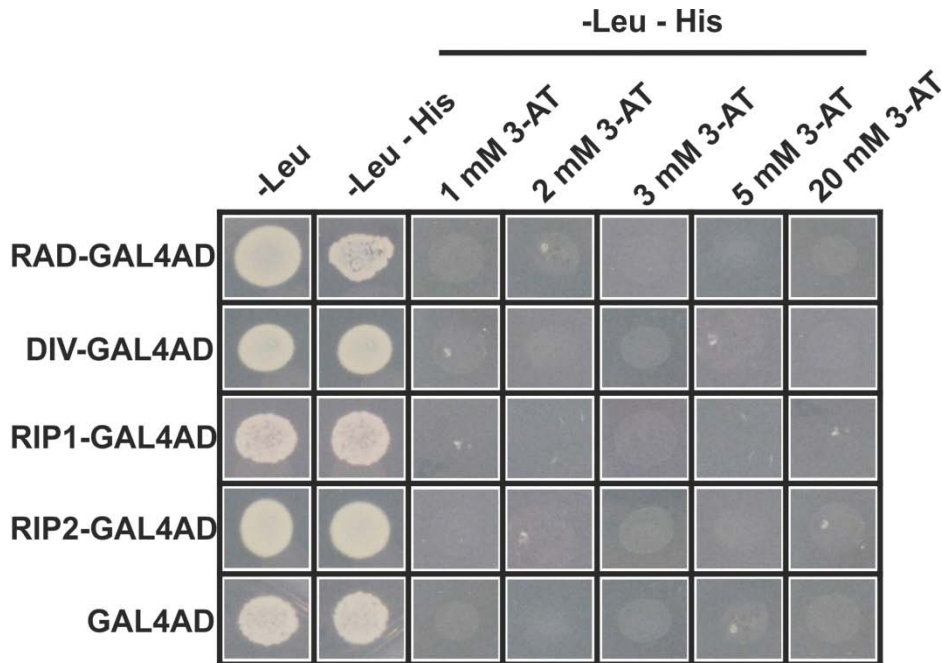


**Figure 35-** Analysis of yeast cell growth in media with and without 3-AT. AH109 yeast cells transformed with constructs containing the proteins fused to the AD<sub>GAL4</sub>, and these were able to grow in the selective media (-Leucine) and in media without histidine (-His). Adding 1 mM 3-AT was enough to abolish minimal growth in medium lacking histidine. Different final concentrations of 3-AT were used (1-20 mM).

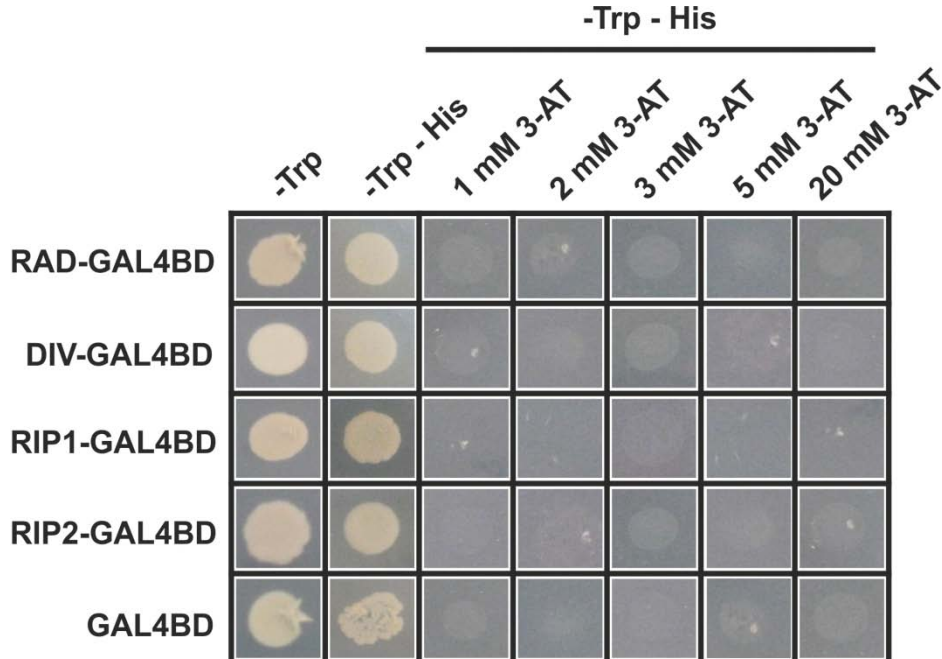


**Figure 36-** Analysis of yeast cell growth in media with and without 3-AT. AH109 yeast cells transformed with constructs containing the proteins fused to the BD<sub>GAL4</sub>, and these were able to grow in the selective media (-Tryptofan) and in media without histidine (-His). Adding 1 mM 3-AT was enough to abolish minimal growth in medium lacking histidine. Different final concentrations of 3-AT were used (1-20 mM).

### 3.5.2 RIP1 and RIP2 interact with RAD and DIV in a yeast two-hybrid assay

The conventional yeast two-hybrid assay requires the pair of possible interactors to be expressed in the same yeast cell. *RAD*, *DIV*, *RIP1* and *RIP2* cDNA cloned in the  $BD_{GAL4}$  or  $AD_{GAL4}$  vectors were co-transformed into AH109 yeast cells in all combinations. It is worth to mention, that *DIV* fused to the  $AD_{GAL4}$  was not used in this assay because it was able to alone activate the transcription of the reporter genes (data not shown), due to the presence of the transcriptional activation domain. To test whether the combined proteins were able to initiate transcription of the *HIS3* or *LacZ* reporter genes, co-transformants were plated on selection medium lacking leucine, triptofan, either with or without histidine. After incubation at 30°C for three days, the  $\beta$ -galactosidase activity was assayed by a colony-lift filter assay. In this assay, in the presence of  $\beta$ -galactosidase X-gal (lactose analogous) was cleaved yielding galactose and 5-bromo-4-chloro-3-hydroxyindole. The latter was then oxidized into 5,5'-dibromo-4,4'-dichloro-indigo, an insoluble blue product, allowing colorimetric detection.

Every co-transformant grew in the selective medium (lacking leucine and triptofan). However, only cells containing the combined interacting proteins grew in medium lacking histidine (figure 37). No growth was observed in the control transformants (protein- $BD_{GAL4}$ /empty vector- $AD_{GAL4}$  and empty vector- $BD_{GAL4}$ /protein- $AD_{GAL4}$ ) (figure 37a, b, c and d). *RAD*- $BD_{GAL4}$  fusion protein interacts with both *RIP1* and *RIP2*, but do not interact with itself or with *DIV* (figure 37d). *RAD*- $AD_{GAL4}$  is also capable of interacting with *RIP1* and *RIP2* (figure 37 b and c). Both *RIP1* and *RIP2* interact with *DIV* (figure 37 b and c). There are no evidences of homodimerization of *RAD*, *RIP1* or *RIP2* fusion proteins (figure 37b, c and d).

The  $\beta$ -galactosidase colony-lift filter assay demonstrated that all the interacting partners, tested positive for the *HIS3* reporter gene, were also able to activate the transcription of the *LacZ* gene (figure 37). However, in contradiction with the *HIS3* selection, a small blue spot was observed when testing *RIP1* homodimerization (figure 37b). This small amount of  $\beta$ -galactosidase activity could suggest a weaker homodimerization of *RIP1*, however, this result needs to be confirmed.

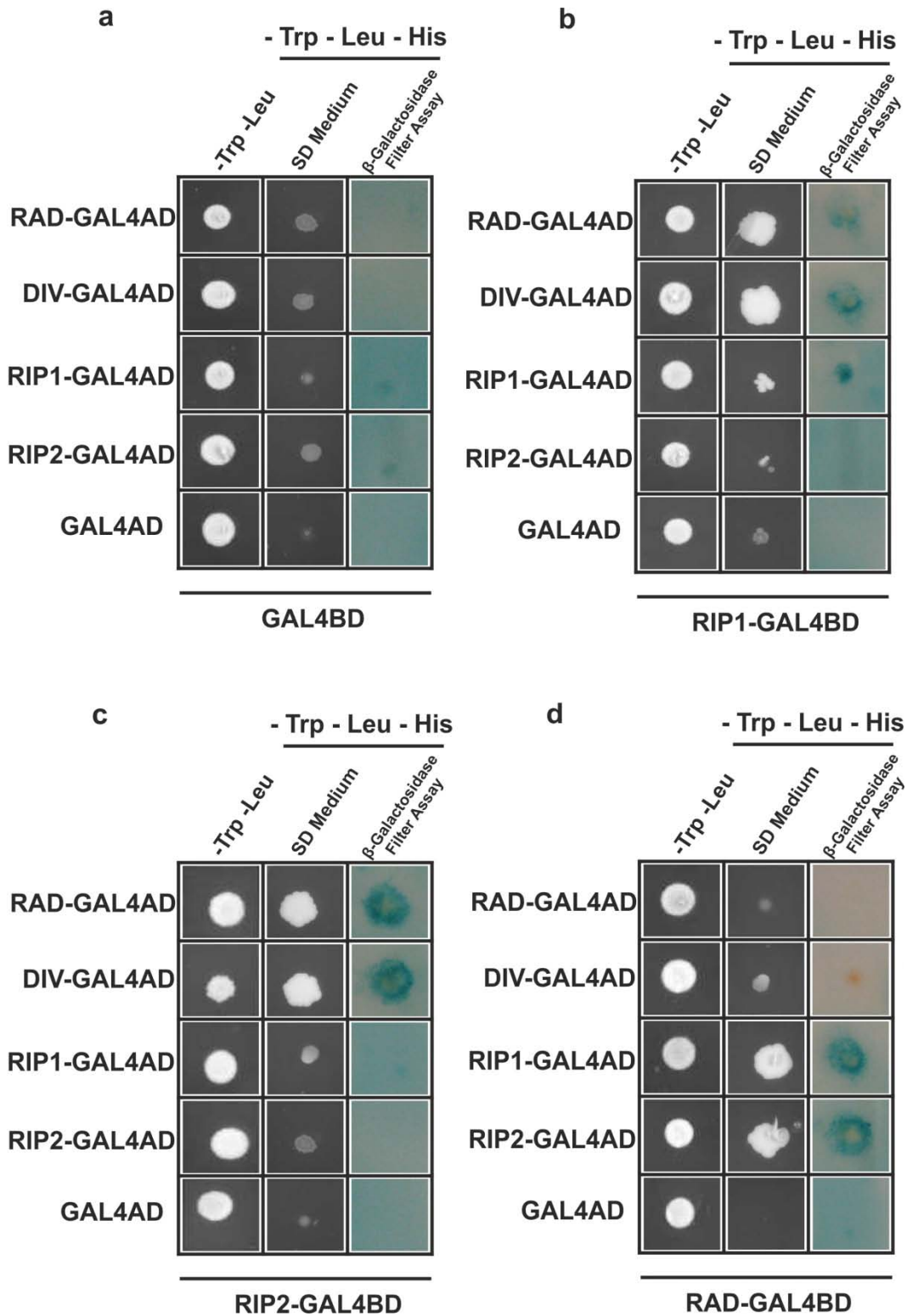


**Figure 37-** Analysis of the interaction between RAD, DIV, RIP1 and RIP2 proteins by growth in selective medium (-His) and by the  $\beta$ -galactosidase filter assay. **a)** colonies of co-transformed yeast with BD<sub>GAL4</sub> empty vector and the AD<sub>GAL4</sub> constructs; **b)** colonies of co-transformed yeast with RIP1-BD<sub>GAL4</sub> and the AD<sub>GAL4</sub> constructs; **c)** colonies of co-transformed yeast with RIP2-BD<sub>GAL4</sub> and AD<sub>GAL4</sub> vectors and **d)** colonies of co-transformed yeast with RAD-BD<sub>GAL4</sub> and the AD<sub>GAL4</sub> constructs.

These results not only confirm the previous assessment that RIP1 and RIP2 interact with RAD and DIV but also confirm the results obtained in the EMSA experiment, that RAD does not interact directly with DIV. From those results it is also possible to conclude that neither the RAD-BD<sub>GAL4</sub> fusion protein nor the RIP-BD<sub>GAL4</sub> fusion proteins were able to activate transcription by itself (no growth when the RAD-BD<sub>GAL4</sub>/AD<sub>GAL4</sub>, RIP1-BD<sub>GAL4</sub>/AD<sub>GAL4</sub>, RIP2-BD<sub>GAL4</sub>/AD<sub>GAL4</sub> were expressed in the same yeast cell), which could mean that these proteins do not have a transcriptional activation domain.

### **3.5.3 Determination of the interaction strength by the $\beta$ -galactosidase liquid assay**

The results described so far represent just a qualitative assessment of the interaction between the proteins, which translates in their ability to interact. So, after establishing which pairs of fusion proteins interacted, a quantitative  $\beta$ -galactosidase liquid assay was performed to quantify the interaction strength of each pair. This assay is based on the principle that the interaction strength is proportionally correlated with the transcription rate of *LacZ* gene. Thus, a stronger interaction generates a higher amount of  $\beta$ -galactosidase and its product, 5,5'-dibromo-4,4'-dichloro-indigo, when compared with a weaker interaction. In this quantitative assay, *ortho*-Nitrophenyl- $\beta$ -galactoside (ONPG) was used as substrate for  $\beta$ -galactosidase. All the fusion proteins combined with empty vectors showed the same amount of activity as the negative control (figure 38, 39 and 40). According to the results revealed in figure 38, the highest  $\beta$ -galactosidase activity was detected when RAD-AD<sub>GAL4</sub> fusion protein interacted with RIP2-BD<sub>GAL4</sub> fusion protein (47.9 miller units). The interaction between the RAD-BD<sub>GAL4</sub>/RIP2-AD<sub>GAL4</sub> pair gave the second highest  $\beta$ -galactosidase activity (29.9 miller units) followed closely by the RIP1-BD<sub>GAL4</sub>/RAD-AD<sub>GAL4</sub> pair (26.3 miller units) (figure 38). There was, however, an odd result that is worth mentioning. The lower  $\beta$ -galactosidase activity generated by the interaction of RAD-BD<sub>GAL4</sub>/RIP1-AD<sub>GAL4</sub>, only 5.8 miller units, is a amount five times lower than the RIP1-BD<sub>GAL4</sub>/RAD-AD<sub>GAL4</sub> but, nevertheless, five times higher than the negative control (1.1 miller units) (figure 38).

This lower value could be correlated with a structural fault during the GAL4 transcription factor functional assemble.

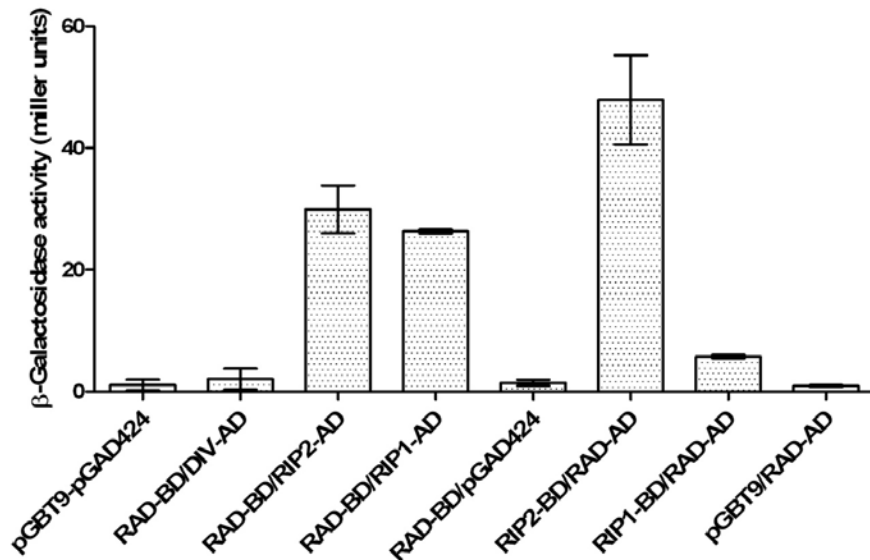


**Figure 38-**  $\beta$ -galactosidase quantitative liquid culture assay.  $\beta$ -galactosidase activity (miller units) was measured between RAD fusion proteins and its putative interaction partners tested. Each column represents the mean  $\beta$ -galactosidase activity of three independent colonies (three replica for experiment). (The scaled bar represents standart deviation). pGAD424/pGBT9 is the negative control.

The  $\beta$ -galactosidase activity generated by the interaction between DIV and the RIP proteins was significant but found weaker when compared with RAD (18.6 for RIP1 and 16.5 for RIP2) (figure 39). As expected, RAD did not interact directly with DIV (2,1 miller units). According to Kosugi and Ohashi (2002), an interaction of 25 miller units of  $\beta$ -galactosidase is considered a strong interaction whereas Moon *et al.* (1999) considers a strong protein interaction above 10 units. Thus, by comparing with previously published data, it is possible to infer that both RAD and DIV proteins have strong affinities for the RIP1 and RIP2 proteins.

The homodimerization ability of the RIP proteins was also tested. The results show clearly that neither RIP1 nor RIP2 formed homodimers. The amount of  $\beta$ -galactosidase activity generated when the proteins were tested for homodimerization was found very similar to the negative control, pGBT9/pGAD424 (1.1 miller units) (figure 40). Also, no activity was detected when RIP1 and RIP2 fusion proteins were tested for interaction. The results show clearly that RAD/RIP2 interaction is stronger

than the RAD/RIP1 interaction. Nonetheless, RAD appears to have a higher affinity with the RIP proteins than DIV. According to the results it is also possible to put aside the idea that RAD, RIP1 and RIP2 proteins are capable of homodimerization and the idea that RAD interacts with DIV.

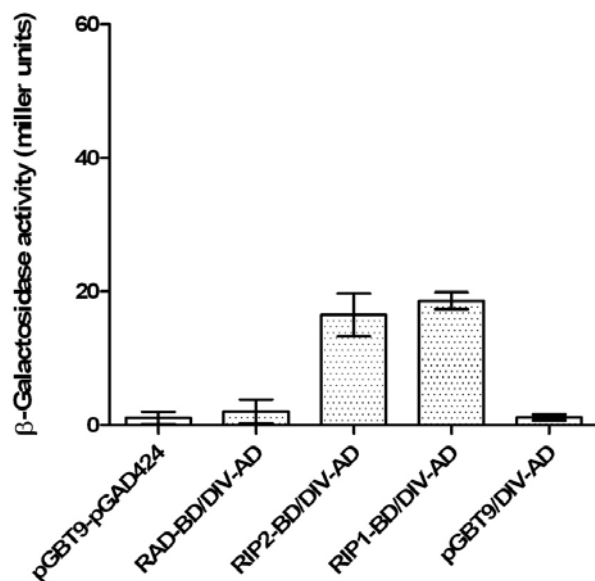


**Figure 39-**  $\beta$ -galactosidase quantitative liquid culture assay.  $\beta$ -galactosidase activity (miller units) was measured between DIV fusion proteins and its putative interaction partners tested. Each column represents the mean  $\beta$ -galactosidase activity of three independent colonies (three replica for experiment). (The scaled bar represents standard deviation). pGAD424/pGBT9 is the negative control.

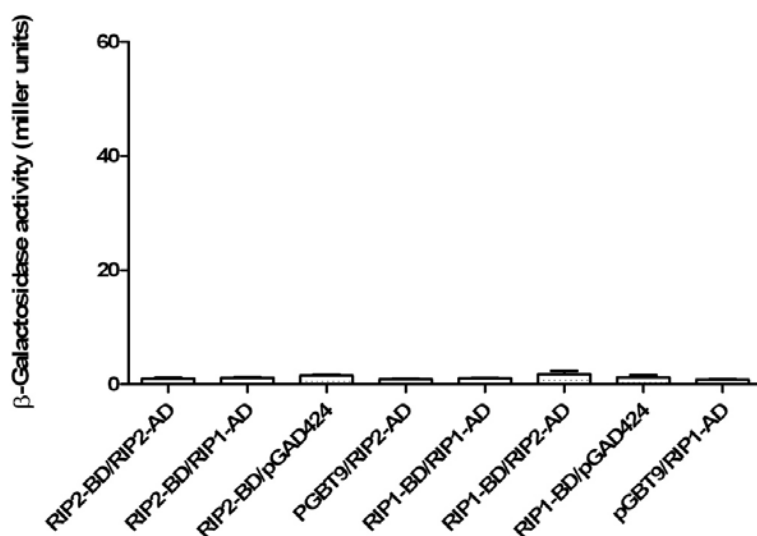


**Figure 40-**  $\beta$ -galactosidase quantitative liquid culture assay.  $\beta$ -galactosidase activity (miller units) was measured to test the homo and heterodimerization ability of the RIP fusion proteins. Each column represents the mean  $\beta$ -galactosidase activity of three independent colonies (three replica for experiment). (The scaled bar represents standard deviation). pGAD424/pGBT9 is the negative control.

## 3.6 Sub-cellular localisation of RAD, DIV and RIP proteins

When testing for protein-protein interactions it is important to consider the fact that two interacting partners could not be able to interact *in vivo* due to different sub-cellular localizations. Thus, to establish whether the RAD and DIV proteins are able to interact with the RIP proteins in the same sub-cellular compartment, the ORFs of the four genes were cloned in fusion with fluorescent protein tags, and the sub-cellular localisation detected by fluorescence microscopy. Sub-cellular localisation assays in *N. benthamiana* are very common in transient expression experiments (Walter *et al.*, 2004; Bracha-Dori *et al.*, 2004; Bhat *et al.*, 2006; Citovsky *et al.*, 2006; Bowen *et al.*, 2010). The fluorescence emission of the fluorescent proteins does not require any co-factor or substrate, which enables its fluorescence to be observed without making any pre-treatment of the tissue.

Using gateway-based technology *RIP1* and *RIP2* ORFs were cloned in fusion with *GFP6* in the pMDC43 vector, while *RAD* and *DIV* were cloned in fusion with the *EYFP* gene in the pH7WGY2 plasmid. The fusion proteins were then transiently expressed in *N. benthamiana*, after *A. tumefaciens* transformation and the fluorescence emission detected by epifluorescence or fluorescence confocal microscopy.

### 3.6.1 Plasmids construction

An experimental plan was designed to fuse *RIP1*, *RIP2*, *RAD* and *DIV* ORFs to specific fluorescent-tagged vectors using Gateway technology. The Gateway technology provides a rapid and highly efficient way to clone DNA sequences into multiple vector systems for functional analysis and protein expression (Hartley *et al.*, 2000). It is a universal cloning method based on the site-specific recombination properties of the bacteriophage lambda. Lambda based recombination is catalysed by a mixture of enzymes that bind to specific sequences (*att* sites), bring together the target sites, cleave them, and covalently attach the DNA (Landy, 1989).

The first step on this process is to generate PCR products suitable for use as substrates for the recombination reaction with a donor vector. Accordingly, *attB* sites are introduced to the ORFs flanking sites by PCR amplification. Two recombination

reactions constitute the basis of the Gateway Technology as described in figure 41: the BP reaction, where the recombination of an *attB* substrate (*attB*-PCR product or a linearized *attB* expression clone) with an *attP* substrate (donor vector) occurs to create an *attL*-containing entry clone (catalysed by the BP Clonase enzyme); and the LR reaction, where the recombination of an *attL* substrate (entry clone) with an *attR* substrate (destination vector) to create an *attB*-containing expression clone (catalyzed by LR Clonase enzyme) (Hartley *et al.*, 2000).

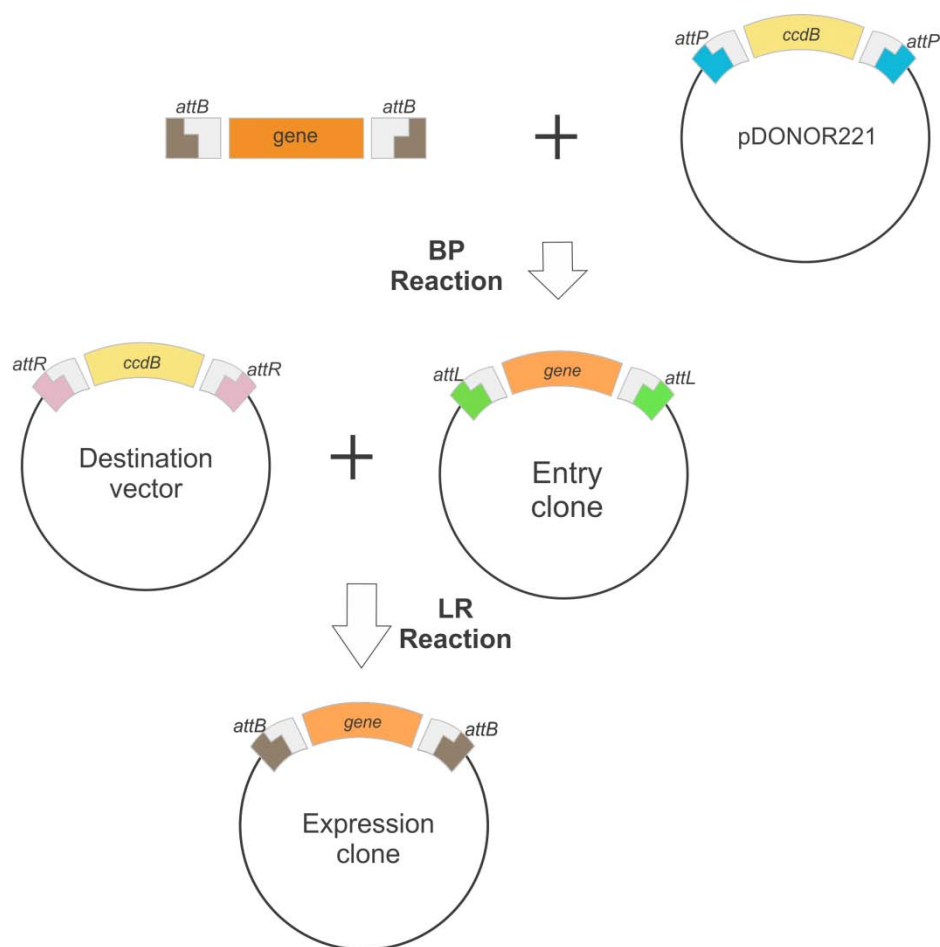


**Figure 41-** Gateway cloning procedure. Two recombination reactions constitute the basis of the Gateway Technology: the BP reaction that facilitates recombination of an *attB* substrate (*attB*-PCR product) with an *attP* substrate (donor vector) to create an *attL*-containing entry clone catalysed by the BP Clonase II enzyme; and the LR Reaction that facilitates recombination of an *attL* substrate (entry clone) with an *attR* substrate (destination vector) to create an *attB*-containing expression clone. This reaction is catalyzed by LR Clonase II enzyme mix.

The amplification of the gene ORFs for Gateway cloning was divided in two distinct PCR reactions. Concerning the first PCR reaction, no unspecific amplification



occurred (figure 42, lane 1). The PCR product of the first amplification reaction and *primers* containing the complete *attB* sequence were used for a new PCR amplification reaction (figure 42, lane 2). To prevent non-specific amplification of the PCR product, a control reaction (without *attB* primers) was set-up for each amplification. According to figure 42, the ORFs were significantly amplified when compared to the control reactions.

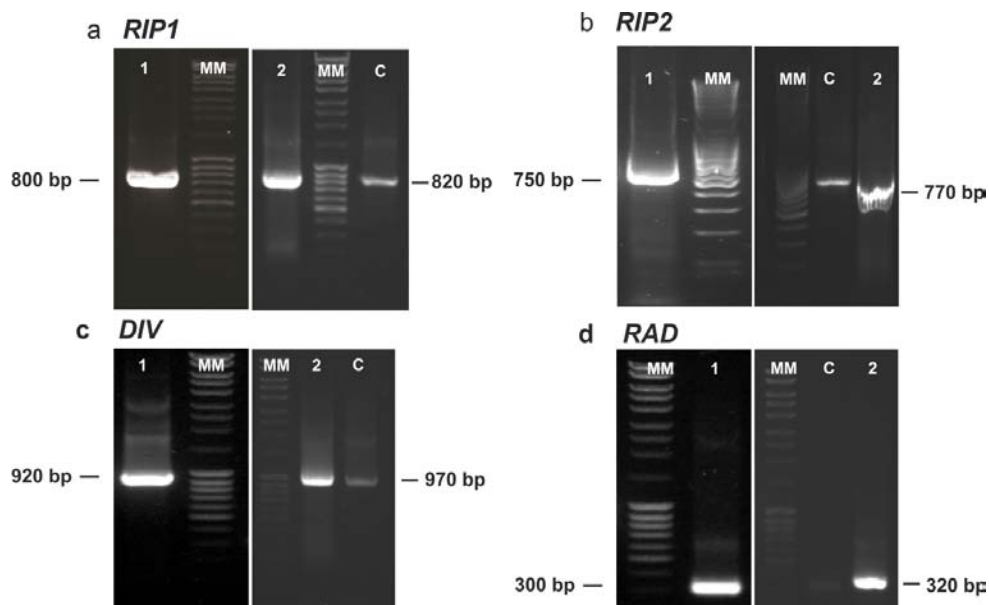


**Figure 42-** PCR amplification of the *RAD*, *DIV*, *RIP1* and *RIP2* ORFs for Gateway cloning was divided in two different amplification reactions. In the first PCR reaction the ORFs were amplified whereas in the second reaction the *attB* are introduced in the flanking sites of the ORFs. C- control of the second PCR reaction (no *attB* primers). A 10 kb ladder (MM, Fermentas) was run in each of the 1% agarose gels.

a) *RIP1* ORF amplification:

Lane 1- product of the first PCR reaction (800 bp fragment amplification);

Lane 2- product of the second PCR reaction (820 bp fragment amplification);

b) *RIP2* ORF amplification:

Lane 1- product of the first PCR reaction (750 bp fragment amplification);

Lane 2- product of the second PCR reaction (770 bp fragment amplification);

c) *DIV* ORF amplification:

Lane 1- product of the first PCR reaction (920 bp fragment amplification);

Lane 2- product of the second PCR reaction (970 bp fragment amplification);

d) *RAD* ORF amplification:

Lane 1- product of the first PCR reaction (300 bp fragment amplification);

Lane 2- product of the second PCR reaction (320 bp fragment amplification).

The BP reaction was then performed to recombine the flanked *attB* product with the pDONOR vector. The reaction mixture was then used to transform XL1-Blue *E. coli* competent cells and putative positives were identified as the colonies were able to grow in selective medium (LB supplemented with kanamycin). A colony PCR was then conducted to screen for positive clones using pDONOR specific forward and reverse

*primers* (figure 43). A control reaction was also performed using the same set of *primers* and the empty vector as template (1500 bp product expected size).

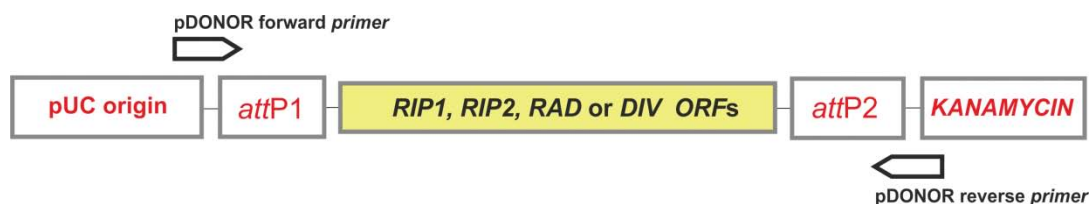


**Figure 43-** Primers chosen for the screening of  $RIP1_{pDONOR}$ ,  $RIP2_{pDONOR}$ ,  $RAD_{pDONOR}$ ,  $DIV_{pDONOR}$ , positive clones by colony PCR amplification.

As described in figure 44a only the amplified product of clone 13 fitted with the expected size for a *RIP1* ORF successful amplification (1080 bp size DNA fragment). Clones 1, 2-7, 9-11, 13, 14 and 16 showed the expected amplified product size (1020 bp) for a positive amplification of the *RIP2* ORF (figure 44b). The colony screening for amplified *DIV* ORF generated only one amplified product with the expected size (1220 bp) (figure 44c, lane 5). The same was found in the *RAD* colony screening where just one positive amplification was observed (figure 44d, lane 6, 600 bp amplified DNA fragment). Plasmids of clones 13 ( $RIP1_{pDONOR}$ ), 1 ( $RIP2_{pDONOR}$ ), 7 ( $DIV_{pDONOR}$ ) and 6 ( $RAD_{pDONOR}$ ) were isolated and sent for sequencing. Sequencing results showed that the ORF of all genes were cloned in the correct orientation with no PCR errors.

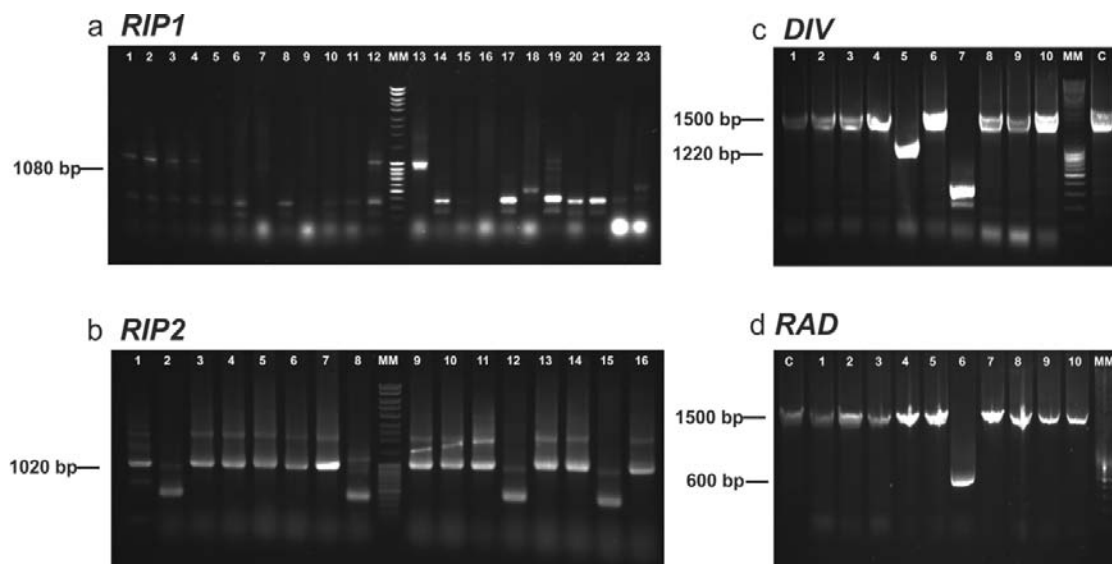


**Figure 44-** BP reaction. Following transformation with the reaction mixtures, *E. coli* XL1-Blue cells were plated in selective medium (LB with kanamycin). A colony PCR was then conducted to screen for positive clones. A 10 kb molecular marker (MM, Fermentas) was run in each of the 1% agarose gels. C- pDONOR amplification (control).

- a) *RIP1* clones screening, lanes 1-23 (the positive clone generated a 1080 bp amplified product);
- b) *RIP2* clones screening, lanes 1-16 (the positive clones generated a 1020 bp amplified product);
- c) *DIV* clones screening, lanes 1-10 (the positive clone generated a 1220 bp amplified product);
- d) *RAD* clones screening, lanes 1-10 (the positive clone generated a 600 bp amplified product).

The LR reaction was then conducted to recombine  $RIP1_{pDONOR}$  and  $RIP2_{pDONOR}$  constructs with the pMDC43 vector, and  $DIV_{pDONOR}$  and  $RAD_{pDONOR}$  constructs with the pH7WGY2 vector. Following transformation in *E. coli* XL1-Blue competent cells and growth in selective medium (LB supplemented with hygromycin 50  $\mu\text{g mL}^{-1}$ ), positive clones were screened by colony PCR using the vectors specific forward and reverse primers (figure 45).

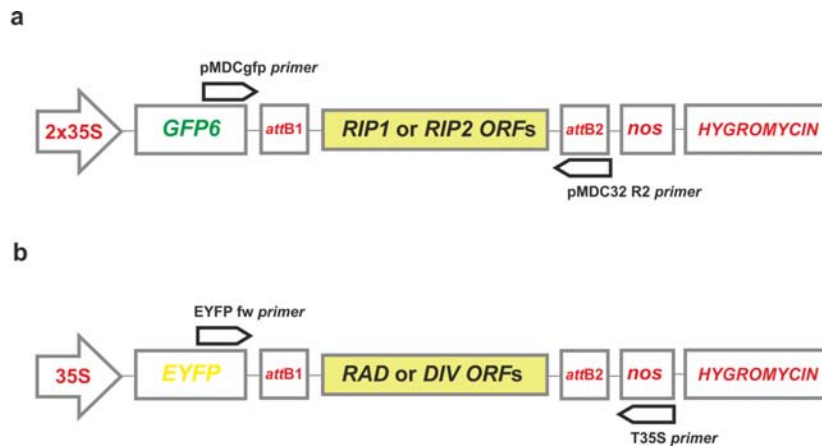


**Figure 45-** Primers used in a colony PCR amplification performed to screen *E. coli* colonies for: a)  $RIP1_{pMDC43}$ ,  $RIP2_{pMDC43}$ ; and b)  $RAD_{pH7WGY2}$ ,  $DIV_{pH7WGY2}$ .

A control PCR amplification was also performed using the same set of primers and the empty vectors as template (a 1750 bp product size for both plasmids). Concerning *RIP1*, only one clone grew in the selective medium, however, the amplification product size generated by PCR amplification was similar to the expected size (800 bp) (figure 46a, lane 1). In the case of *RIP2*, four amplification products were observed with the predictable size (740 bp, figure 46b, lanes 7, 9, 10 and 14). From the three clones tested only two proved to be positive for the amplification of the *DIV* ORF (1089 bp, figure 46c, lanes 1 and 2). All the seven *RAD* clones that grew in selective medium proved to be positive (447 bp) (figure 46d, lanes 1-7). Plasmids of clones 1

(RIP1<sub>pMDC43</sub>), 7 (RIP2<sub>pMDC43</sub>), 1 (DIV<sub>pH7GWY2</sub>) and 1 (RAD<sub>pH7GWY2</sub>) were isolated and sent for sequencing. Sequencing results showed that the ORF of all genes were cloned in the correct orientation with no PCR errors.

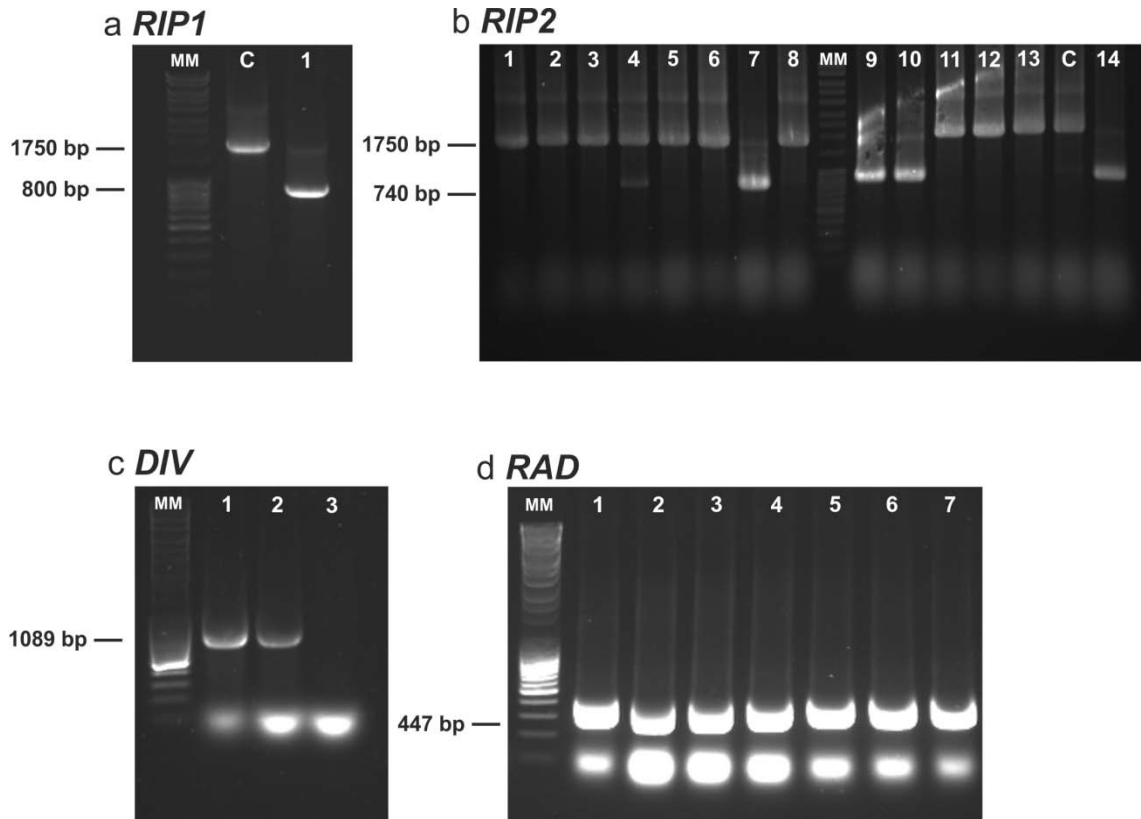


**Figure 46-** LR reaction. Following transformation with the reaction mixtures, *E. coli* XL1-Blue cells were plated in selective medium (LB plus hygromycin). A colony PCR amplification was then conducted to screen for positive clones. A 10 kb molecular marker (MM, Fermentas) was run in each of the 1% agarose gels. C- pMDC43 or pH7WGY2 amplification (control).

**a)** *RIP1* clone screening (pMDC43), lane 1 (the positive clone generated a 800 bp amplified product);  
**b)** *DIV* clones screening (pH7WGF2), lanes 1-14 (the positive clones generated a 740 bp amplified product);  
**c)** *RIP2* clones screening (pMDC43), lane 1 and 2 (the positive clones generated a 1089 bp amplified product);  
**d)** *RAD* clones screening (pH7WGF2), lanes 1-7 (the positive clone generated a 447 bp amplified product).

### 3.6.2 Transient expression in *N. benthamiana*

For transient expression in *N. benthamiana*, competent cells of the EHA105 *A. tumefaciens* strain were transformed with the above described constructions (RIP1<sub>pMDC43</sub>, RIP2<sub>pMDC43</sub>, DIV<sub>pH7GWY2</sub> and RAD<sub>pH7GWY2</sub>). Positive clones were screened in a colony PCR using the vectors specific forward and reverse *primers* (figure 45). All

the colonies screened for  $RIP1_{pMDC43}$  were positive (800 bp expected size, figure 47a). Despite the weaker signals of the  $RIP2_{pMDC43}$  amplification product in the gel, all the amplified products were of the expected size (740 bp, figure 46b). All  $RAD_{pH7GWY2}$  and  $DIV_{pH7GWY2}$  clones were positive (figure 46c and d. respectively).

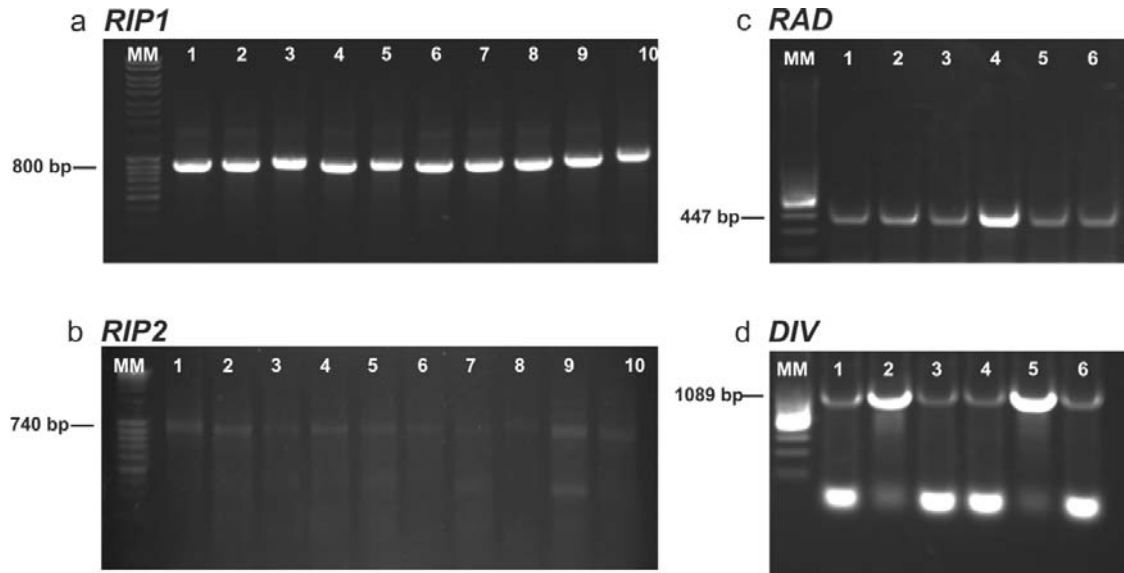


**Figure 47-** Screening of *Agrobacterium* colonies by PCR amplification. *Agrobacterium* competent cells were transformed with  $RIP1_{pMDC43}$ ,  $RIP2_{pMDC43}$ ,  $DIV_{pH7GWY2}$  and  $RAD_{pH7GWY2}$  vectors and plated in selective medium (LB plus rifampicin and kanamycin or streptomycin) A colony PCR amplification was then performed to screen for positive clones. A 10 kb molecular marker (MM, Fermentas) was run in each of the 1% agarose gels.

- a)**  $RIP1$  clones screening ( $pMDC43$ ), lanes 1-10 (amplification of the positive clones generated a 800 bp amplified product);
- b)**  $RIP2$  clones screening ( $pMDC43$ ), lanes 1-10 (amplification of the positive clones generated a 1089 bp amplified product);
- c)**  $RAD$  clones screening ( $pH7WGF2$ ), lanes 1-6 (amplification of the positive clone generated a 447 bp amplified product);
- d)**  $DIV$  clones screening ( $pH7WGF2$ ), lanes 1-6 (amplification of the positive clones generated a 740 bp amplified product).

Expanded leaves (fourth to sixth) of *N. benthamiana* plants were infiltrated with an overnight culture of *A. tumefaciens* EHA105 containing the above-mentioned constructs. Infiltrated plants were kept in obscurity and the infiltrated leaves analysed under the microscope after 48 hours. Sections (0.5 cm<sup>2</sup>) were cut from leaves, distal to the primary infiltration site, and sections were mounted in water and analyzed for *GFP6* or *EYFP* expression by epifluorence or confocal microscopy. A control transformation was prepared, by inoculating *N. benthamiana* with *A. tumefaciens* harboring a vector expressing *GFP6*. According to Curtis and Grossniklaus (2003), the GFP6 protein does

not have a nuclear localization signal, however, GFP is a small proteins and should be visible in the entire cell including the nucleus.

GFP6 protein was excited at 488 nm and emission was detected at 507 nm. Epifluorescence microscopy imaging analysis revealed that in the control GFP6 signal was detected in the entire cell (figure 48a). GFP6-RIP1 fusion protein was located primarily in the nucleus, but the signal was also observed in the cytoplasm and in a filamentous network surrounding the nucleus (could correspond to transport of the GFP6-RIP1 through the endoplasmatic reticulum) (figure 48b).

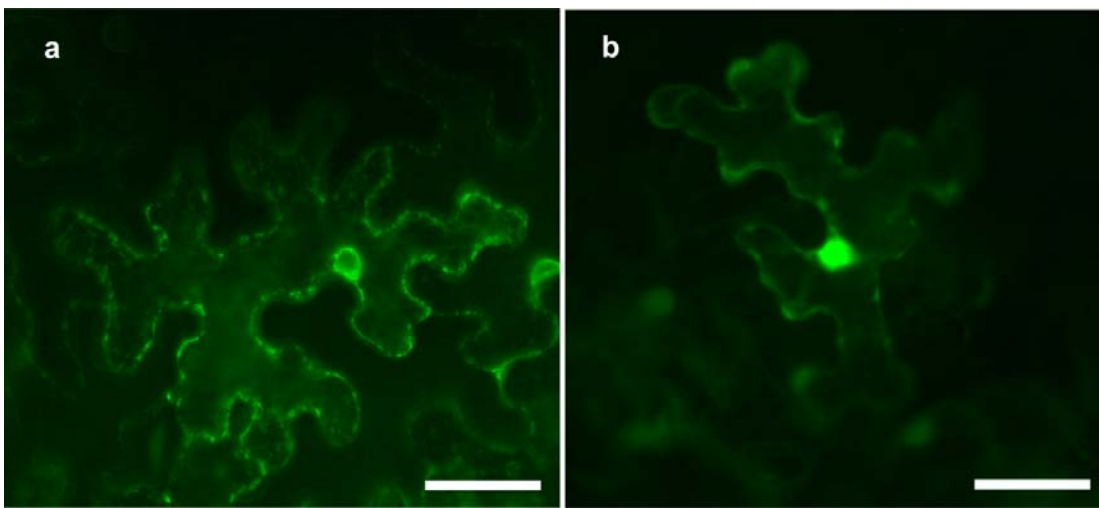


**Figure 48-** GFP-RIP1 fusion protein sub-cellular localization. Epifluorescent images of **a)** *N. benthamiana* cells transiently expressing GFP6 (control) and **b)** *N. benthamiana* cells transiently expressing GFP6-RIP1, were obtained in the *Leica DM5000 B* microscope. GFP6 was excited at 488 nm and emission was detected in the 507 nm wavelength. Bar corresponds to 50  $\mu\text{m}$ .

To confirm these results, GFP6-RIP1 expressing cells were analysed by fluorescent laser scanning confocal microscopy with a *Leica SP2 AOBS SE* microscope. Imaging analysis confirmed that the GFP6-RIP1 fusion protein was localised in the nucleus (figure 49b). The nuclear signal is clearly stronger when compared with the control (figure 49a). Confocal imaging also revealed a network surrounding the nucleus but in contradiction with the epifluorescent localization images no signal was observed in the cytoplasm. However, the mentioned network does not have a signal as strong as the observed in the control.

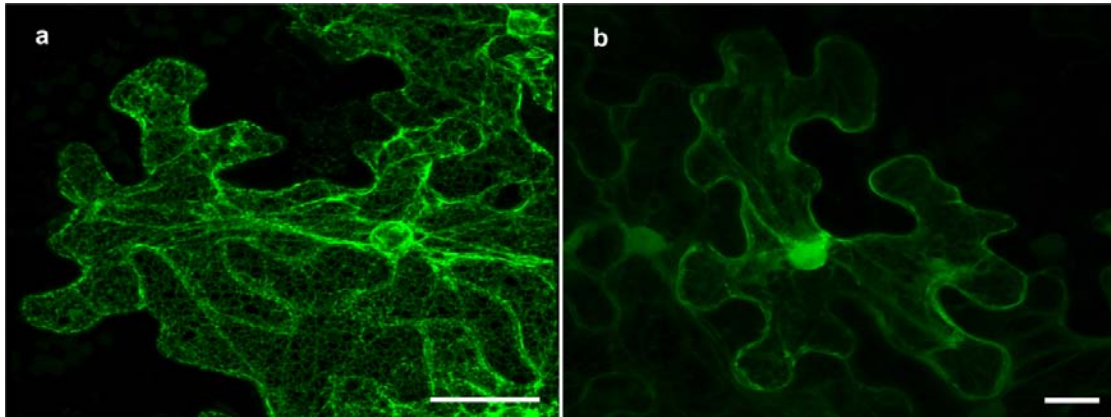


**Figure 49-** GFP6-RIP1 fusion protein sub-cellular localization. Fluorescent laser scanning confocal images of **a)** *N. benthamiana* cells transiently expressing *GFP6* (control); and **b)** *N. benthamiana* cells transiently expressing GFP6-RIP1 were obtained in a *Leica SP2 AOBs SE* microscope. GFP6 was excited at 488 nm and emission was detected at 507 nm. Bar corresponds to 10  $\mu$ m.

Epifluorescence microscope imaging of *N. benthamiana* cells expressing the GFP6-RIP2 fusion protein, suggested a nuclear localization as seen in figure 50b. When compared with control images (figure 50a) the nuclear signal is clearly stronger when cells were expressing the GFP6-RIP2 fusion protein. However, contrarily to GFP6-RIP1 no fluorescent signal was detected in filamentous networks surrounding the nucleus. This result could suggest a different sub-cellular localization profile for the RIP proteins.

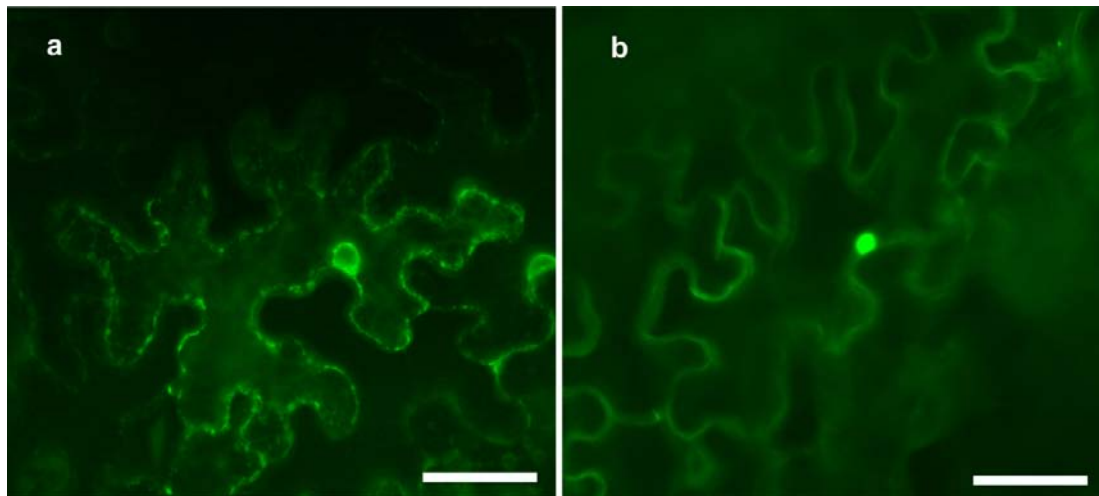


**Figure 50-** GFP6-RIP2 fusion protein sub-cellular localization. Fluorescent confocal images of **a)** *N. benthamiana* cells transiently expressing *GFP6* (control); and **b)** *N. benthamiana* cells transiently expressing GFP6-RIP2, were obtained in the *Leica DM5000 B* microscope. GFP6 was excited at 488 nm and emission was detected at 507 nm. Bar corresponds to 50  $\mu$ m.

*RAD* and *DIV* were identified as transcription factors (Galego and Almeida, 2002; Corley *et al.* 2005). Thus, their sub-localization should be in the nucleus. EYFP was excited at 503 nm and the emission was detected at 518 nm. Fluorescent laser scanning confocal microscopy (*Leica SP2 AOBS SE* microscope) imaging of *N. benthamiana* cells expressing EYFP-*RAD* and EYFP-*DIV* fusion proteins revealed a sub-cellular localization profile very similar to the GFP6-RIP1 fusion protein. Analysis revealed that *RAD* and *DIV* fusion proteins are localised in the nucleus (figure 51a and b). Curiously, a weak filamentous signal throughout the cell was observed in both cases very similar to the signal observed in cells expressing GFP6-RIP1 (figure 48b). Unfortunately no control experiment was performed because no vector was available to express EYFP protein.

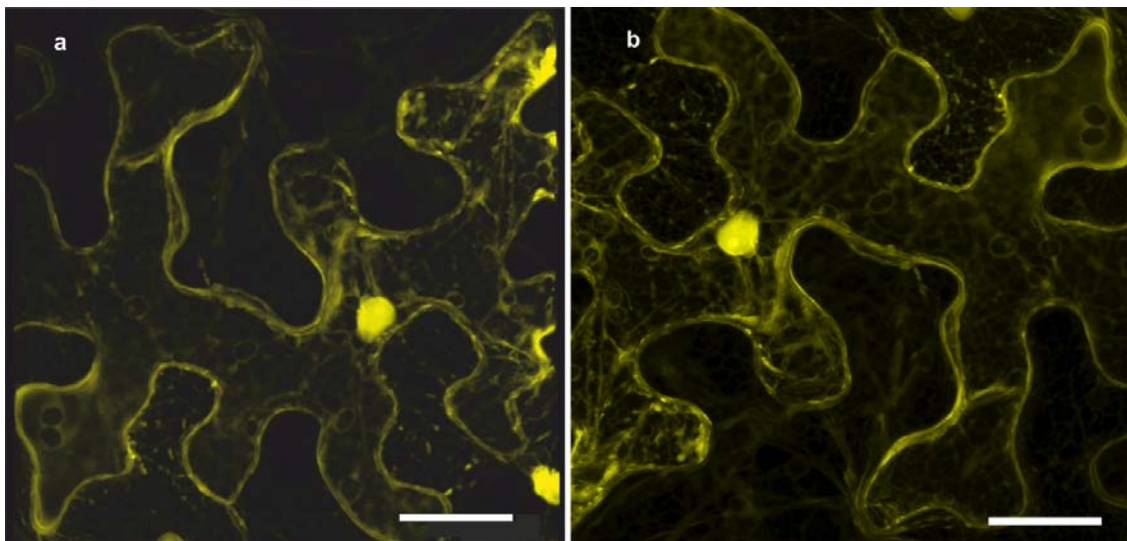


**Figure 51-** EYFP-*DIV* and EYFP-*RAD* fusion proteins sub-cellular localizations. Fluorescent laser scanning confocal images of *N. benthamiana* cells transiently expressing a) EYFP-*RAD*; and b) EYFP-*DIV* were obtained in a *Leica SP2 AOBS SE* microscope. EYFP was excited at 488 nm and emission was detected at 670 nm. Bar corresponds to 25  $\mu$ m.

### 3.6.3 Co-localization assay

The results obtained in the sub-cellular localization assay suggested that the interacting partners co-exist in the same sub-cellular compartment, the nucleus. To further test the ability of the proteins to interact in the same sub-cellular compartment, a co-localization assay was performed. Much similar to the methodology above described,



the co-localization assay offers the possibility to analyse two different expression profiles in the same cell based on different excitation and emission wavelengths of the fluorescent proteins. Using appropriate microscopy software the different fluorescent images can be overlaid, generating an image with the two colours combined. In this assay, a strategy was planned to co-localise GFP6-RIP1 with either EYFP-RAD or EYFP-DIV, based on differences between the excitation and emission wavelengths of the GFP6 and EYFP proteins. This assay methodology differs from the previous, because prior to infiltration the two *A. tumefaciens* cultures (containing GFP6-RIP1 and EYFP-RAD or EYFP-DIV) were mixed evenly and infiltrated together in the same *N. benthamiana* leaf. Images obtained from the laser scanning confocal microscope were acquired separately for each fusion protein and overlapped using appropriate software (*Leica LCS Lite*). According to figure 52a, GFP6-RIP1 expression was observed in the nucleus as expected. In the same way EYFP-DIV was also detected in the nucleus (figure 52b).

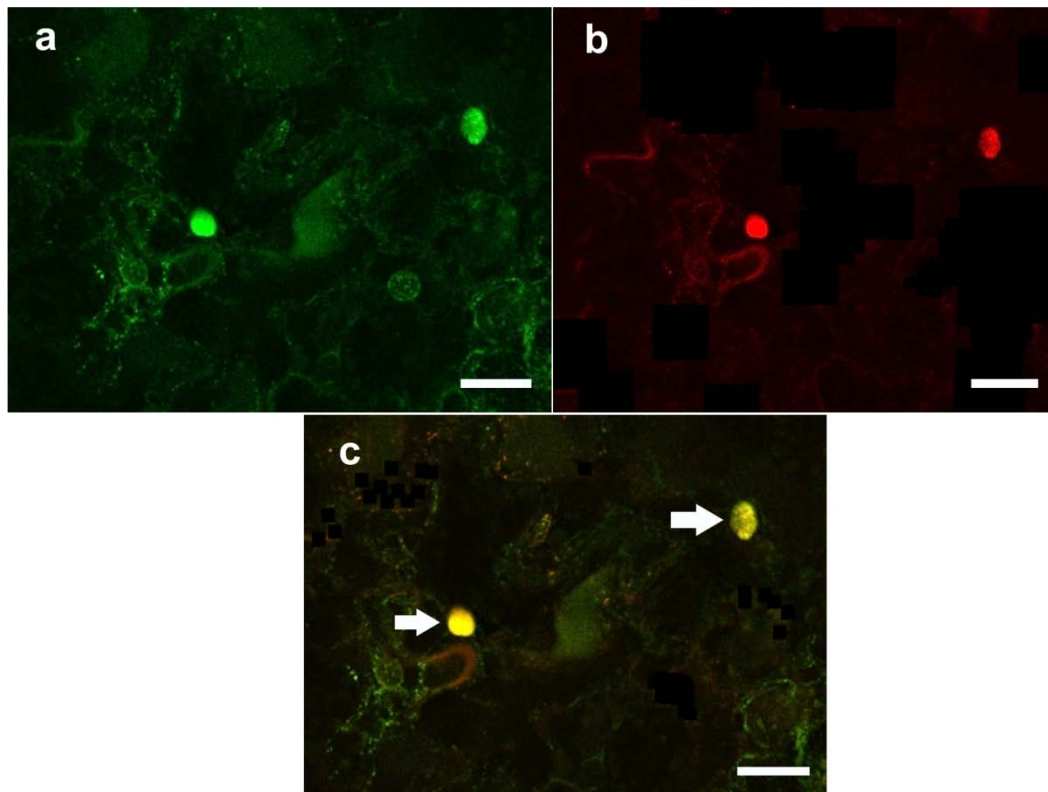


**Figure 52-** YFP-DIV and GFP6-RIP1 co-localize in the nucleus. Fluorescent confocal images of *N. benthamiana* cells expressing a) GFP6-RIP1; and b) YFP-DIV, were obtained in a *Leica SP2 AOBS SE* microscope. c) Merged images using the *Leica LCS Lite* software. White arrows represent positive co-localization. Bar corresponds to 25  $\mu\text{m}$

Overlapping the GFP6-RIP1 and EYFP-DIV emission images, it was possible to verify that DIV and RIP1 fusion proteins co-localize in the nucleus (figure 52c, white arrows). The same result was observed when co-localizing GFP6-RIP1 and YFP-RAD. In figure 53c it is possible to observe that both fusion proteins co-localized in the nucleus.

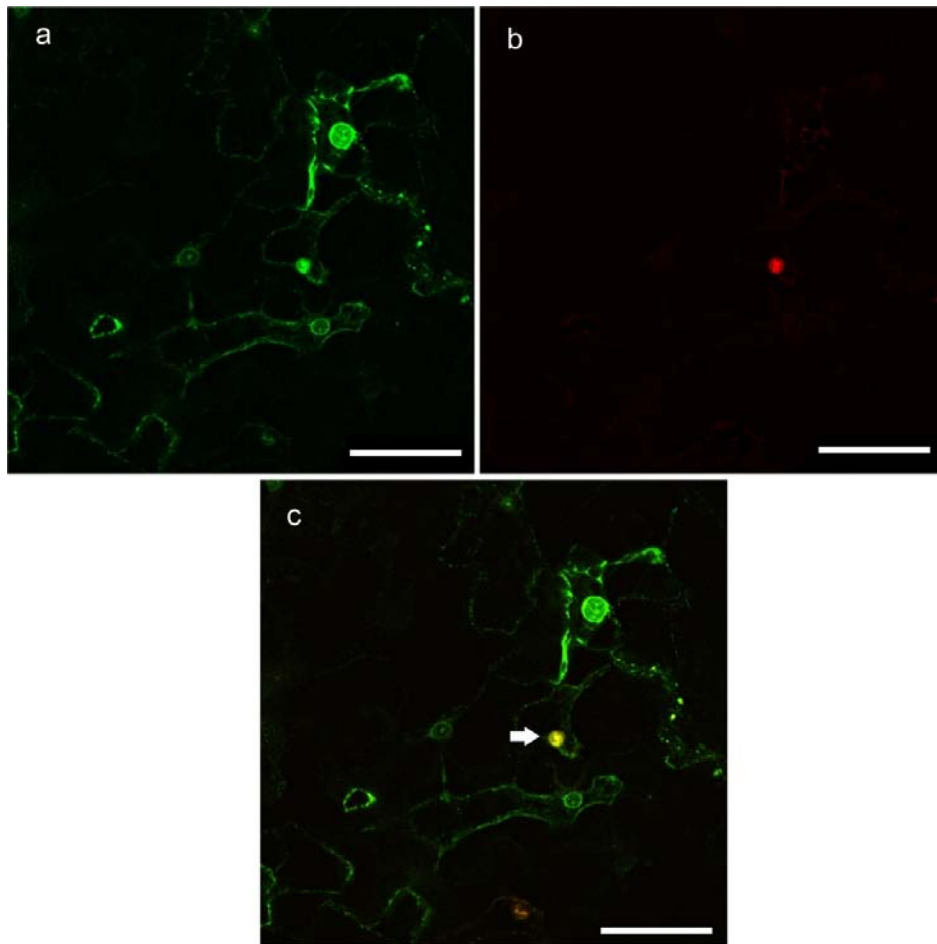


**Figure 53-** YFP-RAD and GFP-RIP1 co-localize in the nucleus. Fluorescent confocal images of *N. benthamiana* cells expressing **a)** GFP-RIP1; and **b)** YFP-RAD, were obtained in a *Leica SP2 AOBS SE* microscope. **c)** Merged images using the *Leica LCS Lite* software. White arrows represent positive co-localization. Bar corresponds to 25  $\mu\text{m}$ .

Single and co-localisation studies show clearly that the proteins co-localized in the nucleus. However, it is important to point out that the expression profiles observed are the result of the transient expression in *N. tabacum* and, so, permanent expression in *A. thaliana* should be conducted to confirm these results. The interaction between the proteins should also be confirmed *in planta*.

### **3.7 Testing the interaction between RAD-RIP and DIV-RIP proteins *in planta* by Bimolecular Fluorescence Complementation**

One of the possible drawbacks of screening plant specific protein-protein interactions in the yeast two-hybrid is that some interactions depend upon post-translational modifications that do not, or inappropriately, occur in yeast. The most frequent modifications include the formation of disulfide bridges, glycosylation and most commonly phosphorylation (Van Crieling and Beyart, 1999). In order to analyse the protein complexes under native conditions, a Bimolecular Fluorescence Complementation (BiFC) assay was planned. The BiFC assay has been widely and successfully used in plant studies. It has been used to study protein-protein interactions involved in hormonal signaling pathways (Feng *et al.*, 2008; Chini *et al.*, 2009), in the *Arabidopsis* floral development (Marion *et al.*, 2008), in cell morphogenesis (Uhrig *et al.*, 2007) or in the formation of vacuolar channels (Voelker *et al.*, 2006).

The BiFC assay is based on the observation that N- and C-terminal fragments of a fluorescent protein do not spontaneously reconstitute a functional fluorophore when expressed in the same cell. However, if fused to interacting proteins, two non-functional halves of the fluorophore are brought into tight contact, refold together and generate *de novo* fluorescence (Hu *et al.*, 2003) (figure 54). Thus, BiFC can easily monitor the interaction status of two proteins monitored via fluorescence emission upon excitation with a suitable wavelength.

Since both fused proteins may be directed to distinct sub-cellular organelles or compartments, the reconstructed signal is confined to specific sub-cellular structures, allowing not only for the detection, but also the localization of the interacting proteins in living cells (Walter *et al.*, 2004).

#### **3.7.1 Plasmids construction**

An experimental plan was designed to clone *RIP1*, *RIP2*, *RAD* and *DIV* ORFs in specific BiFC vectors using Gateway technology. The vectors employed in this study were the same that Zhong *et al.* (2008) used to confirm with success the interaction between the ethylene receptor and the CTR1-like proteins in tomato. In these vectors,

the N' terminus fragment of *YFP* variant *Venus* (1-154 aa) or the C' terminus fragment of *YFP* variant *Venus* (155-238 aa) are under the control of the 35S promoter. The *YFP* fragments are downstream of the *attB* sites, so, the gene ORFs needed to be cloned without the stop codon.

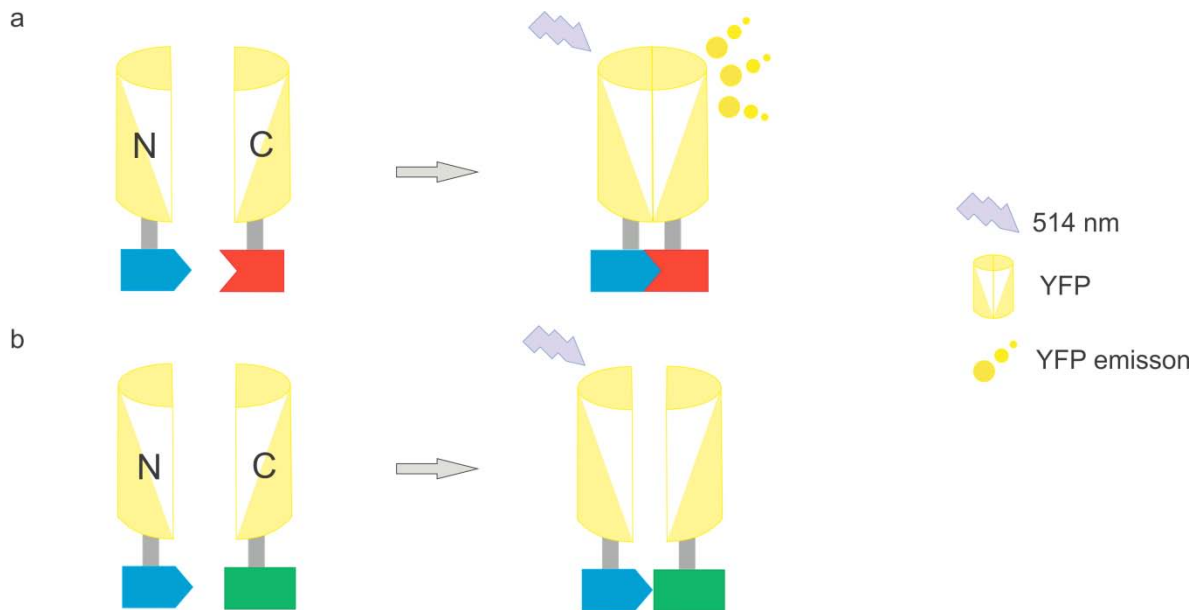


**Figure 54-** Principles of the BiFC assay. **a)** When two non-functional halves of the fluorophore are fused to a pair of interacting proteins, the fluorophore is reconstituted and occurs fluorescence emission following excitation; **b)** when there is no interaction the fluorophore is not reconstituted and no fluorescence is emitted following excitation.

In the first step, the gene *ORFs* were amplified by PCR in two steps to avoid using primers with a high number of non-homologous base pairs, similarly to previous amplifications for Gateway purposes. In the first step *RAD*, *DIV*, *RIP1* and *RIP2* *ORFs* were amplified using specific primers. The amplified product obtained was the expected (figure 55a). In the second step, the PCR product of the first amplification reaction and *primers* containing the complete *attB* sequence were used for a new PCR reaction (figure 55b). To prevent non-specific amplification of the PCR product, a control reaction (without *attB* primers) was set-up for each amplification. No significant amplification occurred in the negative control reactions (figure 55b, lanes 2, 4, 6 and 8).

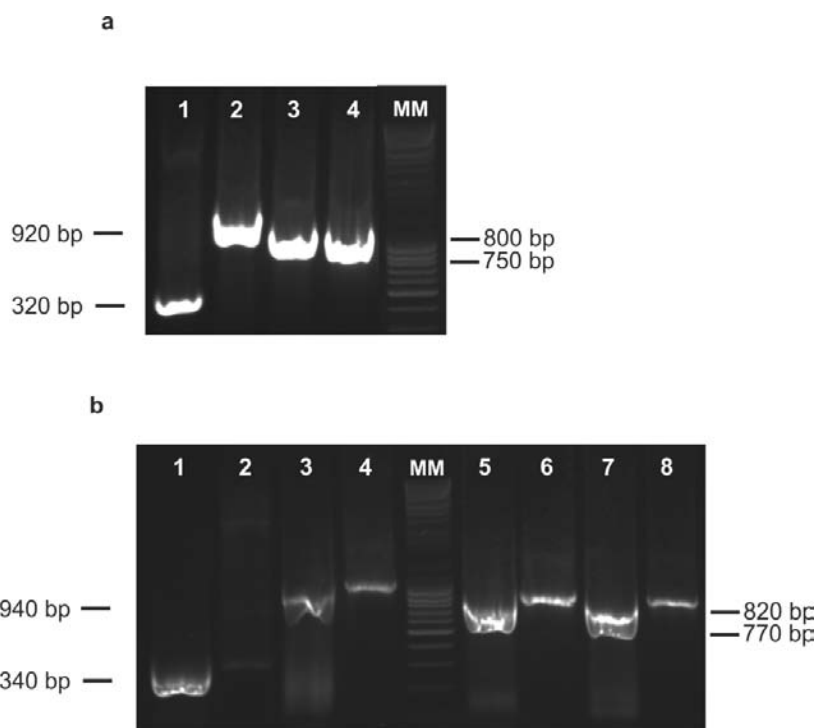


**Figure 55-** PCR amplification of the *RAD*, *DIV*, *RIP1* and *RIP2* ORF for cloning in BiFC vectors using Gateway technology. Amplification was performed in two different PCR reactions. A 10 kb molecular marker (MM, Fermentas) was run in each of the 1% agarose gels.

**a)** First PCR amplification,

Lane 1- *RAD* product amplification (expected amplified product: 320 bp);

Lane 2- *DIV* product amplification (expected amplified product: 920 bp);

Lane 3- *RIP1* product amplification (expected amplified product: 800 bp);

Lane 4- *RIP2* product amplification (expected amplified product: 750 bp);

**b)** Second PCR amplification,

Lane 1- *RAD* product amplification (expected amplified product: 340 bp);

Lane 3- *DIV* product amplification (expected amplified product: 940 bp);

Lane 5- *RIP1* product amplification (expected amplified product: 820 bp);

Lane 7- *RIP2* product amplification (expected amplified product: 770 bp);

Lanes 2, 4, 6 and 8- *RAD*, *DIV*, *RIP1* and *RIP2* negative controls, respectively.

Following the BP reaction, where the flanked *attB* fragments were introduced in pDONOR by recombination using the BP Clonase enzyme, the reaction mixtures were used to transform *E. coli* XL1-Blue competent cells. A colony PCR amplification using pDONOR forward and reverse *primers* (figure 43) was then performed to screen for positive clones in colonies that grew in selective medium (LB supplemented with kanamycin). Figure 56 shows the electrophoretic separation of the amplification products of each colony PCR amplification performed. A control amplification was also performed with pDONOR as template and the *primers* described above (a 1500 bp amplified product was expected). For *RIP1*, a positive amplification was expected to generate a 1080 bp size fragment. Several amplifications produced the desired sized

product (figure 56a) and one of those, clone 9, was selected, the plasmid isolated and sequenced. A positive amplification of *RIP2* was expected to generate a 1040 bp size fragment (figure 56b), and accordingly, clone 8 was selected, the plasmid isolated and sequenced. By examining the PCR amplification results of *DIV* transformants, it was possible to select clone 10. However, the clone PCR amplification produced not only the expected product (amplification of a 1220 bp size fragment), but also a second band with approximately 600 bp (figure 56c). Nevertheless, the plasmid was isolated and sequenced. Finally by analysing the colony PCR result of RAD, clone 10 was selected as positive (amplification of a 600 bp size fragment) (figure 56d), and the plasmid was isolated and sent for sequencing. The results of the sequencing confirmed that the ORFs of the genes were cloned in the entry vector and that no mutation occurred during the PCR amplifications.

Entry vectors were then used in the LR reaction. Each entry clone was recombined with Gateway-compatible BiFC vectors based on the pDH51 and pGreenII backbones with the fragmented YFP variant Venus fluorescent protein tag, pDH51-GW-YFPn (YFPn) and pDH51-GW-YFPc (YFPc) (Zhong *et al.*, 2008). In the former, the ORFs were cloned in fusion to the first 154 amino acids of the fluorescence tag whereas in the latter, ORFs were cloned in fusion to the last 84 amino acids of the fluorescent tag. *E. coli* XL1-Blue competent cells were then transformed with the LR reaction mixtures.

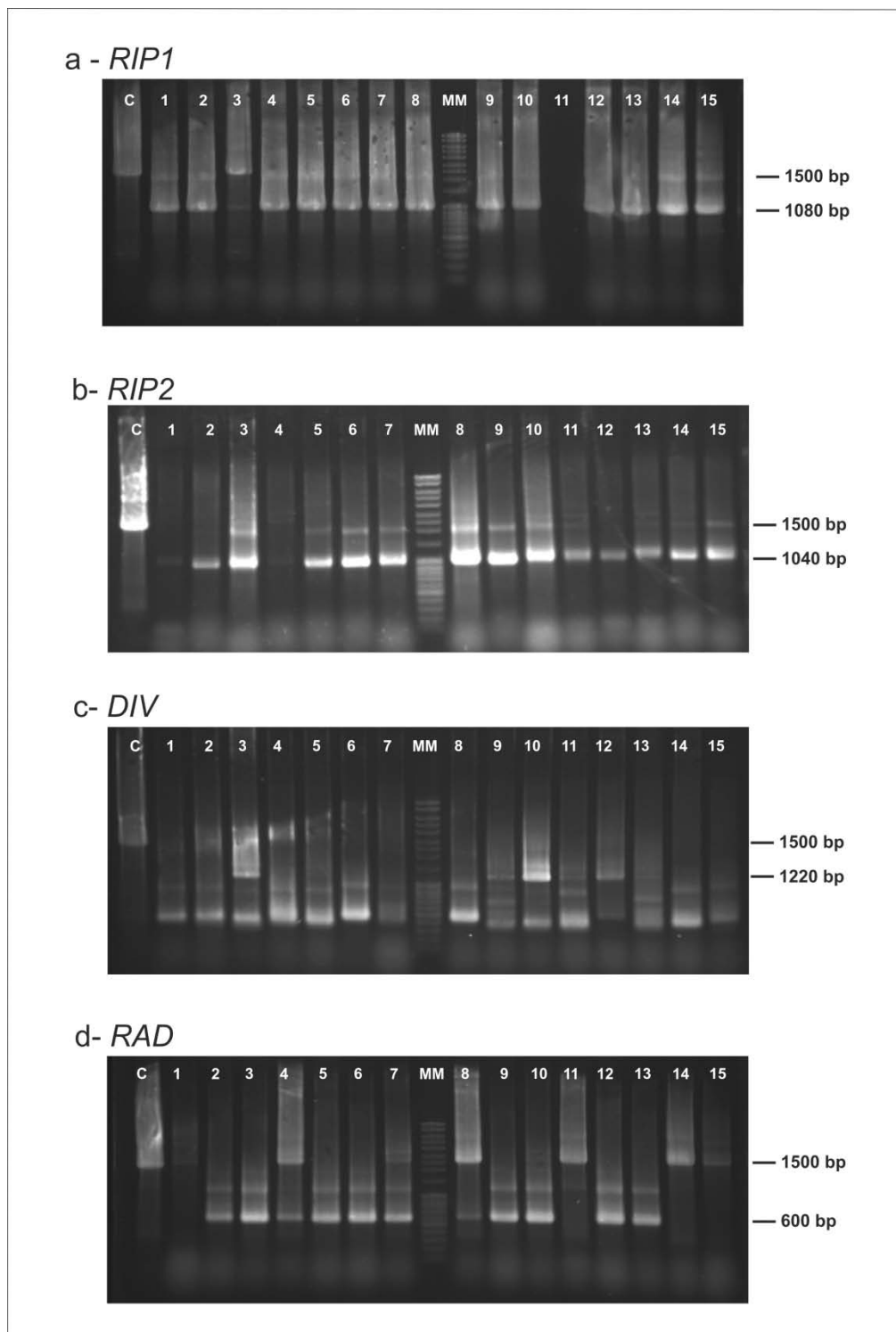


**Figure 56-** Analysis by colony PCR amplification of colonies that grew in selective medium following transformation of *E. coli* XL1-Blue cells with the BP reaction mixture. A 10 kb molecular marker (MM, Fermentas) was run in each of the 1% agarose gels. C- amplification product of the pDONOR vector (control, 1500 bp amplified fragment).

- a)** *RIP1* clones screening, lanes 1-15, (positive amplification: 1080 bp size fragment);
- b)** *RIP2* clones screening, lanes 1-15 (positive amplification: 1040 bp size fragment);
- c)** *DIV* clones screening, lanes 1-15 (positive amplification: 1220 bp size fragment);
- d)** *RAD* clones screening, lanes 1-15 (positive amplification: 600 bp size fragment).

A colony PCR amplification using appropriate pDH51-YFPn and pDH51-YFPc forward and reverse *primers* (figure 57) was then performed in colonies that grew in selective medium (LB supplemented with kanamycin) to screen for positive clones.

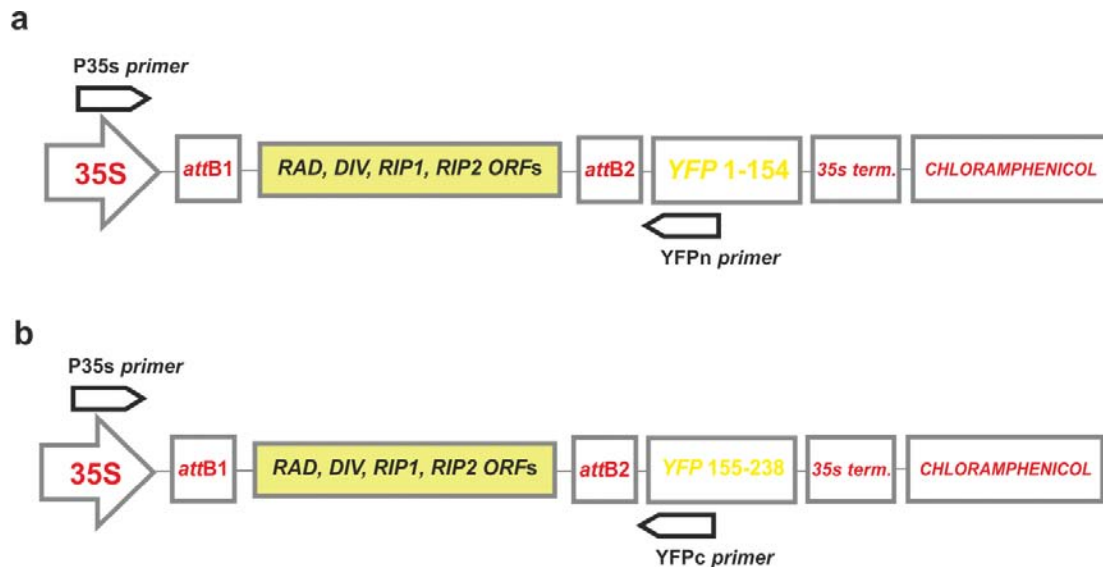


**Figure 57-** Primers used in a colony PCR amplification performed to screen *E. coli* colonies for: **a)**  $RIP1_{pDH51YFPn}$ ,  $RIP2_{pDH51YFPn}$ ;  $RAD_{pDH51YFPn}$ ,  $DIV_{pDH51YFPn}$  and **b)**  $RIP1_{pDH51YFPc}$ ,  $RIP2_{pDH51YFPc}$ ;  $RAD_{pDH51YFPc}$ ,  $DIV_{pDH51YFPc}$ .

A PCR amplification reaction was also set up using the pDH51-YFP vector as template and the same set of *primers* (control), and in this case a 1500 bp amplified fragment was observed (figure 58a, lane 1). *RIP1* was successfully amplified from the YFPn (figure 58a, lanes 3, 7 and 10) and YFPc vectors (figure 58a, lanes 11, 13 and 16-20) (where a positive amplification was expected to generate a 900 bp size product). Analyzing *RIP2* colony PCR gel, two clear positive amplifications were identified for YFPc (figure 58b, lanes 5 and 6) whereas for YFPn four positive amplifications were observed (figure 58b, lanes 11, 13, 14 and 16) (a 860 bp size amplified fragment was expected for a positive clone). All the colonies tested for RAD and DIV were positive amplifications (a expected 420 and 1040 bp size amplified product for a positive amplification, respectively) (figure 58c and d). Plasmids of clones 7 ( $RIP1_{YFPc}$ ), 19 ( $RIP1_{YFPn}$ ), 6 ( $RIP2_{YFPc}$ ), 13 ( $RIP2_{YFPn}$ ), 10 ( $DIV_{YFPc}$ ), 12 ( $DIV_{YFPn}$ ), 2 ( $RAD_{YFPc}$ ) and 16 ( $RAD_{YFPn}$ ) were isolated and sent for sequencing. All the gene ORFs were correctly orientated, with no mutations and *in frame* with the truncated fluorescent genes



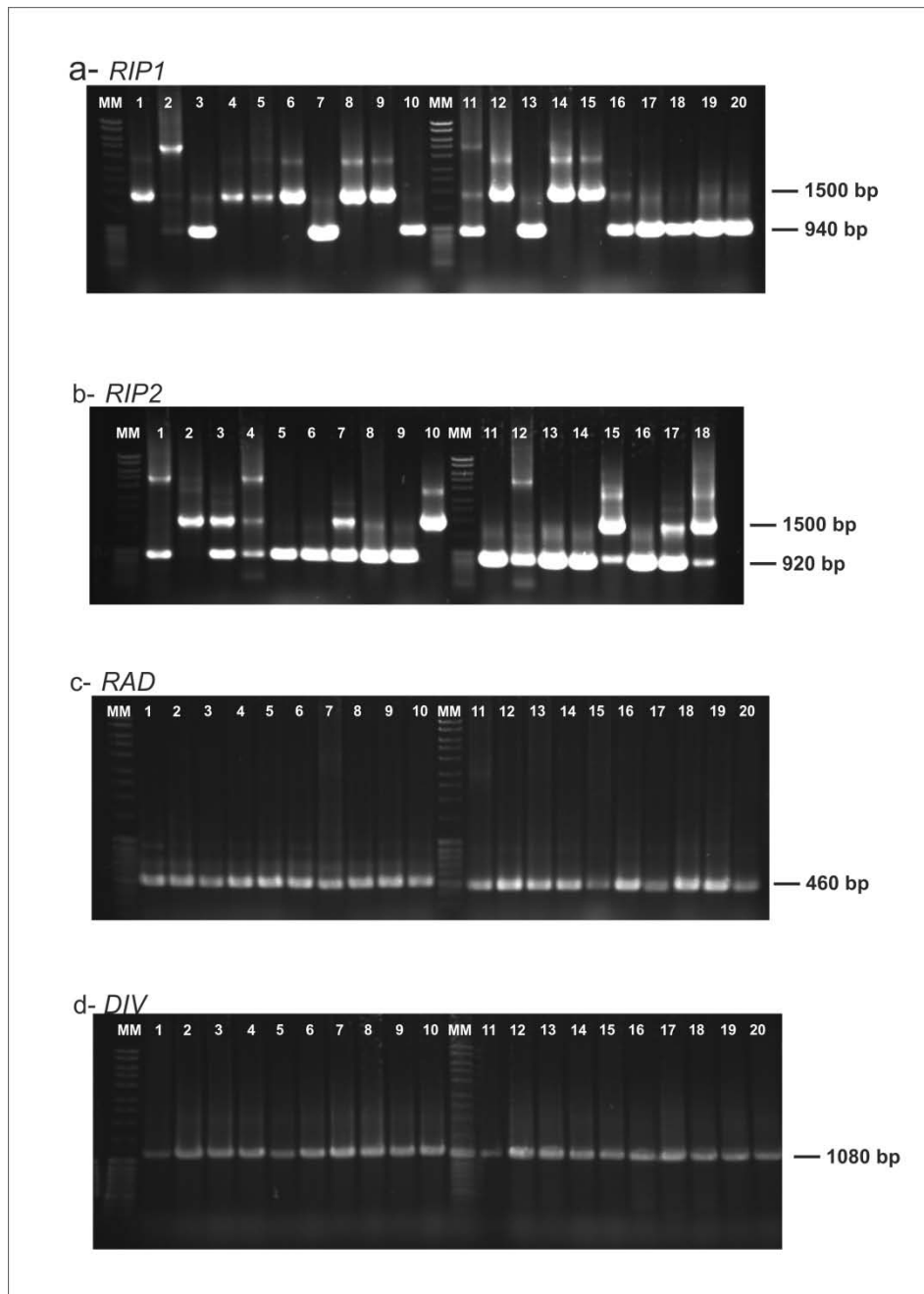


**Figure 58-** Analysis by colony PCR amplification of colonies that grew in selective medium following transformation of *E. coli* XL1-Blue cells with the LR reaction mixture. A 10 kb molecular marker (MM, Fermentas) was run in each of the 1% agarose gels. C- amplification of the pDH51-YFP vector (control, 1500 bp amplified fragment).

**a)** *RIP1* clones screening (pDH51YFPn), lanes 1-10; (pDH51YFPc), lanes 11-20 (positive amplified product: 940 bp size);

**b)** *RIP2* clones screening (pDH51YFPn), lanes 1-10; (pDH51YFPc), lanes 11-18 (positive amplified product: 920 bp size);

**c)** *RAD* clones screening (pDH51YFPn), lanes 1-10; (pDH51YFPc), lanes 11-20 (positive amplified product: 460 bp size);

**d)** *DIV* clones screening (pDH51YFPn), lanes 1-10; (pDH51YFPc), lanes 11-20 (positive amplified product: 1080 bp size).

BiFC experiments were not performed during the course of this work due to time constraints. Biolistic-mediated transformation, a highly efficient method that is used to transform plant cells, will be used to test each pair of interacting partners. This method was chosen because not only the vectors are appropriate for this methodology, because of their small size, but also due to the large number of combinations to be tested. Thus, in a future experiment, transient gene expression will be carried out in onion epidermal cells or in *A. majus* petals using a biolistic particle delivery system. The BiFC analysis will undoubtedly confirm the interaction between the RAD, DIV and RIP proteins and give some insight on the biological function of the RIP proteins.

### **3.8 Ectopic expression of the RIP proteins in *Arabidopsis***

Another common methodology to study function *in planta* is to express ectopically the gene. Thus parallel to the BiFC assay, a construct was prepared with the full-length *RIP1* ORF under the control of a single copy of the 35S CaMV promoter. Already available was the 35S:RIP2 construct. This construct has the RIP2 ORF cloned in the pBI121, under the control of a 35S promoter and in fusion with the  $\beta$ -*GLUCORUNIDASE*, which will allow for detection of expression in a GUS assay (Jefferson *et al.*, 1987). These two constructs were then used to transform *Arabidopsis* plants.

Using Gateway technology, a LR recombinant reaction was performed between  $RIP1_{\text{pDONOR}}$  (obtained previously, see 3.5.1) and the pMDC32 vector (destination vector that has the *attR* sites downstream of a 35S promoter). The reaction mixture was then used to transform *E. coli* XL1-Blue competent cells and a colony PCR amplification was performed to screen for positive clones in colonies that grew in selective medium (LB plus hygromycin). The colony PCR was performed using appropriate pMDC32 forward and reverse *primers*. A control reaction was set up with the same set of primers and the pMDC32 as template (generated a 1750 bp product). Results in figure 59a show six putative positive clones (910 bp fragment amplification, lanes 3, 6, 9, 10, 11 and 12). Plasmid from clone 9 was isolated and sent for sequencing. Sequencing results showed that the *RIP1* ORF was cloned in the correct orientation with no mutations. The construct was then used to transform *A. tumefaciens* EHA105 competent cells.

Following transformation, a colony PCR amplification revealed that all the clones tested were positive (figure 59b).

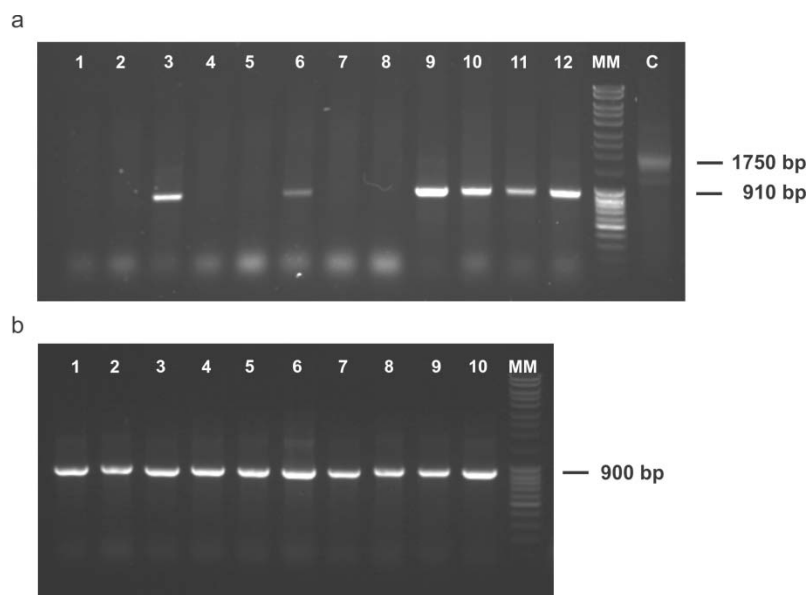


**Figure 59-** Screening for RIP1<sub>pMDC32</sub> with colony PCR amplification of *E. coli* and *A. tumefaciens* colonies. C- amplification of the pMDC32 vector (control, 1750 bp amplified product). A 10 kb molecular marker (MM, Fermentas) was run in each of the 1% agarose gels.

**a)** RIP1<sub>pMDC32</sub>, clones screening following transformation of the LR reaction in *E. coli* XL1-Blue cells and growth in selective medium (expected positive amplification: 910 bp);

**b)** RIP1<sub>pMDC32</sub> clones screening following transformation of the construct in *A. tumefaciens* and growth in selective medium (expected positive amplification: 900 bp).

For each construct, four different pots of plants were selected for transformation using *A. tumefaciens* and the floral dip transformation method. After two months, seeds from each pot were collected separately and screened in MS medium with the appropriate antibiotic. The screening of positive transformants (generation T1) is still undergoing.

## 4. Discussion

In this study, the case of the *A. majus* floral dorsoventral asymmetry, a key evolutionary trait, that has arisen many times independently during evolution and that is controlled by the activity of transcription factors is addressed (Donoghue *et al.*, 1998). In *Antirrhinum*, TCP-like transcription factors, such as *CYC* (Luo *et al.*, 1996) and *DICH* (Luo *et al.*, 1999), and MYB-like transcription factors, such as *RAD* (Corley *et al.*, 2005; Baxter *et al.*, 2007) and *DIV* (Galego and Almeida, 2002), are involved in determining floral dorsoventral asymmetry. In the early stages of flower development, *RAD* is expressed in the dorsal domain, whereas *DIV* is expressed in all floral organs regardless of their position along the flower dorsoventral axis (Galego and Almeida, 2002; Corley *et al.*, 2005). However, when *RAD* is expressed the *DIV* function is restricted to the ventral domain of the meristem, and when *RAD* is not expressed, *DIV* function expands to the entire floral meristem (Galego and Almeida, 2002; Corley *et al.*, 2005). These facts lead to the hypothesis that *RAD* antagonises *DIV* to promote dorsal identity to the developing flower meristem. The idea that *RAD* is antagonizing *DIV* function is supported by expression and phenotypic data, but is also strengthened by the high homology observed between the first MYB-like/SANT domain of *DIV* and the MYB-like/SANT domain of *RAD*. There is, however, one question that remains to be answered, and that is how does *RAD* antagonize *DIV*.

In this study, three hypotheses were proposed to address this question (figure 12). The first was based on a possible interaction between *RAD* and *DIV* that could be inhibiting the transcriptional activity of *DIV*. The second and third hypotheses were based on the homology between the MYB-like/SANT domains of *RAD* and *DIV*. This homology suggests that these transcription factors could have the same DNA or protein targets. In the former, *RAD* could bind to the DNA targets of *DIV*, functioning as a transcriptional repressor and in the latter, *RAD* and *DIV* could be competing for the same protein targets, in this case the RIP proteins.

## **4.1 RAD does not bind directly to DIV or indirectly to DIV DNA targets.**

As a first approach, the hypothesis that RAD could be antagonizing DIV function indirectly by sequestering the DNA binding sites of DIV targets was tested. A similar behavior was reported for two MYB transcription factors that are expressed during the development of the *A. majus* flower. AmMYB305 and AmMYB340 are structurally very similar throughout their DNA binding domain, and when co-expressed in the same cell compete for the same *cis*-elements of target genes (Moyano *et al.*, 1996). This hypothesis was further co substantiated by the fact that RAD being a R3MYB-like protein, without a clear activation domain, could be acting as a transcription repressor altering the transcription rate of the genes regulated by DIV. Similar R3MYB proteins have been described as transcriptional repressors such as: AtMYBL2 involved in the flavonoid biosynthesis, (Matsui *et al.*, 2008); and CPC involved in cell fate (Lee and Schiefelbein, 1999). An EMSA was performed to establish if RAD recombinant protein was able to bind to a DNA probe containing the GATAA sequence, the DNA consensus-binding site of DIV (previously obtained using a Random Site Binding Selection assay). A binding reaction with the probe and DIV recombinant protein was used as positive control. As expected, a DIV/probe complex was observed. No retardation of the migration of the probe was observed when incubated with RAD protein. This lack of retardation could be due to the binding conditions not being optimal for RAD DNA binding. To optimise the binding conditions several variables were altered: pH, presence of non-ionic detergents, protein concentration, type of bulk carrier DNA and KCl, NaCl and MgCl<sub>2</sub> concentrations. However, no retardation was observed. This could mean that RAD protein might be incapable of targeting the DNA targets of DIV. Nevertheless, these results need to be confirmed by testing other reaction variables such as: probe concentration, temperature and incubation reaction time length. One possibility for the inability of RAD to bind to the probe is that RAD recombinant protein might not be properly folded and therefore not fully active. Post-translation modifications, such as phosphorylation, glycosylation or disulfide bond formation do not occur in *E. coli* (Mann and Jensen, 2003) and this could explain a lack of proper folding and the failure

in rescuing the binding site. Thus, the RAD ability to bind to the DNA binding consensus of DIV should be tested in a eukaryotic expression system where the great majority of the post-translation modifications are available.

The GATAA sequence is the consensus-binding site characteristic of the I-box transcription factors (Giuliano *et al.*, 1988). Rose *et al.* (1999) described the first plant transcription factor capable of binding to the I-box sequence and curiously this MYB-like transcription factor has high similarity with DIV. This R2R3MYB-like transcription factor depends on the second MYB-like repeat to bind and activate transcription and the same authors also found that the first MYB-like repeat is not involved in DNA-binding. Thus, it may be that the DNA binding activity of DIV depends in the same way on its second MYB-like repeat and not to the first MYB-like/SANT repeat. If the first DIV MYB-like/SANT domain share a homology with the RAD MYB-like/SANT domain, it is possible that RAD could be unable to bind to DNA and activate or repress transcription.

RAD and DIV homologous MYB-like/SANT have been linked to several biological functions such as the chromatin remodeling (Aasland *et al.*, 1996), or involved in protein-protein interactions (Boyer *et al.*, 2004). Choi *et al.* (2007) reported that in *Arabidopsis* the PIE3 and SUF3 MYB-like/SANT proteins are not involved in DNA binding but interact with each other in a nucleosomal complex that repress *FLC*. The same authors assume that the MYB-like/SANT domain of these proteins is essential for the protein-protein interactions. Thus, another possibility is that RAD might be antagonizing DIV function by sequestering directly DIV protein. Results presented in this work indicate that RAD and DIV proteins do not interact with each other. The first evidence was provided by the result obtained in the gel-shift analysis. When RAD and DIV recombinant proteins were incubated with the DNA probe, a complex was formed resembling the one obtained when incubating DIV and the probe alone. This result indicates that RAD is unable to disrupt the DIV-DNA complex and that RAD protein does not form a multi-protein/DNA complex with DIV protein *in vitro*. The second evidence was provided by the results of the yeast two-hybrid assay. Clones containing either RAD or DIV proteins fused to the truncated fragments of GAL4 were incapable of activating the transcription of the *HIS3* and *LacZ* reporter genes.

## 4.2 RAD and DIV interact strongly with the RIP proteins

Transcription factors heterodimers and even higher-order protein complexes often mediate transcription (Zhang *et al.*, 2010). Accordingly, there are examples of transcription factors that have, as an absolute requirement for activity, a structural domain that is capable of directing the formation of homo and/or heteromeric dimers. Dimerisation increases the number of transcription factor complexes that can be formed from a smaller number of homomeric components and can have a positive or negative influence on their DNA-binding characteristics, activation potential or nuclear localization (Kosugi and Ohashi, 2002). Schwarz-Sommer *et al.* (1992) reported that the *Antirrhinum* proteins DEFICIENS (DEF) and GLOBOSA (GLO) can bind DNA *in vitro* only in the presence of each other. Also Egea-Cortines *et al.* (1999) work revealed that the *Antirrhinum* DEF, GLO and SQUAMOSA (SQUA) proteins have the capacity for higher-order complex formation. The ability of DIV to control transcription could depend on the formation of a transcriptional complex with non-DNA-binding proteins that may act as ‘bridging factors’ between DIV and the basal transcription machinery. Those bridging factors could be stabilizing the DNA binding complex or changing the specificity for the target sequences (Riechmann *et al.*, 2000). Thus, RAD might be antagonizing DIV by sequestering its interacting partners on the transcriptional complex. This hypothesis was consolidated by the identification in a yeast two-hybrid assay of two MYB-like/SANT proteins that were able to interact with RAD and DIV, the RIP1 and RIP2 proteins. In this study, the yeast two-hybrid assay was used to confirm the ability of RAD and DIV proteins to interact with RIP1 and RIP2. The results demonstrated that RAD and DIV were able to interact with the RIP proteins by activating the transcription of the *HIS3* reporter gene, granting the hypothesis that the molecular antagonism between RAD and DIV could be due to molecular competition for the RIP proteins. Based on this assumption, RAD might have a higher affinity for the competing partners than DIV in order to successfully antagonize DIV. Alternatively, RAD could have the same affinity than DIV for the RIP proteins, but to successfully inhibit DIV function the amount of RAD protein in the flower meristem might be significantly higher than the amount of DIV to rescue a higher amount of RIP proteins. In a third scenario, RAD and DIV could form a multi-protein complex with the RIP

proteins and in this case the affinity of RAD and DIV for the RIP proteins could be equal.

A quantitative yeast two-hybrid liquid assay was performed to test if there were any differences in the affinity of RAD and DIV for the RIP proteins. Results showed that RAD and DIV share a strong affinity with the RIP proteins when comparing with the  $\beta$ -galactosidase activity generated from known interacting partners (Moon *et al.*, 1999; Kosugi and Ohashi, 2002). Importantly, the results demonstrated that RAD has a greater affinity for the RIP1 and RIP2 proteins than DIV. It is worth mentioning the case of the RIP1-BD<sub>GAL4</sub> and RAD-AD<sub>GAL4</sub> interaction that generated a smaller  $\beta$ -galactosidase activity when compared to the one generated by the RAD-BD<sub>GAL4</sub>/RIP1-AD<sub>GAL4</sub> interaction. One possibility to explain this situation is that the GAL4 reconstituted by this interaction might not be fully active due to incorrect folding. Another explanation could be that the GAL4 transcription factor access to the GAL2 promoter (*LacZ*) might be partially inhibited by this specific protein-protein conformation. Kosugi and Ohashi (2002) reported a similar situation. In this study the interaction of PCF6-BD<sub>GAL4</sub>/PCF5-AD<sub>GAL4</sub> was able to induce the transcription of the reporter gene whereas the interaction of PCF5-BD<sub>GAL4</sub>/PCF6-AD<sub>GAL4</sub> was not. However, the authors did not present an explanation for this particular result.

Based on these results, a model for the antagonisation of DIV by RAD through the competition for the RIP proteins can be hypothesized. DIV probably exerts its functions by binding to the promoter in target genes. However, in order for DIV to be able to control transcription, it needs to form a transcriptional complex with either the RIP1 or RIP2 proteins. When RAD is expressed in the dorsal domain of the floral meristem and transported non-cell autonomously to the lateral domain of the floral meristem, the RIP1 and/or RIP2 proteins are sequestered by RAD inhibiting the formation of the transcriptional complex of DIV, or RAD could sequester the entire RIP/DIV complex. In a future experiment, these two hypotheses could be discriminated using a yeast-three hybrid approach. In this assay, the RIP proteins could be cloned in a third yeast plasmid and tested for interaction with RAD and DIV fused either to the BD<sub>GAL4</sub> or AD<sub>GAL4</sub>. If the RIP proteins are mediating the formation of a complex between RAD and DIV the reporter genes are activated, whereas if RAD is sequestering



the RIP proteins, the transcription of the reporter genes would not occur. Favaro *et al.* (2003) used a similar approach when testing the involvement of AGAMOUS, SEPALLATA3 and SEEDSTICK in a transcription complex in the development of carpels and ovules in *Arabidopsis*.

Yeast two-hybrid results also showed that there was no evidence for homodimerisation between the RIP1 or RIP2 proteins, nor evidence of heterodimerisation between RIP1 and RIP2 proteins. These results could suggest that DIV and either RIP1 or RIP2 proteins form the transcriptional complex. This model of interactions could be very similar to the one where the R3MYB-like transcription factor CPC and the R2R3Myb-like WER control the epidermal cell differentiation in *Arabidopsis* (Tominaga *et al.*, 2007). WER promotes differentiation to the non-hair cell fate whereas CPC is critical in the induction of hair cell fate (Lee and Schiefelbein, 1999; Wada *et al.*, 2002). Koshino-Kimura *et al.* (2005) reported that the transcription of GL2, which encodes a homeodomain-leucine zipper protein and is thought to act farthest downstream in the root hair regulatory pathway is controlled by a protein complex that includes WER, GL3, ENHANCER OF GLABRA3 (EGL3), and TRANSPARENT TESTA GLABRA1 (TTG1) proteins. The CPC protein was proposed to disrupt this protein complex by competitive binding with WER, leading to repression of GL2 expression (Wada *et al.*, 2002; Koshino-Kimura *et al.*, 2005). However in this case, the antagonism is through a direct interaction between the R3MYB and the R2R3MYB, whereas in the *A. majus* flower dorsoventral asymmetry case, a third MYB-like protein might mediate the antagonism.

Another interesting result retrieved from the yeast two-hybrid assay was that neither RAD nor the RIP proteins alone were able to activate transcription of the reporter genes. However, DIV when fused to the binding domain of GAL4 was able to activate the transcription of the reporter genes (results not shown). These results clearly indicate that DIV has an active transcriptional activation domain and that the RAD and RIP proteins do not. Alignment of the second MYB-like repeats of DIV and homologous sequences like LeMYB1 (Rose *et al.*, 1999) and CCA1 (Wang and Tobin, 1998) proteins revealed a highly conserved sequence, the SHAQK(Y/F)F motif that could be essential for the DNA-binding and transcription regulation. An interesting next step

would be to site direct mutagenise the SHAQKYF motif to evaluate the role of if this motif in DIV function. In the same way, this approach could be used to target specific regions on the first MYB-like/SANT domain of DIV and the unique MYB-like/SANT domain of RAD and the RIP proteins to understand which motifs are responsible for the protein-protein interaction. As mentioned before, DIV has a high similarity with CCA1. Interestingly, Daniel *et al.* (2004) reported that in *Arabidopsis* the phosphorylation of CCA1 by the regulatory ( $\beta$ ) subunit of the protein kinase CK2 is needed for DNA binding. Phosphorylation of transcription factors has been reported to modulate their DNA-binding activity, cellular localization, stability and interaction with other proteins (Bontems *et al.*, 2002). It would be interesting to study the possible effects of phosphorylation in DIV function by using, for example, specific phosphorylation inhibitors.

To prove that the RIP proteins could be involved in the formation of a transcriptional complex with DIV, a gel-shift assay was planned. The objective of this assay was to test if the RIP proteins could form a transcriptional complex with DIV, and if the complex could be disrupted by RAD. If the RIP and DIV recombinant proteins are able to form a protein-protein complex with DIV, the shift of the probe might be able to be observed in the gel. When adding RAD recombinant protein, two outcomes could be expected: RAD could disrupt the RIP-DIV protein complex and the super-shifted band corresponding to RIP/DIV/probe would disappear; or RAD could form a higher complex with RIP and DIV and a band with even higher molecular weight should be observed in the gel. However, this assay was not performed, due to the fact that it was not possible to obtain purified RIP recombinant protein. Heterologous expression of the RIP proteins was performed in *E. coli*. This system is frequently used to obtain purified recombinant protein, however, there are several constraints that could affect the production of viable recombinant protein. The lack of expression of the recombinant proteins in this study could be due to the codon usage bias or proteolytic activity during the expression. Also, the recombinant proteins could induce toxicity to the *E. coli* cells. Codon usage bias refers to differences in the frequency of occurrence of synonymous codons in coding DNA (Comeron and Aguadé, 1998). Optimal codons in *E. coli* reflect the composition of their respective genomic tRNA pool. Analysing the *RIP2* sequence, it is possible to

identify several codons that are frequently rare in *E. coli*: AGG, AGA, CGA (arginine), CCC (proline), ATA (isoleucine) and CTA (Leucine). From these codons, the most limiting is the AGG codon (1.7% frequency). By analysis of the *RIP1* sequence the same rare codons were observed, however, it was also observed repeated (AGG-AGG) and consecutive (GGG-CCC) rare codons. Roche and Sauer (1999) found that tmRNA-mediated tagging occurs at a run of rare codons on an mRNA where the ribosome is expected to stall due to the deficiency of cognate tRNAs. TmRNA-mediated tagging is a process that allows the release of the stalled ribosome and the marking of the incomplete polypeptide for degradation by ATP dependent proteases (Karzai *et al.*, 2000). Moreover, Bendtsen *et al.*, 2005 consider that the repeated twin arginines (AGG-AGG sequence) are a common signal for proteolytic activity in bacteria. The presence of the rare codons and the twin arginines could be responsible for the lack of visible expression of the RIP1 and RIP2 proteins or the expression of truncated forms.

To solve this problem, there is the hypothesis of using of a different *E. coli* expression strain. One of these is the *E. coli* BL21-CodonPlus strain (Stratagene), that contains a ColE1-compatible plasmid encoding extra copies of the argU and proL tRNA genes that rescue the translational process restricted by either AGG/AGA codons or CCC codons. Alternatively, the heterologous expression of the recombinant RIP proteins could be performed in another system, preferably a eukaryotic system where post-translational modifications like phosphorylation, formation of disulfide bridges or glycosylation are available (Mann and Jensen, 2003).

### **4.3 RAD and DIV co-localise with the RIP proteins in the nucleus**

A potential problem concerning the study of physical interactions between proteins is that the interacting proteins could be expressed at different time and space points during development. In a study carried out by Raimundo (2010), *RIP1* and *RIP2* transcripts were identified in floral organs. In the same work, an *in situ* hybridization assay comproved that the *RIP* transcripts are present and co-expressed with *RAD* and *DIV* in the developing flower meristem of *A. majus*.

When testing for protein-protein interactions it is also very important to consider the proteins sub-cellular localisation because it is possible that the proteins, despite being able to interact *in vitro*, are never in close proximity to each other within the cell (Van Crielinge, 1999). Two interacting proteins tested on a yeast-two hybrid assay could be expressed in different cell types, or even when found in the same cell could localize in distinct sub-cellular compartments. As discussed, RAD, DIV, RIP1 and RIP2 show sequence similarity to known transcription factors. However, to act as transcriptional regulators the proteins would need to localise in the nucleus. A nuclear localisation serves as a regulatory mechanism in the activity of the transcription factors. According to the WolfPSORT algorithm (Horton *et al.*, 2006), software commonly used to predict sub-cellular localization, RAD, DIV, RIP1 and RIP2 proteins co-localize in the nucleus. To test this theoretical assumption, *GFP6* was fused to the N-terminus of *RIP1* and *RIP2* whereas *EYFP* was fused the N-terminus of *DIV* and *RAD*. Protein fusions to either GFP or its variants, is a practical method of assessing cellular localisation in plant cells. The fluorescent proteins are relatively small proteins that tolerate well being fused to another protein and, therefore, are widely used as fluorescent tags (Chiu *et al.*, 1996). Single and co-localization fluorescence studies confirmed that the all the above-mentioned proteins fused to fluorescent tags co-localized in the nucleus. The nuclear localisation of the RIP proteins could be correlated with the presence of a Robins and Dingwall consensus NLS. The NLS might be able to drive the fusion protein into the nucleus.

There was no evidence for any type of NLS in the RAD primary sequence. However, it is possible that RAD might enter the nucleus by diffusion. According to Gorlich and Mattaj (1996), the estimated size exclusion limit for bidirectional diffusion through nuclear pore complexes is between 40-60 kDa. In the cells expressing EYFP-RAD (42 kDa), the fusion protein could enter the nucleus by diffusion. The GFP-DIV fusion protein is larger than this exclusion limit (72 kDa) and it was found in the nucleus of *N. benthamiana* cells, suggesting that the DIV protein contains at least one NLS, which is able to drive the fusion protein to the nucleus. A Robins and Dingwall consensus NLS was predicted in the analysis of the DIV protein primary sequence (*RKSSSGRPSEQE RKKGV*), which could explain the presence of this protein in the nucleus.

The results obtained clearly indicate that the fusion proteins co-localise in the nucleus. Therefore, the model proposed for the RAD, DIV and RIP proteins interactions is perfectly viable because the proteins are able to physically interact in the same cellular compartment.

According to Palmer and Freeman (2004), proteins fused to fluorescent tags could have different sub-cellular localizations depending on the type of fusion (fused to the C or N terminus). The authors implied that the tested C-terminus tagged proteins were localized correctly, but this was not the case for more than half of the N-terminus tagged proteins. Thus, the sub-cellular localisation assay here described should be complemented with the sub-cellular localisation of the RAD, DIV and RIP proteins fused to the N terminus of the fluorescent tag.

The described fused tagged proteins could also be used in different assays. For example, a co-immunoprecipitation assay using specific GFP antibodies could be performed to screen for interacting partners of the RIP proteins using *A. majus* protein extracts. Chandler *et al.* (2007) used a similar approach to detect a protein-protein interaction between two transcription factors in *Arabidopsis*.

#### **4.4 Testing the RAD, DIV and RIPs interactions *in planta***

The last part of this study focused on the planning of a strategy to prove that the interactions between RAD, DIV and the RIP proteins occur *in planta*. One of the disadvantages of using the yeast two-hybrid system to test plant protein interactions is that some interactions depend upon post-translational modifications that do not, or inappropriately, occur in yeast. Among them are the formation of disulfide bridges, glycosylation and most commonly phosphorylation (Van Crieling and Beyart, 1999). Also this system does not preclude indirect interaction of two proteins through a third component present in yeast cells. Due to the importance of analyzing protein complexes under native conditions, several methods have been developed to facilitate the detection and imaging of protein-protein interactions in living cells. Recent methods such as the fluorescence resonance energy transfer (FRET) and bioluminescence resonance energy transfer (BRET) assays have been successfully used to monitor protein associations in living cells. However, use of these methods is rather challenging due to various technical

and biological limitations, including autofluorescence, photobleaching, the need for luciferin and for specialized equipment and software for imaging and data analysis (Citovsky *et al.*, 2008). A more direct approach to visualizing protein–protein interactions in living cells is the bimolecular fluorescence complementation (BiFC) assay (Hu *et al.*, 2002; Bracha-Dori *et al.*, 2004; Walter *et al.*, 2004). BiFC offers several advantages over the use of FRET or BRET for monitoring protein–protein interactions in living cells. These include higher sensitivity, relative technical simplicity and the ability to use epifluorescence microscopy as a low-cost alternative to confocal microscopy (Rebois *et al.*, 2008). Unfortunately, the BiFC assay was not performed due to lack of time.

Further experiments based on the BiFC technique could be used to reveal the nature of the relation between the RIP, RAD and DIV proteins. Testing complementation with truncated or mutated proteins could reveal the motifs necessary for the protein-protein interaction. Also, with the aim of characterize even further the protein interactions it could be very interesting to measure the protein-protein interaction kinetics (*e.g.*, association constants, interaction time length or specific inhibitors of interaction). Robida and Kerppola (2009) determined the kinetics of the BiFC complex formation. Using flow cytometry, the authors described magnitudes of the increases in fluorescence in response to a ligand-inducible protein interaction. Also, in the same study the effects of different ligand concentrations on BiFC complex formation were compared to determine if the fluorescence intensity reflected the proportion of the interaction partners that associate with each other, and also the reversibility of BiFC complex formation using competitive inhibitors of ligand binding. Another approach could be to combine BiFC and resonance energy transfer with the purpose of discover if the RAD, RIP and DIV proteins form a multi-protein complex in living cells. In this assay, a fluorophore reconstituted by BiFC could serve as a donor for resonance energy transfer to a third partner (acceptor). This would allow discriminating the simultaneous presence of three or more proteins in a single complex. In a study developed by Kwaaitaal *et al.* (2010) a BiFC combined with FRET assay based on the cerulean fluorescent protein as a donor and reconstituted yellow fluorescent protein as an

acceptor was used to study the formation of a ternary protein assembly between a set of barley SNARE proteins and their orthologous in *Arabidopsis*.

## 4.5 The RIPs biological function

The most important question to be answered in future studies is the biological function of the *RIP1* and *RIP2* genes. Their role in the establishment of flower dorsoventral asymmetry in *A. majus* appears to be plausible, but this will only be firmly established when the *A. majus rip* mutant are to be isolated. Also, a contribution on the knowledge about the RIP function could be given by the ectopic expression in *Arabidopsis*. The constitution of the RIP MYB-like/SANT domain differs from the DIV and RAD MYB-like/SANT domains. The alteration in the aromatic residues could be functionally significant since it is the first time that a MYB-like protein is described with this combination of conserved amino acids. Moreover, Saikumar *et al.* (1990) implied that the replacement of two aminoacids, asparagine and lysine, that flank the last tryptophan with other acidic amino acids completely abolished their DNA-binding activity. By analysis of the RIP amino acidic sequences it is possible to observe that the last tryptophan of the MYB-like/SANT domain is not flanked by either a asparagine or a lysine, which could mean that this proteins are not involved in DNA-binding but exclusively in protein-protein interactions. The conserved DUF3755 domain, a 40 amino acids long protein domain is found in several organisms such as *P. patens patens*, *P. sitchensis*, *Z. mays*, *O. sativa*, *V. vinifera*, *R. communis* and *A. thaliana*, however, its biological meaning is still unknown. The role of the DUF3755 domain in the RIP function particularly in their ability to establish protein-protein interactions is a question that should be answered in future studies.

## 4.6 Concluding Remarks

This investigation has given insight on the molecular antagonism between RAD and DIV in the establishment of floral dorsoventral asymmetry in *A. majus*. Results show that RAD and DIV do not interact directly and that the molecular antagonism could be mediated by competition for the RIP proteins. Moreover, RAD appears to have a higher affinity for the RIP proteins than DIV. This result suggests the idea that the RIP

proteins are co-factors in the molecular antagonism of RAD over DIV function during floral development. Accordingly, the RIP proteins might be essential co-factors for DIV to exert its functions and to determine ventral identity of the flower. In the dorsal domain, where RAD is expressed, the interaction of DIV and RIP proteins is inhibited by RAD, therefore, restricting DIV function to the ventral domain of the flower.

There is ample evidenced that during evolution *RAD* and *RAD*-like genes were co-opted to establish floral dorsoventral asymmetry in several *taxa* (Corley *et al.*, 2005, Baxter *et al.*, 2007, Zhou *et al.*, 2008; Preston *et al.*, 2009; Yang *et al.*, 2010). However, there is little evidence in *A. majus* and in other *taxa* of the downstream targets of RAD and RAD-like proteins. Also, there is little indication about the involvement of *DIV*-like genes in the establishment of flower dorsoventral asymmetry, with the exception of the study carried out by Howarth and Donoghue (2009) and Zhou *et al.* (2008). However, it is likely that the RAD molecular antagonism towards DIV could also be conserved in other species. If this proves to be right, the RIP function in mediating the molecular antagonism between RAD and DIV could also be conserved among other *taxa*. Because life reinvents itself by remodelling already existing pathways, it will be of great interest to determine whether the interactions between these three types of MYB-like proteins have been recruited in other species for different developmental processes, providing a good example of heterotopic expression of existing functions. Understanding the interactions between the genes in this network presents an exciting challenge for the future and will provide a deeper understanding of how molecular changes have evolved to generate new forms and functions, producing biological diversity.



## 5. Bibliography

- Aasland, R., Stewart, A.F., and Gibson, T.** (1996). The SANT domain: a putative DNA-binding domain in the SWI-SNF and ADA complexes, the transcriptional co-repressor N-CoR and TFIIB. *Trends Biochemical Science* **21**, 87-89.
- Almeida, J., Rocheta, M., and Galego, L.** (1997). Genetic control of flower shape in *Antirrhinum majus*. *Development* **124**, 1387-1392.
- Araki, S., Ito, M., Soyano, T., Nishihama, R., and Machida, Y.** (2004). Mitotic cyclins stimulate the activity of c-MYB-like factors for transactivation of G2/M phase-specific genes in tobacco. *Journal of Biological Chemistry* **279**, 32979-32988.
- Ballesteros, M.L., Bolle, C., Lois, L.M., Moore, J.M., Vielle- Calzada, J.P., Grossniklaus, U., and Chua, N.H.** (2001). LAF1, a MYB transcription activator for phytochrome A signaling. *Genes Development* **15**, 2613-2625.
- Barg, R., Sobolev, I., Eilon, T., Gur, A., Chmelnitsky, I., Shabtai, S., Grotewold, E., and Salts, Y.** (2005). The tomato early fruit specific gene *Lefsm1* defines a novel class of plant-specific SANT/MYB domain proteins. *Planta* **221**, 197-211.
- Bartel, P. L., Chien, C.-T., Sternglanz, R., and Fields, S.** (1993). Using the two-hybrid system to detect protein-protein interactions. In *Cellular Interactions in Development: A Practical Approach*, ed. Hartley, D. A. (Oxford University Press, Oxford), 153–179.
- Baxter, C.E.L., Costa, M.M.R., and Coen, E.S.** (2007). Diversification and co-option of RAD-like genes in the evolution of floral asymmetry. *The Plant Journal* **52**, 105-113.
- Belting, H.G., Shashikant, C.S., and Ruddle, F.H.** (1998). Modifications of expression and *cis*-regulation of *Hoxc8* in the evolution of diverged axial morphology. *Proceedings National Academy Science U. S. A.* **95**, 2355-2360.
- Bendtsen, J.D., Nielsen, H., Widdick, D., Palmer, T., and Brunak, S.** (2005). Prediction of twin-arginine signal peptides. *BMC bioinformatics* **6**, 167-170.
- Bhasin, M., and Raghava, G.P.S.** (2004). ESLpred: SVM based method for subcellular localization of eukaryotic proteins using dipeptide composition and PSI-BLAST. *Nucleic Acids Research* **32**, 414-419
- Bianchi, A., Stansel, R.M., Fairall, L., Griffith, J.D., Rhodes, D., and de Lange, T.** (1999). TRF1 binds a bipartite telomeric site with extreme spatial flexibility. *European Molecular Biology Organization Journal* **18**, 5735-5744.
- Bontems, S., Di Valentin, E., Baudoux, L., Rentier, B., Sadzot-Delvaux, C. and Piette, J.** (2002). Phosphorylation of Varicella-Zoster Virus IE63 protein by casein kinases influences its cellular localization and gene regulation activity. *Journal of Biological Chemistry* **277**, 21050-21060.
- Borello, U., Ceccarelli, C., and Giuliano, G.** (1993). Constitutive, light-responsive and circadian clock-responsive factors compete for the different *I* box elements in plant light-regulated promoters. *The Plant Journal* **4**, 611-619.
- Boyer, L.A., Latek, R.R., and Petersen, C.L.** (2004). The SANT domain: a unique histone-tail-binding module? *Nature Reviews Molecular Cell Biology* **5**, 158-163.
- Bracha-Drori, K., Shichrur, K., Katz, A., Oliva, M., Angelovici, R., Yalovsky, S., and Ohad, N.** (2004). Detection of protein–protein interactions in plants using

- bimolecular fluorescence complementation. *The Plant Journal* **40**, 419-427.
- Braun, E.L., and Grotewald, E.** (1999). Newly discovered plant *c-Myb*-like genes rewrite the evolution of the plant *Myb* gene family. *Plant Physiology* **121**, 21-24.
- Breeden, L., and Nasmyth, K.** (1985). Regulation of the Yeast HO Gene. *Cold Spring Harbour Symposium Quantification Biology* **50**, 643-650.
- Brent, R. and Finley, R.L.** (1997). Understanding gene and allele function with two-hybrid methods. *Annual Reviews Genetics* **31**, 663-704.
- Bullock, W.O., Fernandez, J.M., and Short, J.M.** (1987). XL1-Blue: a high-efficiency plasmid transforming *recA Escherichia coli* strain with beta-galactosidase selection. *Biotechniques* **5**, 376-380.
- Busch, A. and Zachgo, S.** (2007). Control of corolla monosymmetry in the Brassicaceae *Iberis amara*. *Proceedings National Academy Science U. S. A.* **104**, 16714-16719.
- Carroll, S.B., Grenier, J.K., and Weatherbee, S.D.** (2005). *From DNA to Diversity: Molecular Genetics and the Evolution of Animal Design*, Second Edition (Malden, MA: Blackwell Publishing).
- Carroll, S.B., Grenier, J.K., and Weatherbee, S.D.** (2001). *From DNA to diversity*. Blackwell Science.
- Carpenter, R. and Coen, E.S.** (1990). Floral homeotic mutations produced by transposon-mutagenesis in *Antirrhinum majus*. *Genes Development* **4**, 1483-1493.
- Causier, B., and Davies, B.** (2002). Analysing protein-protein interactions with the yeast two-hybrid system. *Plant Molecular Biology* **50**, 855-870.
- Chandler, J.W., Cole, M., Flier, A., Grewe, B., and Werr, W.** (2007). The AP2 transcription factors DORNROSCHEN and DORNROSCHEN-LIKE redundantly control *Arabidopsis* embryo patterning via interaction with PHAVOLUTA. *Development* **134**, 1653-1662.
- Chen, K., and Rajewsky, N.** (2007). The evolution of gene regulation by transcription factors and microRNAs. *Nature Reviews Genetics* **8**, 93-103.
- Chini, A., Fonseca, S., Chico, J.M., Fernández-Calvo, P., and Solano, R.** (2009). The ZIM domain mediates homo- and heteromeric interactions between Arabidopsis JAZ proteins. *The Plant Journal* **59**, 77-87.
- Chiu, I.-W., Niwa, Y., Zheng, W., Hirano, T., Kobayashi, H., Sheen J.** (1996). Engineered GFP as a vital reporter in plants. *Current Biology* **6**, 325-330.
- Choi, K., Park, C., Lee, J., Oh, M., Noh, B., and Lee, I.** (2007). *Arabidopsis* homologs of components of the SWR1 complex regulate flowering and plant development. *Development* **134**, 1931-1941.
- Clough, S.V., and Bent, A.F.** (1998). Floral dip: a simplified method for *Agrobacterium*-mediated transformation of *Arabidopsis thaliana*. *The Plant Journal* **16**, 735-743.
- Coen, E.S. and Meyerowitz, E.M.** (1991). The war of the whorls: genetic interactions controlling flower development. *Nature* **353**, 31-37.
- Coen, E.S., and Nugent, J.M.** (1994). Evolution of flowers and inflorescences. *Development (Suppl.)*, 107-116.
- Cohn, M.J., and Tickle, C.** (1999). Developmental basis of limbleness and axial patterning in snakes. *Nature* **399**, 474-479.

- Comeron, J.M., and Aguadé, M.** (1998). An evaluation of measures of synonymous codon usage bias. *Journal of Molecular Evolution* **47**, 268-274.
- Corley, S.B., Carpenter, R., Copsey, L., and Coen, E.** (2005). Floral asymmetry involves interplay between TCP and MYB transcription factors in *Antirrhinum*. *Proceedings National Academy Science U. S. A.* **102**, 5068-5073.
- Costa, M.M.R., Fox, S., Hanna, A.I., Baxter, C., and Coen, E.** (2005). Evolution of regulatory interactions controlling floral asymmetry. *Development* **132**, 5093-5101.
- Crane, P.R., Friis, E.M., and Pedersen, K.R.** (1995). The origin and early diversification of angiosperms. *Nature* **374**, 27-33.
- Crepet, W.L.** (1996). Timing in the evolution of derived floral characters. Upper Cretaceous (Turonian) taxa with tricolpate and tricolpatederived pollen. *Review Palaeobotany Palynology* **90**, 339-359.
- Cronk, Q.** (2001). Plant evolution and development in a post-genomic context. *Nature Review Genetics* **2**, 607-619.
- Cubas, P., Lauter, N., Doebley, J., and Coen, E.** (1999). The TCP domain: a motif found in proteins regulating plant growth and development. *The Plant Journal* **18**, 215-222.
- Curtis, M.D., and Grossniklaus, U.** (2003). A gateway cloning vector set for high-throughput functional analysis of genes in planta. *Plant Physiology* **133**, 462-469.
- Daniel, X., Sugano, S., and Tobin, E.** (2004). CK2 phosphorylation of CCA1 is necessary for its circadian oscillator function in *Arabidopsis*. *Proceedings National Academy Science U. S. A.* **9**, 3292-3297.
- Doebley, J., and Lukens, L.** (1998). Transcriptional regulation and the evolution of plant form. *Plant Cell* **10**, 1075-1082.
- Donoghue, M.J., Ree, R.H., and Baum, D.A.** (1998). Phylogeny and the evolution of flower symmetry in the Asteridae. *Trends Plant Science* **3**, 311-317.
- Dubendorff, J.W. and Studier, F.W.** (1991). Controlling basal expression in an inducible T7 expression system by blocking the target T7 promoter with lac repressor. *Journal Molecular Biology* **219**, 45-59.
- Dubos, C., Stracke R., Grotewold, E., Weisshaar, B., Martin, C., and Lepiniec, L.** (2010). MYB transcription factors in *Arabidopsis*. *Trends in Plant Science Article in Press*, 1-9.
- Durfee, T., Becherer, K., Chen, P. L., Yeh, S. H., Yang, Y., Kilburn, A.E., Lee, W.H. and Elledge, S. J.** (1993). The retinoblastoma protein associates with the protein phosphatase type 1 catalytic subunit. *Genes Development* **7**, 555-569.
- Egea-Cortines, M, Saedler, H., and Sommer, H.** (1999). Ternary complex formation between the MADS-box proteins SQUAMOSA, DEFICIENS and GLOBOSA is involved in the control of floral architecture in *Antirrhinum majus*. *EMBO Journal* **18**, 5370-9.
- Endress, P.K.** (1994). *Diversity and Evolutionary Biology of Tropical Flowers*. Cambridge University Press.
- Endress, P.K.** (1999). Symmetry in flowers: diversity and evolution. *International Journal Plant Science* **160**, 3-23.
- Endress, P.K.** (2001). Evolution of floral symmetry. *Current Opinion Plant Biology* **4**, 86-89.

- Esch, J.J., Chen, M.A., Hillestad, M. and Marks, M.D.** (2004). Comparison of TRY and the closely related At1g01380 gene in controlling Arabidopsis trichome patterning. *The Plant Journal* **40**, 860-869.
- Favaro, R., Pinyopich, A., Battaglia, R., Kooiker, M., Borghi, L., Ditta, G., Yanofsky, M.F., Kater, M.M., and Colombo, L.** (2003). MADS-box protein complexes control carpel and ovule development in Arabidopsis. *The Plant Cell* **15**, 2603-2611.
- Feilotter, H.E., Hannon, G.J., Ruddel, C.J., and Beach, D.** (1994). Construction of an improved host strain for two-hybrid screening. *Nucleic Acids Research* **22**, 1502-1503.
- Feng, X., Zhao, Z., Tian, Z., Xu, S., Luo, Y., Cai, Z., Wang, Y., Yang, J., Wang, Z., Weng, L., Chen, J., Zheng, L., Guo, X., Luo, J., Sato, S., Tabata, S., Ma, W., Cao, X., Hu, X., Sun, C., and Luo, D.** (2006). Control of petal shape and floral zygomorphy in *Lotus japonicus*. *Proceedings National Academy Science U. S. A.* **103**, 4970-4975.
- Feng, S., Martinez, C., Gusmaroli, G., Wang, Y., Zhou, J., Wang, F., Chen, L., Yu, L., Iglesias-Pedraz, J.M., Kircher, S., Schäfer, E., Fu, X., Fan, L-M., and Deng, X.W.** (2008). Coordinated regulation of Arabidopsis thaliana development by light and gibberellins. *Nature* **451**, 475-480.
- Fields, S.** (1993). The two-hybrid system to detect protein-protein interactions. *Methods* **5**, 116-124.
- Forwood, J.K., and Jans, D.A.** (2006). Quantitative analysis of DNA-protein interactions using double-labeled native gel electrophoresis and fluorescence-based imaging. *Electrophoresis* **27**, 3166-3170.
- Fried, M. and Crothers, D.M.** (1981). Equilibria and kinetics of lac repressor-operator interactions by polyacrylamide gel electrophoresis. *Nucleic Acids Research* **9**, 6505-6525.
- Galego, L., and Almeida, J.** (2002). Role of DIVARICATA in the control of dorsoventral asymmetry in *Antirrhinum* flowers. *Genes Development* **16**, 880-891.
- Gao, Q., Tao, J.H., Yan, D., and Wang, Y.Z.** (2008). Expression differentiation of CYC-like floral symmetry genes correlated with their protein sequence divergence in *Chirita heterotricha* (Gesneriaceae). *Development Genes and Evolution* **218**, 341-351.
- Garner, M.M., and Revzin, A.** (1981). A gel electrophoresis method for quantifying the binding of proteins to specific DNA regions: application to components of the Escherichia coli lactose operon regulatory system. *Nucleic Acids Research* **9**, 3047-3060.
- Gasteiger E., Hoogland C., Gattiker A., Duvaud S., Wilkins M.R., Appel R.D., Bairoch A.** (2005). Protein Identification and Analysis Tools on the ExPASy Server. *The Proteomics Protocols Handbook*, Humana Press, 571-607.
- Gaudin, V., Lumness, P.A., Fobert, P.R., Towers, M., Riou-Khamlichi, C., Murray, J.A.H., Coen, E., and Doonan, J.H.** (2000). The Expression of D-Cyclin Genes Defines Distinct Developmental Zones in Snapdragon Apical Meristems and Is Locally Regulated by the Cycloidea Gene. *Plant Physiology* **122**, 1137-1148.
- Gellon, G., and McGinnis, W.** (1998). Shaping animal body plans in development and evolution by modulation of Hox expression patterns. *BioEssays* **20**, 116-125.

- Giuliano, G., Pichersky, E., Malik, V.S., Timko, M.P., Scolnik, P.A. and Cashmore, A.R.** (1988). An evolutionarily conserved protein binding sequence upstream of a plant light-regulated gene. *Proceedings National Academy Science U. S. A.* **85**, 7089-7093.
- Gorlich, D., and Mattaj, I.W.** (1996). Nucleocytoplasmatic transport. *Science* **271**, 1513-1518.
- Griffin, H.G., and Griffin, A.M.** (1994). *PCR Technology: Current Innovations*. Boca Raton: CRC Press.
- Grune, T., Brzeski, J., Eberharter, A., Clapier, C.R., Corona, D.F., Becker, P.B., and Muller, C.W.** (2003). Crystal structure and functional analysis of a nucleosome recognition module of the remodeling factor ISWI. *Molecular Cell* **12**, 449-60.
- Hansen, L.H., Knudsen, S., and Sørensen, S.J.** (1998). The effect of the lacY gene on the induction of IPTG inducible promoters, studied in *E. coli* and *P. fluorescens*. *Current Microbiology* **36**, 341-347.
- Harper, J.W., Adami, G.R., Wie, N., Keyomarsi, K. and Elledge, S.J.** (1993). The p21 Cdk-Interacting protein cipl is a potent inhibitor of G1 Cyclin- dependent Kinases. *Cell* **75**, 805-816.
- Harrison, C.J., Corley, S.B., Moylan, E.C., Alexander, D.L., Scotland, R.W., and Langdale, J.A.** (2005). Independent recruitment of a conserved developmental mechanism during leaf evolution. *Nature* **434**, 509-514.
- Hartley, J.L., Temple, G.F., and Brasch, M.A.** (2000). DNA cloning using in vitro site-specific recombination. *Genome Research* **10**, 1788-1795.
- He, X., and Zhang, J.** (2005). Rapid subfunctionalization accompanied by prolonged and substantial neofunctionalization in duplicate gene evolution. *Genetics* **169**, 1157-1164.
- Hellmann, L.M.; and Fried, M.G.** (2007). Electrophoretic mobility shift assay (EMSA) for detecting protein–nucleic acid interactions. *Nature Protocols* **2**, 1849-1861.
- Higginson, T., Li, S.F., and Parish, R.W.** (2003). *AtMYB103* regulates tapetum and trichome development in *Arabidopsis thaliana*. *The Plant Journal* **35**, 177-192.
- Hileman, L.C., and Baum, D.A.** (2003). Why do paralogs persist? Molecular evolution of *CYCLOIDEA* and related floral symmetry genes in Antirrhineae (Veronicaceae). *Molecular Biology Evolution* **20**, 591-600.
- Hileman, L.C., Kramer, E.M., and Baum, D.A.** (2003). Differential regulation of symmetry genes and the evolution of floral morphologies. *Proceedings of the National Academy of Sciences U.S.A.* **100**, 12814-12819.
- Hochuli, E., Döbeli, H., and Schacher, A.** (1987). New metal chelate adsorbent selective for proteins and peptides containing neighboring histidine residues. *Journal Chromatography* **411**, 177-184.
- Holland, P.W.H.** (1999). Gene duplication: past, present and future. *Seminars Cell Developmental Biology* **10**, 541-547.
- Hood, E.E., Helmer, G.L., Fraley, R.T., and Chilton, M.D.** (1986). The hypervirulence of *Agrobacterium tumefaciens* A281 is encoded in a region of pTiBo542 outside of T-DNA. *Journal Bacteriology* **168**, 1291-1301.

- Horton, P., Park, K.-J., Obayashi, T., and Nakai, K.** (2006). Protein Subcellular Localization Prediction with WoLFPSORT. Proceedings of Asian Pacific Bioinformatics Conference APBC06, 39-48.
- Howarth, D.G., and Donoghue, M.J.** (2006). Phylogenetic analysis of the ‘ECE’ (CYC/TB1) clade reveals duplications predating the emergence of the core eudicots. Proceedings National Academy Science U. S. A. **103**, 9101-9106.
- Howarth, D.G., and Donoghue, M.J.** (2009). Duplications and expression of *DIVARICATA*-like genes in Dipsicales. Oxford University Press on behalf of the Society for Molecular Biology and Evolution.
- Hsieh, T.F., Hakim, O., Ohad, N. and Fischer, R.L.** (2003). From flour to flower: how Polycomb group proteins influence multiple aspects of plant development. Trends Plant Science **8**, 439-445.
- Hu, C.D. and Kerppola, T.K.** (2003) Simultaneous visualization of multiple protein interactions in living cells using multicolor fluorescence complementation analysis. Nature Biotechnology **21**, 539-545.
- Hu, C.D., Chinenov, Y. and Kerppola, T.K.** (2002). Visualization of interactions among bZIP and Rel family proteins in living cells using bimolecular fluorescence complementation. Molecular Cell **9**, 789-798.
- Huang, J., Villemain, J., Padilla, R. and Sousa, R.** (1999). Mechanisms by which T7 lysozyme specifically regulates T7 RNA polymerase during different phases of transcription. Journal Molecular Biology **293**, 457-475.
- Hughes, A.L.** (1994). The evolution of functionally novel proteins after gene duplication. Proceedings of the Royal. Society London B. Biological Sciences **256**, 119-124.
- Inoue H., Nojima H., and Okayama H.** (1990). High efficiency transformation of *Escherichia coli* with plasmids. Gene **96**, 23-28.
- Ito, M.** (2005). Conservation and diversification of three-repeat Myb transcription factors in plants. Journal of Plant Research **118**, 61-69.
- Ito, H., Fukada, Y., Murata, K., and Kimura, A.** (1983). Transformation of intact yeast cells treated with alkali cations. Journal of Bacteriology **153**, 163-168.
- Jabbour, F., Nadot, S., and Damerval, C.** (2009). Evolution of floral symmetry: a state of the art. Evolution **332**, 219-231.
- Jaffé, F.W., Tattersall, A., and Glover, B.J.** (2007). A truncated MYB transcription factor from *Antirrhinum majus* regulates epidermal cell outgrowth. Journal of Experimental Botany **58**, 1515-1524.
- Jefferson, R.A., Kavanagh, T.A., and Bevan, M.W.** (1987). GUS fusions: B-glucuronidase as a sensitive and versatile gene fusion marker in higher plants. The EMBO Journal **6**, 3901-3907.
- Jensen, L.J., Gupta, R., Blom, N., Devos, D., Tamames, J., Kesmir, C., Nielsen, H. Stærfeldt, H.H., Rapacki, K., Workman, C., Andersen, C.A.F., Knudsen, S., Krogh, A., Valencia, A., and Brunak, S.** (2002). Ab initio prediction of human orphan protein function from post-translational modifications and localization features. Journal Molecular Biology **319**, 1257-1265.
- Jensen, L.J., Stærfeldt, H.H., and Brunak, S.** (2003). Prediction of human protein function according to Gene Ontology categories. Bioinformatics **19**, 635-642.

- Jiang, C., Gu, X., and Peterson, T.** (2004). Identification of conserved gene structures and carboxy-terminal motifs in the MYB gene family of *Arabidopsis* and *Oryza sativa* L. ssp. *indica*. *Genome Biology* **5**, 46-52.
- Jiang, C., Gu, J., Chopra, S., Gu, X., and Peterson, T.** (2004). Ordered origin of the typical two- and three-repeat Myb genes. *Gene* **326**, 13-22.
- Kalderon D., Roberts, B.L., Richardson, W.D., and Smith, A.E.** (1984). A short amino acid sequence able to specify nuclear location. *Cell* **39**, 499-509.
- Kalisz, S., Ree, H.R., and Sargent, R.D.** (2006). Linking floral symmetry genes to breeding system evolution. *Trends Plant Science* **11**, 568-573.
- Kang, J., Lee, M.S., and Gorenstein, D.G.** (2005). Quantitative analysis of chemiluminescence signals using a cooled charge-coupled device camera. *Analytical Biochemistry* **345**, 66-71.
- Karimi, M., Inze, D., and Depicker, A.** (2002). GATEWAY vectors for Agrobacterium-mediated plant transformation. *Trends Plant Science* **7**, 193-195.
- Karzai, A.W., Roche, E.D., and Sauer, R.T.** (2000). The SsrA-SmpB system for protein tagging, directed degradation and ribosome rescue. *Nature Structural Biology* **7**, 449-455.
- Kirik, V., Simon, M., Huelskamp, M. and Schiefelbein, J.** (2004). The *ENHANCER OF TRY AND CPC1* gene acts redundantly with *TRIPTYCHON* and *CAPRICE* in trichome and root hair cell patterning in *Arabidopsis*. *Developmental Biology* **268**, 506-513.
- Koshino-Kimura, Y., Wada, T., Tachibana, T., Tsugeki, R., Ishiguro, S., and Okada, K.** (2005). Regulation of *CAPRICE* transcription by MYB proteins for root epidermis differentiation in *Arabidopsis*. *Plant Cell Physiology* **46**, 817-826.
- Kosugi, S., and Ohashi, Y.** (2002). DNA binding and dimerization specificity and potential targets for the TCP protein family. *The Plant Journal* **30**, 337-348.
- Kozmik, Z., Urbanek, P., and Pam, V.** (1990). Albumin improves formation and detection of some specific protein-DNA complexes in the mobility shift assay. *Nucleic Acids Research* **18**, 2198-2204.
- Kwaaitaal, M., Keinath, N.F., Pajonk, S., Biskup, C., and Panstruga, R.** (2010). Combined Bimolecular Fluorescence Complementation and Forster Resonance Energy Transfer Reveals Ternary SNARE Complex Formation in Living Plant Cells. *Plant Physiology* **152**, 1135-1147.
- Laemmli, U.K.** (1970). Cleavage of structural proteins during the assembly of the head of bacteriophage T4. *Nature* **227**, 680-685.
- Landy, A.** (1989). Dynamic, Structural, and Regulatory Aspects of Lambda Site-specific Recombination. *Annual Reviews Biochemistry* **58**, 913-949.
- Latchman, D.S.** (1997). Transcription factors: an overview. *International Journal Biochemical Cell Biology* **29**, 1305-1312.
- Lee, M.M., and Schiefelbein, J.** (1999). WEREWOLF, a MYB-related protein in *Arabidopsis*, is a position-dependent regulator of epidermal cell patterning. *Cell* **99**, 473-483.
- Levine, M., and Tjian, R.** (2003). Transcription regulation and animal diversity. *Nature* **424**, 147-151.
- Li, J., Yang, X., Wang, Y., Li, X., Gao, Z., Pei, M., Chen, Z., Qu, L.-J., and Gu, H.** (2006). Two groups of MYB transcription factors share a motif, which enhances

- trans-activation activity. *Biochemical and biophysical research communications*. **341**, 1155-1163.
- Luo, D., Carpenter, R., Vincent, C., Copsey, L., and Coen, E.** (1996). Origin of floral asymmetry in *Antirrhinum*. *Nature* **383**, 794-799.
- Luo, D., Carpenter, R., Copsey, L., Vincent, C., Clark, J., and Coen, E.** (1999). Control of organ asymmetry in flowers of *Antirrhinum*. *Cell* **99**, 367-376.
- Mann, M., and Jensen, O.N.** (2003). Proteomic analysis of post-translational modifications. *Nature Biotechnology* **21**, 255-261.
- Marion J., Bach, L., Bellec, Y., Meyer, C., Gissot, L., and Faure, J.D.** (2008). Systematic analysis of protein subcellular localization and interaction using high-throughput transient transformation of *Arabidopsis* seedlings. *The Plant Journal* **56**, 169-179.
- Martin C., Paz-Ares, J.** (1997). MYB transcription factors in plants. *Trends in Genetics* **13**, 67-73.
- Matsui, K., Umemura, Y., and Ohme-Takagi, M.** (2008). AtMYBL2, a protein with a single MYB domain, acts as a negative regulator of anthocyanin biosynthesis in *Arabidopsis*. *The Plant Journal* **55**, 954-967.
- Maxam, A., and Gilbert, W.S.** (1977). A new method for sequencing DNA. *Proceedings National Academy of Science USA* **74**, 560-565.
- Melander, C., Burnett, R., and Gottesfeld, J.M.** (2004). Regulation of gene expression with pyrrole-imidazole polyamides. *Journal of Biotechnology* **112**, 195-220.
- Meyer, T.S.; and Lambert, B.L.** (1965). Use of Coomassie brilliant blue R250 for the electrophoresis of microgram quantities of parotid saliva proteins on acrylamide-gel strips. *Biochim. Biophys. Acta* **107**, 144-145.
- Mitchell, P.J., and Tjian, R.** (1989). Transcriptional regulation in mammalian cells by sequence-specific DNA binding proteins. *Science* **245**, 371-378.
- Moyano, E., Martinez-Garcia, J.F., and Martin, C.** (1996). Apparent redundancy in *myb* gene function provides gearing for the control of flavonoid biosynthesis in *Antirrhinum* flowers. *Plant Cell* **8**, 1519-1532.
- Miller, J.H.** (1972). *Experiments in Molecular Genetics* (Cold Spring Harbor Laboratory, Cold Spring Harbor, NY).
- Miller, J.H.** (1992). In *A Short Course in Bacterial Genetics*. Cold Spring Harbor Laboratory Press, Cold Spring Harbor, 74-99.
- Moffatt, B.A., and Studier, F.W.** (1987). T7 lysozyme inhibits transcription by T7 RNA polymerase. *Cell* **49**, 221-227.
- Murashige, T., and Skoog, F.** (1962). A revised medium for rapid growth and bioassays with tobacco tissue cultures. *Physiological Plant* **15**, 473-497.
- Nakai, K., and Kanehisa, M.** (1991). Expert system for predicting protein localization sites in gram-negative bacteria. *Proteins* **11**, 95-110.
- Neal, P.R., Dafni, A., and Giurfa, M.** (1998). Floral symmetry and its role in plant-pollinator systems: terminology, distribution, and hypotheses. *Annual Review Ecological Systems* **29**, 345-373.
- Ogata, K., Morikawa, S., and Nakamura, H.** (1995). Comparison of the free and DNA-complexed forms of the DNA-binding domain from c-MYB. *Nature Structural & Molecular Biology* **2**, 309-320.



- Ogata, K., Morikawa, S., Nakamura, H., Sekikawa, A., Inoue, T., Kanai, H., Sarai, A., Ishii, S., and Nishimura, Y.** (1994). Solution structure of a specific DNA complex of the MYB DNA binding domain with cooperative recognition helices. *Cell* **79**, 639-648.
- Ohno, S.** (1970). *Evolution by Gene Duplication*. New York: Springer-Verlag.
- Pabo, C.O., and Sauer, R.T.** (1992). Transcription factors, structural families and principles of DNA recognition. *Annual Reviews Biochemistry* **61**, 1053-1095.
- Palmer, E., and Freeman, T.** (2004). Investigation into the use of C- and N-terminal GFP fusion proteins for subcellular localization studies using reverse transfection microarrays. *Comparative and Functional Genomics* **5**, 342-353.
- Patthy, L.** (2008). *Protein Evolution*. Blackwell Publishing, second edition.
- Paz-Ares, J., Ghosal, D., Wienand, U., Peterson, P.A., and Saedler, H.** (1987). The regulatory *c1* locus of *Zea mays* encodes a protein with homology to MYB proto-oncogene products and with structural similarities to transcriptional activators. *European Molecular Biology Organization Journal* **6**, 3553-3558.
- Perbal, M.C., Haughn, G., Saedler, H., and Schwarz-Sommer, Z.** (1996). Non-cell-autonomous function of the *Antirrhinum* floral homeotic proteins DEFICIENS and GLOBOSA is exerted by their polar cell-to-cell trafficking. *Development* **122**, 3433-3441.
- Perez-Rodriguez, M., Jaffé, F.W., Butelli, E., Glover, B.J., and Martin, C.** (2005). Development of three different cell types is associated with the activity of a specific MYB transcription factor in the ventral petal of *Antirrhinum majus* flowers. *Development* **132**, 359-370.
- Porath, J., Carlsson, J., Olsson, I., and Belfrage, G.** (1975). Metal chelate affinity chromatography, a new approach to protein fractionation. *Nature* **258**, 598-599.
- Preston, J.C., and Hileman, L.C.** (2009). Developmental genetics of floral symmetry evolution. *Trends Plant Science* **14**, 147-154.
- Preston, J.C., Kost, M.A., and Hileman, L.C.** (2009). Conservation and diversification of the symmetry developmental program among close relatives of snapdragon with divergent floral morphologies. *New Phytologist* **182**, 751-762.
- Quinn, P.G.** (2002). Mechanisms of basal and kinase-inducible transcription activation by CREB. *Programme Nucleic Acid Research on Molecular Biology* **72**, 269-305.
- Raimundo, J.** (2010). Functional characterisation of a new class of MYB-like genes in *Arabidopsis thaliana* and *Antirrhinum majus*.
- Raymond, S., and Weintraub, L.** (1959). Acrylamide gel as a supporting medium for zone electrophoresis. *Science* **130**, 711-718.
- Rebois, R.V., Robitaille, M., Pétrin, D., Zylbergold, P., Trieu, P., and Hébert, T.E.** (2008). Combining protein complementation assays with resonance energy transfer to detect multipartner protein complexes in living cells. *Methods* **45**, 214-218.
- Ree, R.H., and Donoghue, M.J.** (1999). Inferring rates of change in flower symmetry in Asterid angiosperms. *Systems Biology* **48**, 633-641.
- Reeves, A.P., and Olmstead, R.G.** (2003). Evolution of the TCP gene family in Asteridae: Cladistic and network approaches to understanding regulatory gene family diversification and its impact on morphological evolution. *Molecular Biology Evolution* **20**, 1997-2009.

- Riechmann, J.L., Heard, J., Martin, G., Reuber, L., Jiang, C.-Z., Keddie, J., Adam, L., Pineda, O., Ratcliffe, O.J., Samaha, R.R., Creelman, R., Pilgrim, M., Broun, P., Zhang, J.Z., Ghandehari, D., Sherman, B.K., and Yu, G.-L.** (2000). Arabidopsis transcription factors: genome-wide comparative analysis among eukaryotes. *Science* **290**, 2105-2110.
- Robbins, J., Dilworth, S.M., Laskey, R.A., and Dingwall C.** (1991). Two interdependent basic domains in nucleoplasmin nuclear targeting sequence: Identification of a class of bipartite nuclear targeting sequence. *Cell* **64**, 615-623.
- Robida, A.M., and Kerppola, T.K.** (2009). Bimolecular Fluorescence Complementation Analysis of Inducible Protein Interactions: Effects of Factors Affecting Protein Folding on Fluorescent Protein Fragment Association. *Journal of Molecular Biology* **394**, 391-409.
- Roche, E.D., and Sauer, R.T.** (1999). SsrA-mediated peptide tagging caused by rare codons and tRNA scarcity. *EMBO Journal* **18**, 4579-4589.
- Romero, I., Fuertes, A., Benito, M.J., Malpica, J.M., Leyva, A., and Paz-Ares, J.** (1998). More than 80R2R3-MYB regulatory genes in the genome of *Arabidopsis thaliana*. *The Plant Journal* **14**, 273-284.
- Rose, A., Meier, I., and Wienand, U.** (1999). The tomato I-box binding factor *LeMYB1* is a member of a novel class of Myb-like proteins. *The Plant Journal* **20**, 641-652.
- Rosin, F.M., and Kramer, E.M.** (2009). Old dogs, new tricks: Regulatory evolution in conserved genetic modules leads to novel morphologies in plants. *Developmental Biology* **332**, 25-35.
- Rubio, V., Linhares, F., Solano, R., Martin, A.C., Iglesias, J., Leyva, A., and Paz-Ares, J.** (2001). A conserved MYB transcription factor involved in phosphate starvation signaling both in vascular plants and in unicellular algae. *Genes Development* **15**, 212-2133.
- Rudall, P.J. and Bateman, R.M.** (2004). Evolution of zygomorphy in monocot flowers: iterative patterns and developmental constraints (Tansley Review). *New Phytologist* **162**, 25-44.
- Saikumar, P., Murali, R., and Reddy, E.P.** (1990). Role of tryptophan repeats and flanking amino acids in Myb-DNA interactions. *Proceedings National Academy Science U. S. A.* **87**, 8452-8456.
- Sakai, R.K., Gelfand, D.H., Stoffel, S., Scharf, S.J., Higuchi, R., Horn, G.T., Mullis, K.B., and Erlich, H.A.** (1988). Primer-directed enzymatic amplification of DNA with a thermostable DNA polymerase. *Science* **23**, 487-494.
- Sambrook, J., Fritsch, E. F. and Maniatis, T.** (1989). *Molecular cloning: a laboratory manual*, 2nd edition. Cold Spring Harbor Laboratory, Cold Spring Harbor, New York
- Sargent, R.D.** (2004). Floral symmetry affects speciation rates in angiosperms. *Proceedings of the Royal Society London B. Biological Sciences* **271**, 603-608.
- Schaffer, R., Ramsay, N., Samach, A., Corden, S., Putterill, J., Carré, I. A. and Coupland, G.** (1998). The late elongated hypocotyl mutation of *Arabidopsis* disrupts circadian rhythms and the photoperiodic control of flowering. *Cell* **93**, 1219-1229.
- Schmitz, G., Tillmann, E., Carriero, F., Fiore, C., and Theres, K.** (2002). The tomato *Blind* gene encodes a MYB transcription factor that controls the formation of

- lateral meristems. Proceedings National Academy Science U. S. A. **99**, 1064-1069.
- Schwarz-Sommer, Z.; Hue, I.; Huijser, P.; Flor, P.J.; Hansen, R.; Tetens, F.; Lönnig, W.E.; Saedler, H.; and Sommer, H.** (1992). Characterization of the *Antirrhinum* floral homeotic MADS-box gene *deficiens*: evidence for DNA binding and autoregulation of its persistent expression throughout flower development. The EMBO Journal **11**, 251-63.
- Schwechheimer, C., Zourelidou, M., and Bevan, M.W.** (1998). Plant transcription studies. Annual Reviews in Plant Physiology **49**, 127-150.
- Shiu, S.H., Shih, M.C., and Li, W.H.** (2005). Transcription factor families have much higher expansion rates in plants than in animals. Plant Physiology **139**, 18-26.
- Simon, M., Lee, M.M., Lin, Y., Gish, L. and Schiefelbein, J.** (2007). Distinct and overlapping roles of single-repeat MYB genes in root epidermal patterning. Developmental Biology **311**, 566-578.
- Stevenson, C.E., Burton, N., Costa, M.M., Nath, U., Dixon, R.A., Coen, E.S., and Lawson, D.M.** (2006). Crystal structure of the MYB domain of the RAD transcription factor from *Antirrhinum majus*. Proteins **65**, 1041-1045.
- Stracke, R., Werber, M., and Weisshaar, B.** (2001). The R2R3 MYB gene family in *Arabidopsis thaliana*. Current Opinion Plant Biology **4**, 447-456.
- Studier, F.W.** (1991). Use of bacteriophage T7 lysozyme to improve an inducible T7 expression system. Journal Molecular Biology **219**, 37-44.
- Studier, F.W. and Moffatt, B.A.** (1986). Use of bacteriophage T7 RNA polymerase to direct selective high-level expression of cloned genes. Journal Molecular Biology **189**, 113-130.
- Studier, F.W., Rosenberg, A.H., Dunn, J.J. and Dubendorff, J.W.** (1990). Use of T7 RNA polymerase to direct expression of cloned genes. Methods Enzymology **185**, 60-89.
- Suggs, S.V., Hirose, T., Miyake, E.H., Kawashima, M.J., Johnson, K.I., and Wallace, R.B.** (1981). Using Purified Genes, in *ICN-UCLA Symp. Developmental Biology*, **23**, 683-689.
- Trémousaygue, D., Garnier, L., Bardet, C., Dabos, P., Herveá, C., and Lescure, B.** (2003). Internal telomeric repeats and 'TCP domain' protein-binding sites cooperate to regulate gene expression in *Arabidopsis thaliana* cycling cells. The Plant Journal **33**, 957-966.
- Tominaga, R., Iwata, M., Okada, K. and Wada, T.** (2007). Functional analysis of the epidermal-specific MYB genes *CAPRICE* and *WEREWOLF* in *Arabidopsis*. Plant Cell **19**, 2264-2277.
- Uhrig, J.F., Mutondo, M., Zimmermann, I., Deeks, M.J., Machesky, L.M., Thomas, P., Uhrig, S., Rambke, C., Hussey, P.J., and Hülskamp, M.** (2007). The role of *Arabidopsis* SCAR genes in ARP2-ARP3-dependent cell morphogenesis. Development **134**, 967-977.
- Van Criekinge, W., and Beyart, R.** (1999). Yeast Two-Hybrid: State of the Art. Biological Procedures Online **2**, 1-38.
- Voelker, C., Schmidt, D., Mueller-Roeber, B., and Czempinski, K.** (2006). Members of the *Arabidopsis* AtTPK/KCO family form homomeric vacuolar channels in planta. The Plant Journal **48**, 296-306.

- Wada, T., Kurata, T., Tominaga, R., Koshino-Kimura, Y., Tachibana, T., Goto, K., Marks, M.D., Shimura, Y., and Okada, K.** (2002). Role of a positive regulator of root-hair development, *CAPRICE*, in Arabidopsis root epidermal cell differentiation. *Development* **129**, 5409-5419.
- Walter, M., Chaban, C., Schutze, K., Batistic, O., Weckermann, K., Nake, C., Blazevic, D., Grefen, C., Schumacher, K., Oecking, C., Harter, K. and Kudla, J.** (2004). Visualization of protein interactions in living plant cells using bimolecular fluorescence complementation. *The Plant Journal* **40**, 428-438.
- Wang, R.-L., Stec, A., Hey, J., Lukens, L., and Doebley, J.** (1999). The limits of selection during maize domestication. *Nature* **398**, 236-239.
- Wang, Z. Luo, Y., Li, X., Wang, L., Xu, S., Yang, J., Weng, L., Sato, S., Tabata, S., Ambrose, M., Rameau, C., Feng, X., Hu, X., and Luo, D.** (2008). Genetic control of floral zygomorphy in pea (*Pisum sativum L.*). *Proceedings National Academy Science U. S. A.* **105**, 10414-10419.
- Wang, Z.Y., and Tobin, E.M.** (1998). Constitutive expression of the *CIRCADIAN CLOCK ASSOCIATED 1 (CCA1)* gene disrupts circadian rhythms and suppresses its own expression. *Cell* **93**, 1207-1217.
- West, A.G., Causier, B.E., Davies, B., and Sharrocks, A.D.** (1998). DNA binding and dimerisation determinants of Antirrhinum majus MADS-box transcription factors. *Nucleic Acids Research* **26**, 5277-5287.
- West, R.W.Jr., Yocum, R.R., and Ptashne, M.** (1984). Saccharomyces cerevisiae GAL1-GAL10 Divergent Promoter Region: Location and Function of the Upstream Activating Sequence UASG *Molecular and Cellular Biology* **4**, 2467-2478.
- Weston, K.** (1999). MYB proteins in life, death and differentiation. *Current Opinion on Gene Development* **8**, 76-81.
- Wolberger, C.** (1999). Multiprotein-DNA complexes in transcriptional regulation. *Annual Reviews in Biophysics and Biomolecular Structures* **28**, 29-56.
- Yang, Y.W., Lai, K.N., Tai, P.Y., and Li, W.H.** (1999). Rates of nucleotide substitution in angiosperm mitochondrial DNA sequences and dates of divergence between Brassica and other angiosperm lineages. *Journal of Molecular Evolution* **48**, 597-604.
- Yang, X., Cui, H., Yuan, Z.-L., and Wang Y.-Z.** (2010). Significance of consensus CYC-binding sites found in the promoters of both *ChCYC* and *ChRAD* genes in *Chirita heterotricha* (Gesneriaceae). *Journal of Systematics and Evolution* **48**, 249-256.
- Yanhui, C., Xiaoyuan, Y., Kun, H., Meihua, L., Jigang, L., Zhaofeng, G., Zhiqiang, L., Yunfei, Z., Xiaoxiao, W., Xiaoming, Q., Yunping, S., Li, Z., Xiaohui, D., Jingchu, L., Xing-Wang, D., Zhangliang, C., Hongya, G., e Li-Jia, Q.** (2006). The MYB transcription factor superfamily of Arabidopsis: expression analysis and phylogenetic comparison with the rice MYB family. *Plant Molecular Biology* **60**, 107-124.
- Zhang, L-Y., Bai, M-Y., Wu, J., Zhu, J-Y., Wang, H., Zhang, Z., Wang, W., Sun, Y., Zhao, J., Sun, X., Yang, H., Xu, Y., Kim, S-H., Fujioka, S., Lin, W.H., Chong, K., Lu, T., and Wang, Z-Y.** (2009). Antagonistic HLH/bHLH Transcription Factors Mediate Brassinosteroid Regulation of Cell Elongation and Plant Development in Rice and *Arabidopsis*. *The Plant Cell* **21**, 3767-3780.

- Zhang, J., Tian, Y., Wang, L., and He, C.** (2010). Functional evolutionary developmental biology (evo-devo) of morphological novelties in plants. *Journal of Systematics and Evolution* **48**, 94-101.
- Zhong, S., Lin, Z., Fray, R., and Grierson, D.** (2008). Improved plant transformation vectors for fluorescent protein tagging. *Transgenic Research* **17**, 985-989.
- Zhong, S., Lin, Z., and Grierson, D.** (2008). Tomato ethylene receptor-CTR interactions: visualization of NEVER-RIPE interactions with multiple CTRs at the endoplasmic reticulum. *Journal Experimental Botany* **59**, 965-972.
- Zhou, X.R., Wang, Y.Z., Smith, J.F., and Chen, R.** (2008). Altered expression patterns of TCP and MYB genes relating to the floral developmental transition from initial zygomorphy to actinomorphic in *Bournea* (Gesneriaceae). *New Phytologist* **178**, 532-543.

## 6. Supplementary information

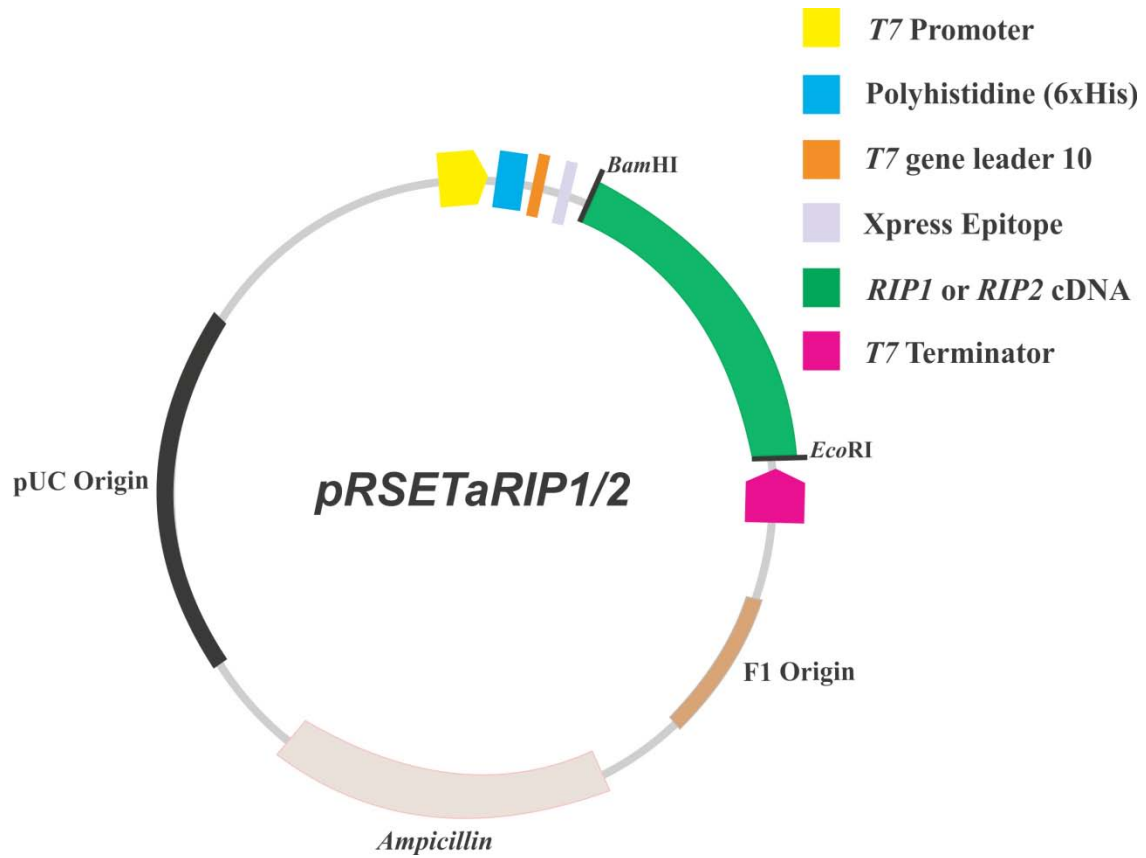


Figure 1 – RIP<sub>pRSETa</sub> constructs.

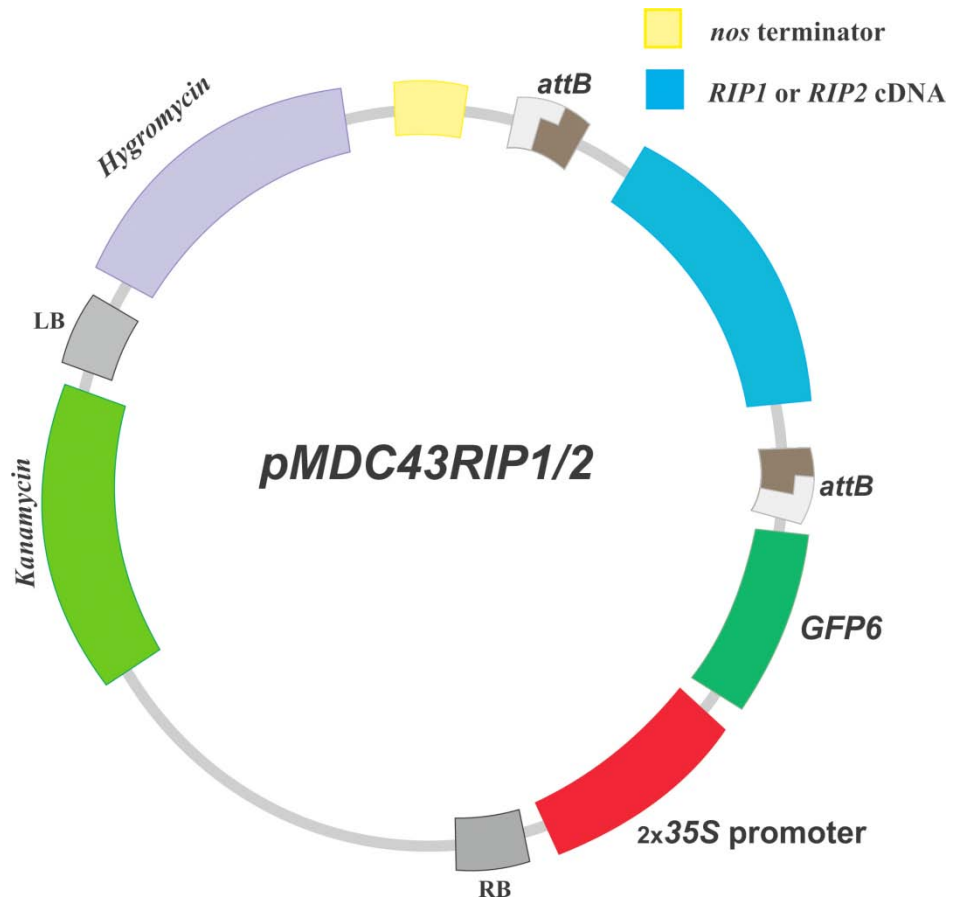


Figure 2 –RIP1<sub>pMDC43</sub> and RIP2<sub>pMDC43</sub> constructs.

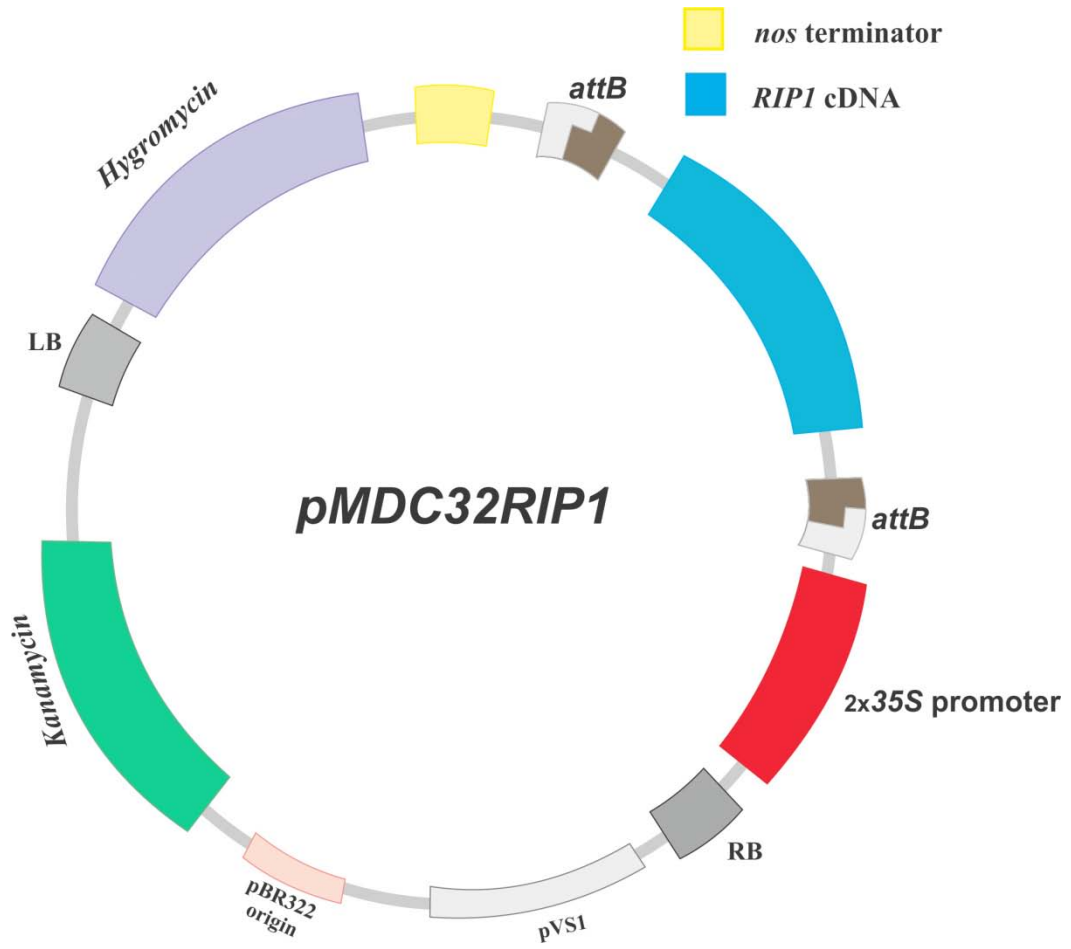


Figure 3–RIP1<sub>pMDC32</sub> construct.



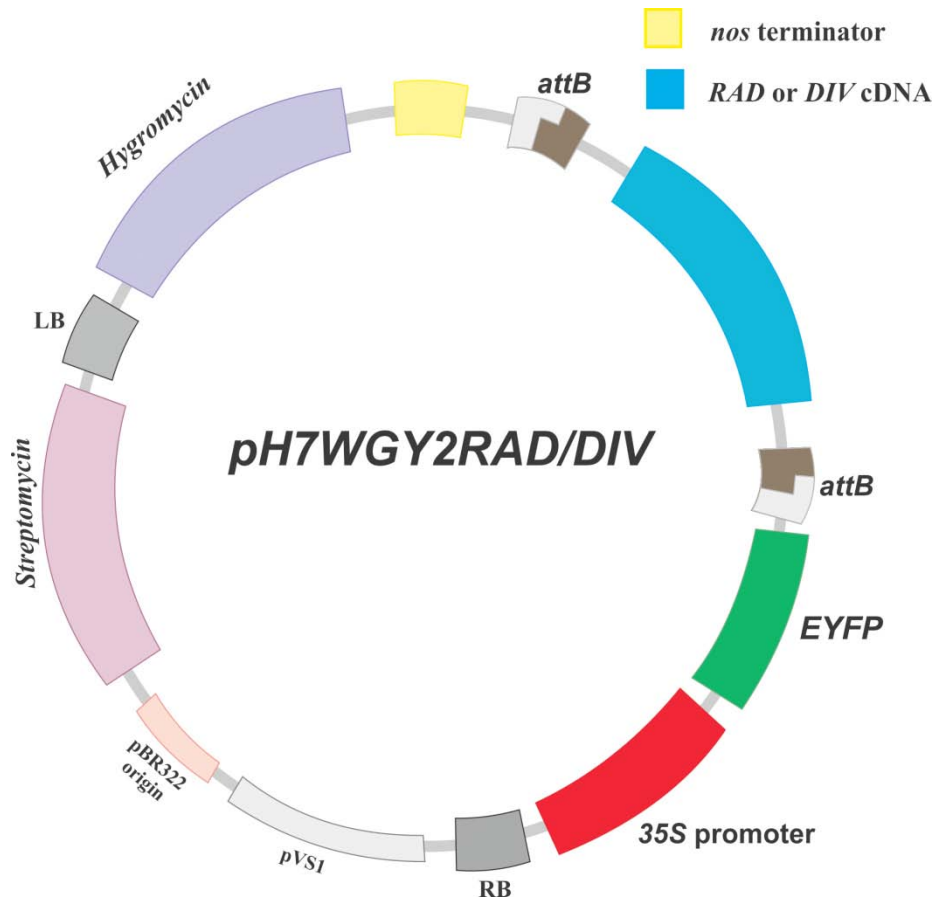


Figure 4 –*RAD/DIV*<sub>*pH7WGY2*</sub> constructs.

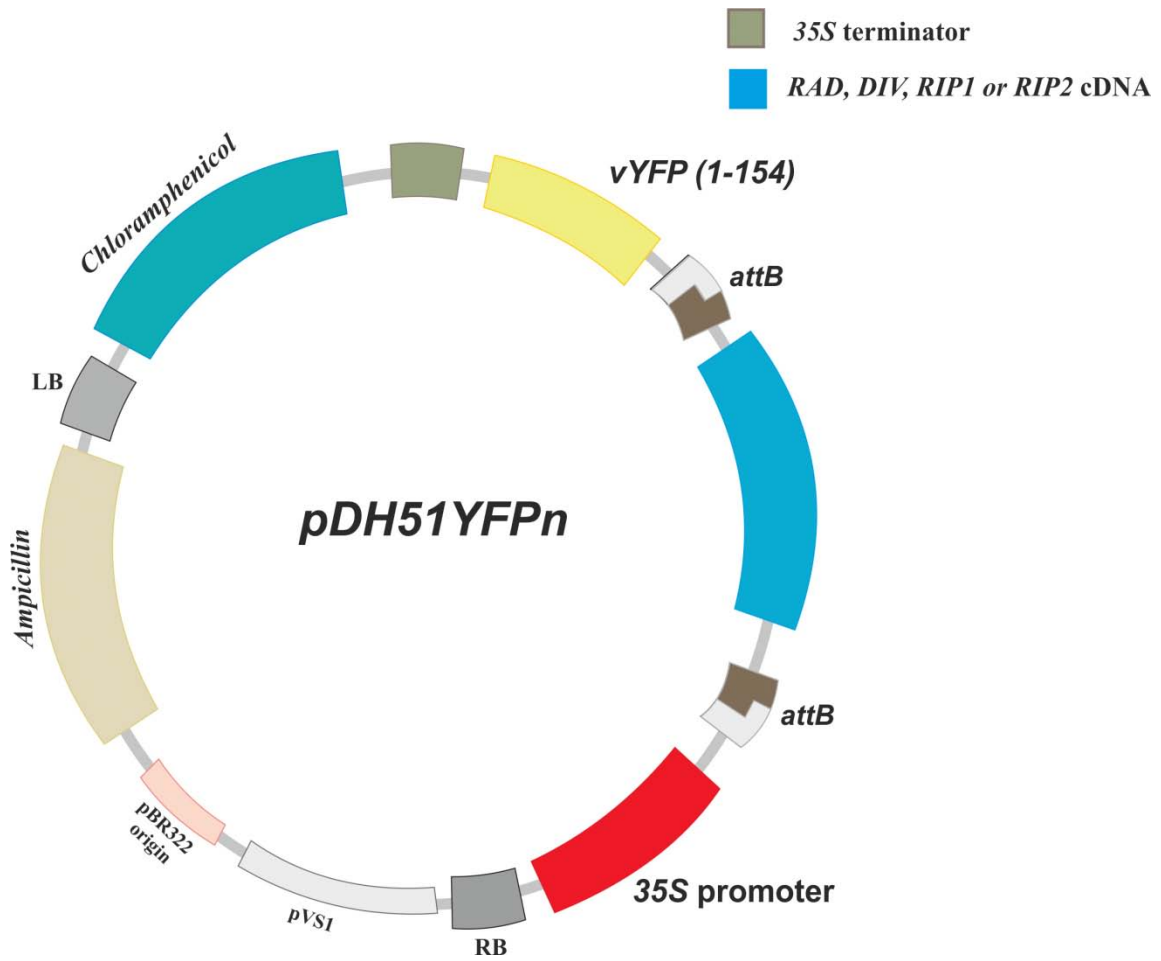


Figure 5 –*pDH51YFPn* constructs.

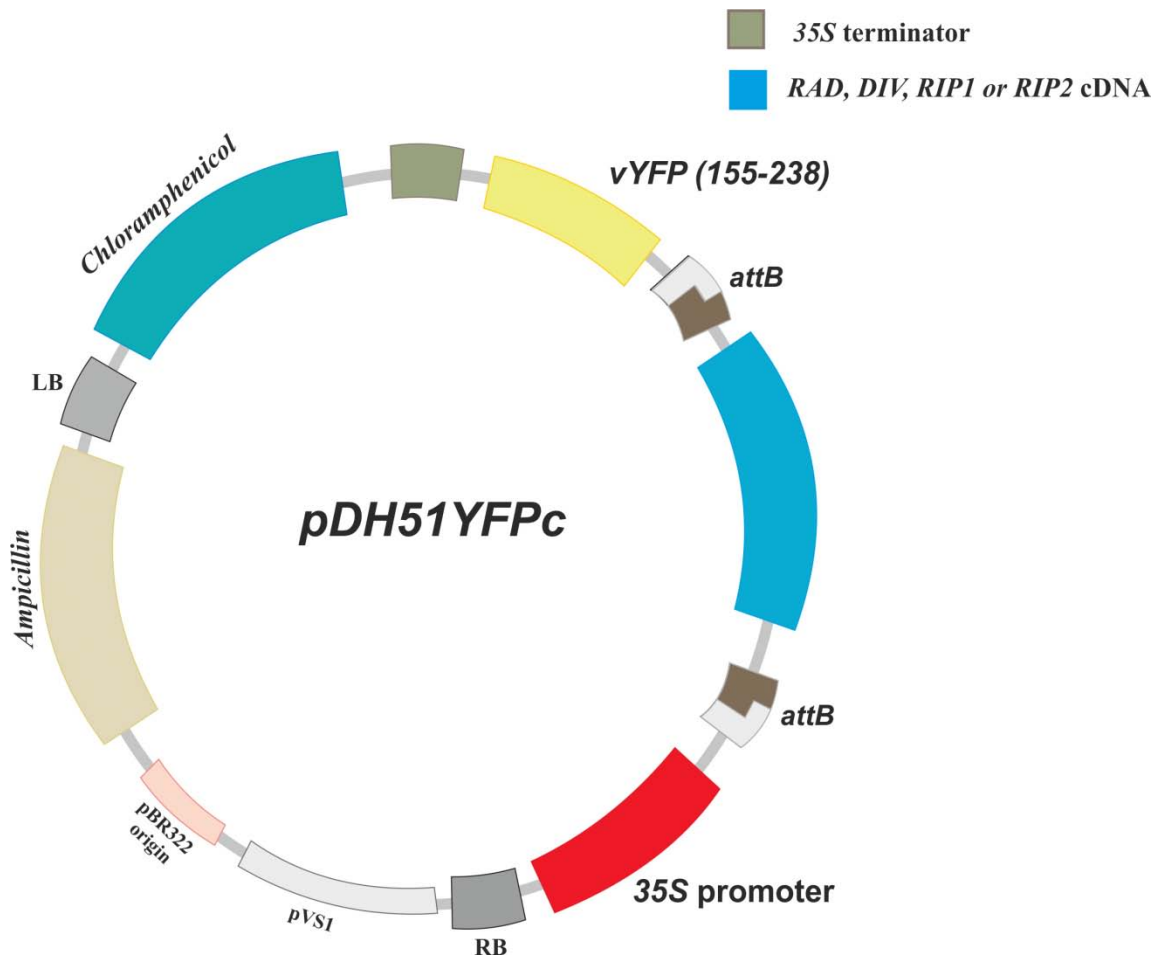


Figure 6 –*pDH51YFPc* constructs.